Non-invasive viral-mediated gene therapy for Machado-Joseph disease

Joana Isabel Rajão Saraiva

Dissertação apresentada à Universidade de Coimbra para cumprimento dos requisitos necessários à obtenção do grau de Mestre em Biologia Celular e Molecular, realizada sob orientação do Professor Doutor Luís Pereira de Almeida (Centro de Neurociências e Biologia Celular) e do Professor Doutor Carlos Duarte (Departamento de Ciências da Vida, Universidade de Coimbra)

Julho de 2016

UNIVERSIDADE DE COIMBRA

Front cover: AAV9 transduction throughout the cerebellum of MJD transgenic mice

Confocal image of a cerebellar section from a MJD transgenic mouse intravenously injected with AAV9, following fluorescence immunohistochemistry: GFP (green), HA (red), DAPI (blue).

O trabalho aqui apresentado foi realizado no grupo de Vectores e Terapia Génica do Centro de Neurociências e Biologia Celular (Universidade de Coimbra, Portugal), sob a orientação do Doutor Rui Jorge Nobre e do Professor Doutor Luís Pereira de Almeida.

Este trabalho foi financiado pela "National Ataxia Foundation" (USA), por Fundos FEDER através do Programa Operacional Factores de Competitividade (COMPETE 2020) e por Fundos Nacionais através da FCT (Fundação para a Ciência e a Tecnologia), no âmbito do projecto Estratégico UID/NEU/04539/2013 e projecto Exploratório EXPL/NEU-NMC/0331/2012.

The present work was performed in Vectors and Gene therapy group, at the Center for Neuroscience and Cell Biology of the University of Coimbra under the supervision of Doutor Rui Jorge Nobre and Prof. Luís Pereira de Almeida

This work was supported by the National Ataxia Foundation, FEDER funds through the Operational Program Competitiveness Factors (COMPETE2020) and Portuguese Foundation for Science and Technology (FCT) through the following grants: UID/NEU/04539/2013 and EXPL/NEU-NMC/0331/2012.

National Ataxia Foundation

COMPETE
PROGRAMA OPERACIONAL FACTORES DE COMPETITIVIDADE

FCT
Fundação para a Ciência e a Tecnologia
MINISTÉRIO DA CIÊNCIA, TECNOLOGIA E ENSINO SUPERIOR

CNC
CENTER FOR NEUROSCIENCE AND CELL BIOLOGY
UNIVERSITY OF COIMBRA, PORTUGAL

Agradecimentos

Queria agradecer a todos os que, de uma forma ou outra, me ajudaram a chegar até aqui e a concluir esta etapa.

Em primeiro lugar, ao Professor Luís Almeida por me ter dado esta oportunidade, pela maneira fantástica como sempre me recebeu no grupo e por todas as palavras de incentivo.

Ao Rui, um agradecimento enorme por me ter deixado entrar neste projecto, que apesar de muito desafiante, me fascinou desde o primeiro dia. Obrigada pela disponibilidade, paciência, por tudo o que me ensinaste e pelo optimismo e entusiasmo que me foste sempre transmitindo.

A todos os membros do grupo, obrigada pela simpatia e boa disposição, mas também por todas as vezes que me ajudaram e tiraram dúvidas. Aprendi muito ao trabalhar convosco. Agradeço também ao João, ao Marco, à Sandra e à Adriana, que me deram uma ajuda essencial ao longo do ano. Queria ainda fazer um agradecimento especial às pessoas que participaram directamente no projecto, principalmente à Clelia, Susana, Sara, Luísa Cortes e Margarida Caldeira. E um grande obrigada à Magda, que este ano foi como uma segunda orientadora e me puxou para cima sempre que precisei.

Queria também agradecer ao Professor Miguel Sena Esteves, pela forma fantástica como me recebeu no laboratório em Worcester. Foi uma experiência muito enriquecedora, que me fez crescer como cientista.

Gostava ainda de agradecer aos professores que no primeiro ano de mestrado me ensinaram imenso, orientaram e transmitiram este gosto pela investigação. A todos os meus colegas e amigos de BCM, obrigada por estes dois anos, sei que me percebem melhor que ninguém. Um beijinho enorme para as "princesas de BCM": obrigada por me fazerem rir quando estou mais triste e por terem partilhado comigo os melhores momentos destes últimos dois anos. Finalmente, queria deixar um agradecimento especial à Laetitia, à Rafi e ao Johnny por todas as vezes que ficaram comigo no laboratório até tarde, me ajudaram a resolver os dilemas da tese e especialmente pelo apoio nesta fase final de escrita. E ainda à Madalena (a minha coleguinha de mesa) e à Marta por me ajudarem nos momentos mais complicados. O trabalho custa muito menos quando podemos contar com amigos assim!

Quero também agradecer aos meus "amigos de sempre" e aos que tive a sorte de encontrar pelo caminho, em Farmácia e Bioquímica, por me terem apoiado não só este ano, mas em todo o meu percurso até aqui.

Por fim, um agradecimento muito especial à minha família, especialmente aos meus pais e irmãs, que sempre acreditaram em mim e que todos os dias me dão força e confiança. Sem vocês nada disto seria possível.

Abbreviations

A.U. - Arbitrary units
AAV - Adeno-associated virus
ATXN-3 – Ataxin-3
BBB - Blood-brain barrier
bp – Base pair
CAG - Cytosine-Adenine-Guanine
cDNA- Complementary DNA
CMV- Cytomegalovirus
CNS - Central Nervous System
CP - Choroid plexus
CSF- Cerebrospinal fluid
DCN - Deep cerebellar nuclei
DMEM - Dulbecco's modified Eagle's medium supplemented
DUB – Deubiquitinating enzyme
EV - Extracellular vesicles
GAPDH - Glyceraldehyde 3-phosphate dehydrogenase
HA - Haemagglutinin
HD - Huntington's disease
HPRT - Hypoxanthine guanine phosphoribosyl transferase
IV - Intravenous
kb - kilobase
LV-Lentivirus
LV-Mut-ATXN3 - Lentiviral vectors encoding for human mutant ataxin-3
LV-WT-ATXN3 - Lentiviral vectors encoding for human wild-type ataxin-3
miR-ATXN3 – microRNA targeting mutant ataxin-3
miR-Control- microRNA Control
miRNA/miR- microRNA
MJD - Machado- Joseph disease
mRNA - Messenger RNA
Mut - Mutant
Mut-ATXN3 Mutant ataxin-3
NES - Nuclear export signal
Neuro2a - Mouse neural crest-derived cell line
NHP - Non-human primates
NIIs – Neuronal intranuclear inclusions
NLS - Nuclear localization signal
P(n) – Postnatal day (n)
PBS - Phosphate-buffered saline
PC - Purkinje cell
PCR - Polymerase chain reaction
PEI - Polyethyleneimine
polyQ - Polyglutamine
pre-miRNAs - Precursor-microRNAs
pri-miRNAs - Primary-microRNAs
qPCR - quantitative real-time PCR
rAAV – recombinant AAV
rAAV9 – recombinant adeno-associated virus serotype 9
rAAV9-miR-ATXN3 – recombinant AAV9 vectors encoding miR-ATXN3
RISC - RNA-induced silencing complex
RNAi - RNA interference
SCA - Spinocerebellar ataxia
SCA3 - Spinocerebellar ataxia type 3
SEM - Standard error of the mean
sh-ATXN3 – shRNA targeting ataxin-3
shRNA - short hairpin RNA
siRNA– small interfering RNA
SNP - Single nucleotide polymorphism
Ub- Ubiquitin
UIM - Ubiquitin interacting motifs
UPS - Ubiquitin-proteasome system
vg – viral genome
WT - Wild-type

Abstract

Machado-Joseph disease (MJD) is a dominant autosomal neurodegenerative disorder characterized by cerebellar dysfunction and loss of motor coordination. This disorder, which corresponds to the most common type of spinocerebellar ataxia worldwide, is caused by a CAG expansion in the coding region of the *MJD1/ATXN3* gene. This mutation is translated into a toxic polyglutamine tract within ataxin-3, which triggers multiple pathogenic mechanisms, ultimately leading to neurodegeneration in several brain regions. The lack of available treatment for MJD encourages further investigation towards possible therapeutic approaches.

One of the most direct, specific and effective solutions to correct MJD would be to inhibit mutant ataxin-3 expression using RNA interference (RNAi), thus targeting the initial cause of the disorder. Several studies have already investigated the impact of mutant ataxin-3 silencing in MJD rodent models, through direct administration of viral vectors into the brain parenchyma. This invasive procedure is associated with potential adverse effects and a limited vector distribution in the brain. As a result, a possible translation to human patients would benefit from a non-invasive delivery system, capable of inducing a widespread therapeutic effect throughout the CNS. Therefore, the main goal of this project was to develop a non-invasive viral-based gene therapy for MJD.

For that purpose, we selected rAAV9 (recombinant adeno-associated virus serotype 9) as the RNAi delivery vector, since this serotype is able to cross the blood-brain barrier (BBB) and efficiently transduce neurons. Moreover, this viral vector mediates a long-term transgene expression and exhibits a good safety profile, being particularly suitable for CNS gene therapy. Taking all of this into account, we developed an AAV9-mediated system encoding an artificial microRNA against mutant ataxin-3 (rAAV9-miR-ATXN3) and test its therapeutic impact in a transgenic mouse model of MJD.

Our first task consisted on the validation of this artificial miR sequence in a neuronal cell line. We concluded that miR-ATXN3 mediates an efficient and allele-specific silencing of mutant ataxin-3, providing confidence to studies *in vivo.*

Next, we analyzed the therapeutic potential of rAAV9-miR-ATXN3 vectors in a severely-impaired MJD transgenic mouse model following intravenous (IV) injection at postnatal day 1. Importantly, viral vectors were found to efficiently cross the BBB and transduce neurons throughout the brain of transgenic mice. Moreover, rAAV9 transduction was detected in Purkinje cells, the neuronal population that expresses mutant ataxin-3 in this particular model.

Subsequently, we assessed the effects of rAAV9-miR-ATXN3 administration in the behavioral performance of MJD transgenic mice. Noteworthy, this treatment successfully alleviated gait, balance and motor coordination impairments. Finally, we also observed a significant amelioration of neuropathological changes in the cerebellum. Accordingly, rAAV9-miR-ATXN3 treated animals exhibited a reduction in the number of mutant ataxin-3 aggregates, as well as a preservation of molecular layer thickness.

Altogether, our results indicate that mutant ataxin-3 silencing through a single AAV9 intravenous injection is an efficient therapeutic approach, alleviating both behavioral and neuropathological impairments. Importantly, our work constitutes the first report of long-term ataxin-3 silencing through a non-invasive viral system, supporting the use of this strategy for MJD therapy.

Keywords: Machado-Joseph disease (MJD), RNA interference (RNAi), Adeno-associated virus serotype 9 (AAV9), Systemic administration

Resumo

A doença de Machado-Joseph (DMJ) é uma doença neurodegenerativa autossómica dominante, caracterizada por disfunção cerebelar e perda de coordenação motora. Esta doença corresponde ao tipo mais comum de ataxia espinocerebelosa a nível mundial e deve-se a uma expansão do número de repetições CAG na região codificante do gene *MJD1/ATXN3*. Esta mutação traduz-se numa longa cadeia de poliglutaminas na proteína ataxina-3, o que induz diversos mecanismos patogénicos, causando morte neuronal em várias regiões cerebrais. Neste momento não existe nenhuma terapia disponível para a DMJ.

A inibição da expressão da ataxina-3 mutante usando RNA de interferência é uma potencial estratégia terapêutica capaz de corrigir a causa inicial da doença, de uma forma directa, específica e eficaz. Vários estudos investigaram anteriormente o impacto desta estratégia de silenciamento em modelos animais da DMJ, com resultados promissores. No entanto, estas experiências envolveram a administração de vectores virais através de uma injecção intracraniana, ou seja, um procedimento invasivo e associado a efeitos secundários. Além disso, este tipo de administração leva a uma dispersão reduzida dos vectores virais no cérebro. Consequentemente, a opção ideal para facilitar futuras aplicações clínicas seria uma via de administração não invasiva, capaz de induzir um efeito terapêutico em todo o Sistema Nervoso Central. Assim sendo, este projecto teve como principal objectivo desenvolver uma estratégia viral não invasiva capaz de induzir o silenciamento da ataxina-3 mutante, como possível terapia para a DMJ.

Para atingir este objectivo, seleccionámos o AAV9 (virus adeno-associado do tipo sérico 9) como vector de entrega da sequência de silenciamento, visto que tem a capacidade de atravessar a barreira hemato-encefálica e transduzir neurónios de forma eficaz. Além disso, este vírus induz a expressão dos transgenes durante largos períodos de tempo, sem induzir toxicidade. Neste sentido, desenvolvemos um sistema baseado no AAV9 capaz de codificar um microRNA artificial específico para a ataxina-3 mutante (rAAV9-miR-ATXN3) e testámos o seu efeito terapêutico num modelo transgénico da DMJ.

Em primeiro lugar, validámos a sequência miR-ATXN3 numa linha celular neuronal, sendo que verificámos um silenciamento eficaz e específico para a forma mutante da ataxina-3. Estes resultados permitiram prosseguir para estudos num modelo animal da doença. Neste contexto, testámos o efeito terapêutico dos vectores rAAV9-miR-ATXN3 em murganhos transgénicos, que receberam uma injeção intravenosa 1 dia após o nascimento. Ao analisar a distribuição do vector, concluímos que ocorreu uma transdução neuronal eficaz em várias regiões do cérebro. De seguida, focámo-nos no cerebelo e em particular nas células de Purkinje, visto que apenas esta população neuronal expressa a ataxina-3 mutante neste modelo. As células de Purkinje mostraram níveis significativos de transdução, indicando que o vector consegue aceder ao nosso principal alvo terapêutico. Consequentemente, avaliámos o efeito desta estratégia no comportamento dos murganhos tratados, sendo que observámos melhorias na coordenação motora e equilíbrio. Além disso, o tratamento permitiu atenuar a neuropatologia no cerebelo, nomeadamente ao reduzir o número de agregados e levando a uma preservação da espessura da camada molecular.

Em conclusão, os resultados obtidos após uma única injeção intravenosa de vectores AAV9 indicam que esta é uma estratégia terapêutica eficaz, capaz de atenuar os problemas motores, bem como a neuropatologia. É importante salientar que este foi o primeiro estudo em que se obteve um silenciamento da ataxina-3 mutante a longo prazo e através de uma administração não invasiva, constuindo por isso uma estratégia muito promissora para a terapia da DMJ.

Palavras-chave: Doença de Machado-Joseph (DMJ), RNA de interferência (RNAi), Vírus adeno-associado do tipo sérico 9 (AAV9), Administração sistémica

1. Introduction

1.1. Machado-Joseph Disease

Machado-Joseph Disease (MJD), also known as Spinocerebellar Ataxia type 3 (SCA3) is a dominant autosomal neurodegenerative disorder. It corresponds to the most common type of spinocerebellar ataxia worldwide (Schols et al., 2004), a group of genetically inherited diseases characterized by progressive cerebellar dysfunction and lack of motor coordination (reviewed in (Seidel et al., 2012)). Similarly to other SCAs, MJD is a late-onset and ultimately fatal disease, whose main symptoms include gait and limb ataxia, as well as balance, speech, swallowing and visual impairments (Taroni and DiDonato, 2004). Firstly described among individuals of Azorean descent (Nakano et al., 1972), this hereditary ataxia is now known to exist worldwide.

The genetic cause of MJD is well described, corresponding to a CAG expansion in the coding region of *MJD1*, identified as the causative gene (Kawaguchi et al., 1994). Consequently, this mutation results in a long polyglutamine tract in the *MJD1*-enconded protein: ataxin-3, leading to a toxic gain of function (Ikeda et al., 1996). As a result, MJD is considered a polyglutamine (polyQ) disorder, sharing important features with this group of neurologic diseases, characterized by an accumulation of aggregates in neurons and a selective neurodegeneration in certain brain regions (reviewed in (Shao and Diamond, 2007). Accordingly, mutant ataxin-3 presents a high propensity to misfold, oligomerize, and form intracellular inclusions, constituting a major MJD hallmark (Paulson et al., 1997). Moreover, the disorder is characterized by neurodegeneration in particular brain regions, including: cerebellum, brainstem, substantia nigra, pontine nuclei and striatum (Rub et al., 2008). A better understanding of MJD pathogenic mechanisms, as well as the development of new therapeutic strategies would be crucial to come up with an effective treatment for this incurable, fatal disorder.

1.1.1. Clinical features

MJD/SCA3 is considered a late-onset fatal neurodegenerative disorder. The mean age of MJD onset is around 40 years, with extremes of 4 and 70 years (Bettencourt and Lima, 2011). Due to disease progression, MJD patients normally become dependent on wheel chairs, bedridden and ultimately present premature death, with a mean survival time after disease onset of 21 years (Kieling et al., 2007).

MJD is considered a rare disorder, whose prevalence exhibits significant geographical and ethnic variations. The highest prevalence has been found in the Azores (Flores Island (1/2390)), followed by a small area of the Tagus River Valley (1/1,000), both in Portugal. Intermediate prevalence rates have been described in Portugal, Germany, the Netherlands, China and Japan (Bettencourt and Lima, 2011).

MJD is a multisystem neurodegenerative disorder, mainly affecting: i) the cerebellum, which is important for motor control; ii) the pyramidal and extrapyramidal systems, two motor pathways

related to fine movements and posture/locomotion, respectively; and iii) the oculomotor system (Coutinho and Andrade, 1978; Rub et al., 2008).

Therefore, most symptoms are caused by progressive ataxia, i.e. a lack of motor coordination that can affect gait, balance, gaze and speech. Accordingly, MJD patients exhibit: i) an ataxic gait, i.e. an unsteady and uncoordinated walk, ii) postural instability, iii) dystonia (sustained muscle contractions), iv) dysphagia (difficulties in swallowing), v) dysarthria (speech problems) and vi) amyotrophy (progressive wasting of muscle tissue) (Burk et al., 1996; Durr et al., 1996; Rub et al., 2008). In some cases, Parkinsonism is also observed, being characterized by bradykinesia (slowness of movement) and rigidity (Bettencourt et al., 2011). Moreover, common symptoms affecting the oculomotor system include: ophthalmoplegia (paralysis or weakness of the eye muscles), diploplia (double vision), bulging eyes and nystagmus (involuntary eye movements) (Gordon et al., 2003; Shimizu et al., 1990). Interestingly, non-motor symptoms have also been described, including sleep disorders, cognitive and psychiatric disturbances, as well as olfactory dysfunction, as reviewed by (Pedroso et al., 2013).

The fact that MJD is caused by dynamic repeat expansions explains its phenotypic heterogeneity (Subramony and Currier, 1996). Therefore, five different subtypes have been described, based on the age of onset and the presence/absence of extrapyramidal and peripheral signs (reviewed in (Bettencourt and Lima, 2011)). Type 2 is the most common MJD subtype, caused by midrange expansions and thus beginning during mid adult years. This subtype is characterized by cerebellar ataxia, progressive external ophthalmoplegia and pyramidal signs (Rosenberg, 1992).

Currently, MJD diagnosis is based on clinical features, family history and genetic testing. However, no efficient therapy has been found for this progressive neurodegenerative disorder up to now. Although incurable, MJD might benefit from symptomatic pharmacological treatments, namely for: dystonia, muscle cramps, Parkinsonism, depression and sleep disturbances. Moreover, physiotherapy and speech therapy might be helpful to attenuate some MJD symptoms (D'Abreu et al., 2010).

1.1.2. Ataxin-3: from gene to protein

MJD1 gene

MJD1/ATXN3, identified as the MJD causative gene, is located on chromosome 14q32.1, spanning about 48 kilobases (kb), with a total of 11 exons (Ichikawa et al., 2001). This gene encodes ataxin-3, a polyubiquitin-binding protein involved in ubiquitin-mediated proteolysis (Burnett et al., 2003). MJD is caused by an unstable expansion of *MJD1* CAG tract present in exon 10, resulting in a mutant form of ataxin-3, with a long polyglutamine stretch at the C-terminus (Ikeda et al., 1996), as illustrated in Figure 1.1. Similarly to the other polyQ disorders, disease will only develop when the (CAG) repeat size exceeds a specific threshold length. In the case of MJD, normal population exhibits 10 to 51 trinucleotide repeats, whereas expansions from 55 to 87 CAGs are present in MJD patients (Gu et al., 2004; Maciel et al., 2001).

Noteworthy, four MJD haplotypes have been found, based on the presence of three distinct intragenic single base pair polymorphisms (SNPs) (Gaspar et al., 2001). In particular, the SNP C987GG/G987GG (rs12895357), which is located immediately after the CAG repeat (Figure 1.1A), is present in 70% of MJD patients and has been investigated as a target for allele-specific silencing (Alves et al., 2008a).

As described for this disorder family, larger CAG expansions are associated with an earlier disease onset and an increased disease severity in MJD, leading to a strong correlation between genotype and phenotype (Maciel et al., 1995). Intergenerational instability of the CAG repeat has been reported in MJD families, since expansions tend to increase in size in successive generations. As a consequence, affected offspring normally present more severe phenotypes and earlier onset ages, a phenomenon known as anticipation (Takiyama et al., 1995). Furthermore, this dynamic feature of the disease-causing mutation may also explain the somatic mosaicism, i.e. differences in CAG length in different cell populations. Although this event can occur in the brain, there is no correlation between large repeats and affected brain regions (Cancel et al., 1998).

The great majority of MJD patients are heterozygous, but extremely rare cases of homozygosity have been reported. Importantly, homozygous patients were found to have earlier disease onset and more severe phenotypes (Carvalho et al., 2008; Zeng et al., 2015). These reports suggest a gene dosage effect, consistent with studies in mice models (Cemal et al., 2002; Goti et al., 2004). Moreover, most patients present a positive family history, with no reported cases of *de novo* mutations and sporadic cases (Paulson, 2012).

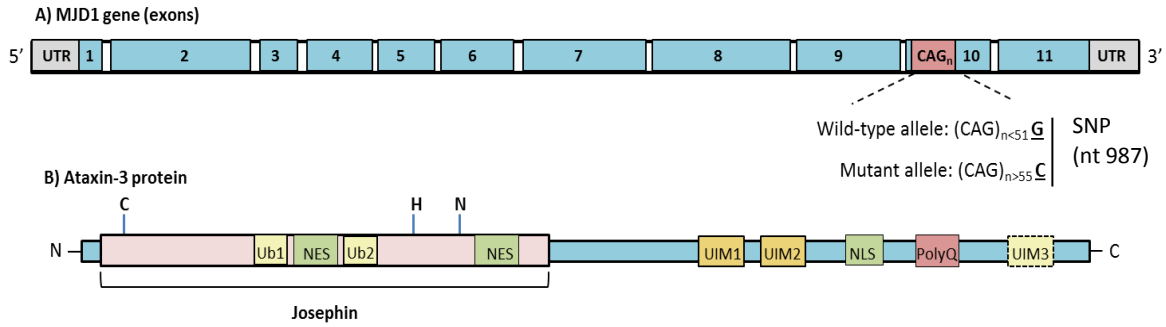

Figure 1.1: Schematic representation of the *MJD1* gene and ataxin-3 protein. A) *MJD1* gene is composed by 11 exons (represented in blue). The CAG repeat is located on exon 10 and MJD is caused by more than 55 repetitions. A SNP was identified immediately after the CAG expansion (nucleotide 987). Normal alleles exhibit a guanine (G) in this position, whereas mutant alleles present a cytosine (C) in 70% of MJD patients (Gaspar et al., 2001).B) Ataxin-3 is composed by an N-terminal Josephin domain (JD), followed by the C-terminal tail. JD displays deubiquitinase function (due to cysteine 14 (C), histidine 119 (H), and asparagine 134 (N), two nuclear export signals (NES) and two ubiquitin binding sites (Ub1 and Ub2). The C tail contains two ubiquitin interacting motifs (UIM), a nuclear localization signal (NLS) and the polyglutamine (polyQ) repeat. Depending on the isoform, a third UIM may exist following the polyQ tract.

Ataxin-3 protein

The *MJD1/ATXN3* gene encodes ataxin-3 (ATXN3), a 42 kilodalton (kDa) soluble protein with deubiquitinase activity, ubiquitously expressed in different body tissues and cell types (Ichikawa et al., 2001). The mechanisms underlying specificity for neuronal vulnerability remain enigmatic. Harris and collaborators. have shown that splicing events might influence ataxin-3 propensity to aggregate and degradation, possibly contributing to selective neuronal toxicity in different brain regions (Harris et al., 2010). Alternatively, specific post-translational events might be crucial for pathogenesis (e.g. phosphorylation, SUMOylation, proteolytic cleavage) (reviewed in (Pennuto et al., 2009)).

- **Structure**

Ataxin-3 is essentially composed by: i) a structured globular N-terminal Josephin domain, which displays catalytic functions and two nuclear export signals (NES), followed by: ii) a flexible C-terminal tail containing two ubiquitin interacting motifs (UIM), a nuclear localization signal (NLS) and the polyglutamine (polyQ) repeat (Albrecht et al., 2004; Masino et al., 2003), as depicted in Figure 1.1B. This polyQ tract is predicted to stabilize protein interactions through coiled-coil regions (Schaefer et al., 2012). Among the 20 possible ataxin-3 isoforms identified so far (Bettencourt et al., 2010), only two have been fully characterized. The predominant isoform in the brain exhibits an additional UIM following the polyQ tract. (Goto et al., 1997; Schmidt et al., 1998).

- **Localization**

Considering intracellular localization, ataxin-3 has been found both in the cytoplasm, nucleus and mitochondria (Pozzi et al., 2008). While in normal conditions ataxin-3 is predominantly cytoplasmatic, the protein tends to accumulate in the nucleus in MJD affected neurons (Schmidt et al., 1998). Subcellular distribution is determined by intrinsic localization signals and posttranslational modifications. Although the NLS was predicted to influence ataxin-3 shutting to the nucleus, this sequence exhibits a weak nuclear import activity *in vitro* (Antony et al., 2009). In contrast, the protein region constituted by the first 27 amino acids was found to be essential for ataxin-3 nuclear localization (Pozzi et al., 2008). Moreover, phosphorylation of three specific serine residues (236, 340 and 352) has been reported to result in nuclear accumulation (Mueller et al., 2009). Considering ataxin-3 translocation from the nucleus to the cytoplasm, two NES show efficient nuclear export activity (Antony et al., 2009).

- **Cellular functions**

In what concerns cellular function, ataxin-3 has been described as a deubiquitinating enzyme (DUB), being responsible for ubiquitin chain removal from target proteins. Accordingly, the inhibition of ataxin-3 activity results in a marked accumulation of polyubiquitin proteins *in vitro* (Berke et al., 2005), similarly to what occurs in ataxin-3 knock-out mice (Schmitt et al., 2007). The Josephin Domain, which is responsible for the isopeptidase activity, contains a catalytic triad characteristic of cysteine proteases (C14, H119 and N134) (Nicastro et al., 2005), as illustrated in Figure 1.1B. The UIMs located at the C-terminal are essential for ataxin-3-ubiquitin (Ub) binding and the selective cleavage of long and complex ubiquitin chains. (Winborn et al., 2008). Moreover, two ubiquitin-binding sites, which have been identified on the Josephin Domain (Figure 1.1B), have shown an important role in DUB activity (ub-binding site 1) and specific linkage recognition (Ub-binding site 2) (Nicastro et al., 2010). In conclusion, all these functional units act in a cooperative manner in ataxin-3 deubiquitinating reaction (Mao et al., 2005). As a result, ataxin-3 is able to cleave excessively long or branched Ub chains on substrates destined for degradation, potentially contributing to their successful delivery of to the proteasome.

Mounting evidence suggests that ataxin-3 is involved in several important cellular mechanisms (reviewed in (Matos et al., 2011), such as: i) protein quality control pathways, including the ubiquitin-proteasome system (UPS) (Doss-Pepe et al., 2003), endoplasmatic-reticulum-associated degradation (ERAD) (Zhong and Pittman, 2006), and aggresome formation (Bonanomi et al., 2014); ii) transcription regulation, by interacting with transcription factors and through histone binding (Li et al., 2002); iii) cytoskeleton organization (Rodrigues et al., 2010).

1.1.3. Neuropathological changes and major hallmarks of the disease

MJD neurodegeneration profile involves neuronal loss in selective regions of the central nervous system (CNS), including: i) the cerebellum (spinocerebellar pathways, Purkinje cell layer and dentate nucleus), ii) brainstem (pons and medulla), iii) substantia nigra, iv) striatum, v) thalamus, vi) spinal cord (particularly Clarke's column nuclei and anterior horn) and v) cranial nerves (Figure 1.2). In the brainstem, the pontine and vestibular nuclei are especially affected. Additionally, systems associated with visual, auditory, vestibular, somatosensory, ingestion and urination abilities are also damaged in the disease (Durr et al., 1996; Rub et al., 2008; Scherzed et al., 2012). Accordingly, magnetic resonance imaging studies in MJD patients have detected a severe atrophy in the brainstem and cerebellum, as well as other brain regions (Liang et al., 2009), (D'Abreu et al., 2012).

One of the major hallmarks of MJD is the accumulation of mutant-ataxin3 inclusions in several brain regions (Paulson et al., 1997). These insoluble aggregates consist of ubiquitin-positive spheres of one to several microns in diameter containing the disease protein and other cellular factors. Normally located in the neuronal nucleus, inclusions are particularly abundant in pontine neurons but have also been observed in other brainstem neuronal populations, thalamus,

substantia nigra and striatum (Hayashi et al., 2003; Yamada et al., 2004). Interestingly, neuronal intranuclear inclusions (NII) have also been detected in brain regions normally spared in MJD, including the cerebral cortex, subthalamic nucleus and raphe nuclei (Yamada et al., 2001; Yamada et al., 2004). This lack of correlation suggests that ataxin-3 immunopositive NII are not immediately decisive for the fate of affected nerve cells but rather represent markers of MJD (Rub et al., 2006).

Moreover, Seidel et al. have described the presence of axonal inclusions in several fiber tracts associated with the oculomotor and motor coordination pathways, which are known to undergo neurodegeneration in MJD (Seidel et al., 2010).

Other MJD-associated neuropathological signs include: deficits in glucose utilization in the cerebellum, brainstem and cerebral cortex (Soong and Liu, 1998), metabolic abnormalities suggestive of axonal dysfunction (D'Abreu et al., 2009), myelin loss and reactive astrogliosis in several brain regions (Rub et al., 2013).

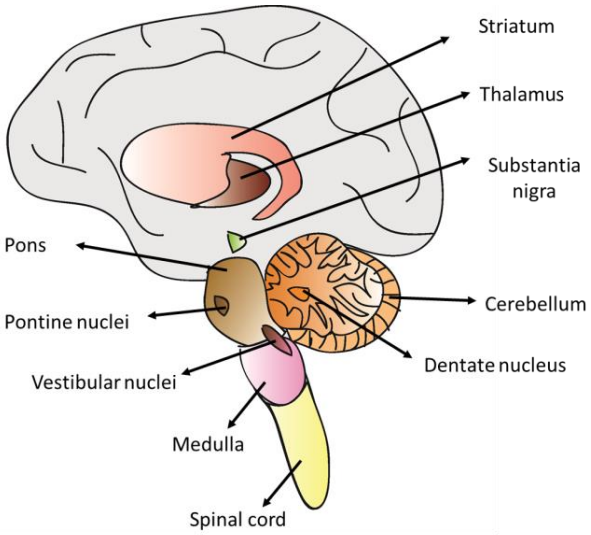

Figure 1.2: Distribution of neuronal loss in the CNS of MJD patients. Schematic representation of the principal sites of neurodegeneration in MJD: cerebellum, brainstem (pons and medulla), substantia nigra, thalamus and striatum. In the brainstem, vestibular and pontine nuclei are particularly affected.

1.1.4. Pathogenesis of MJD

Protein toxicity

In MJD, polyQ expansion induces a conformational modification in ataxin-3, consequently increasing its propensity to aggregate (Nagai et al., 2007) and affecting its stability, localization, and interactions. Altogether, these alterations culminate in cellular dysfunction and neuronal death.

Similarly to other PolyQ disorders, one major hallmark of MJD is the accumulation of intracellular aggregates containing the pathogenic protein. In particular, MJD patients' brains present mainly neuronal intranuclear inclusions, as previously described. Several observations indicate that the nucleus is the main site of mutant ataxin-3 toxicity (Bichelmeier et al., 2007), due to a less efficient

degradation of the protein in this compartment, when compared to the cytoplasm (Breuer et al., 2010). The manipulation of subcellular localization has shown to influence ataxin-3 pathogenic action (Bichelmeier et al., 2007). Moreover, MJD patients also exhibit cytoplasmic inclusions in neurons (Yamada et al., 2004), as well as axonal aggregates in fiber tracts (Seidel et al., 2010). According to *in vivo* studies, disease progression is characterized by an increase in aggregate formation, accompanied by a decrease in soluble mutant ataxin-3 protein in the cerebellum (Nguyen et al., 2013).

Besides mutant ataxin-3, these inclusions contain several cellular components, such as: proteasome constituents, ubiquitin, molecular chaperones, transcription factors, Ub-binding proteins and other polyQ proteins, including normal ataxin-3 (Chai et al., 2002; Donaldson et al., 2003; Schmidt et al., 2002; Uchihara et al., 2001). This sequestration effect might be toxic for the cell, by disturbing quality control systems, altering transcription patterns and inhibiting the cellular function of certain proteins (Yang et al., 2014b).

Nevertheless, there is no clear consensus regarding the contribution of nuclear inclusions to MJD-associated neurotoxicity. Noteworthy, some authors consider this aggregation process as a protective cellular mechanism to cope with expanded proteins instead of a pathogenic event. Accordingly, nuclear inclusion distribution throughout the brain fails to show a correlation with regions of degeneration (Rub et al., 2006; Uchihara et al., 2002). Moreover, one particular *in vitro* study reported less neuronal death in cells exhibiting polyQ inclusions, highlighting their possible neuroprotective role (Arrasate et al., 2004). However, what might work as an adaptive response in the beginning could turn into a 'snowball effect', leading to the recruitment and dysfunction of increasingly more cellular components. In fact, the aggregation process might work as a vicious cycle in which mutant ataxin-3 compromises the cellular systems that are designed to defend cells from polyQ expanded proteins.

Alternatively, soluble amyloid oligomers and ataxin-3 monomers might act as the predominant toxic species in MJD. PolyQ oligomers were found to be cytotoxic *in vitro* (Takahashi et al., 2008), possibly through membrane destabilization or sequestration of important cellular components, similarly to what has been described for aggregates (Hands and Wyttenbach, 2010). On the other hand, the proteolytic cleavage of mutant ataxin-3 has also been suggested as an important pathogenic mechanism in MJD. This 'toxic fragment hypothesis' has been corroborated by the presence of C-terminal fragments in both cellular and animal models, showing an association with enhanced aggregation and toxicity (Colomer Gould et al., 2007). Importantly, the same fragments have been detected in MJD patients, particularly in brain-affected regions (Goti et al., 2004). This proteolytic cleavage might be catalyzed by caspases or calpains (Berke et al., 2004; Hubener et al., 2013). Interestingly, calpain-mediated ataxin-3 cleavage might possibly explain neuronal vulnerability to MJD pathology. According to *in vitro* findings, excitation-mediated calcium influx, an event characteristic of this cellular type, is required for ataxin-3 cleavage by calpains and subsequent aggregation (Koch et al., 2011). The neurotoxic effect of these C-terminal fragments might be related to: i) their marked accumulation in the nucleus (Goti et al., 2004), since they lack the nuclear export signals located in the Josephin Domain. As a consequence, they are able to

escape from cytoplasmatic clearance mechanisms, including chaperones and the UPS; ii) a possible enhancement in their ability to form toxic oligomers or disturb ataxin-3 normal function and interactions (Haacke et al., 2006). Another hypothesis relates to a possible neuroprotective role of ataxin-3 Josephin Domain (Warrick et al., 2005), which would be eliminated with proteolytic cleavage.

In conclusion, mutant ataxin-3 toxic gain of function might be explained by its propensity to aggregate, to be proteolytically cleaved and generate toxic fragments and by its aberrant interaction with normal partners. Altogether, these events might compromise important cellular functions (reviewed in (Evers et al., 2014)), such as: i) protein clearance systems, including the UPS (Schmidt et al., 2002) and autophagy (Nascimento-Ferreira et al., 2011; Onofre et al., 2016), thus leading to the accumulation of misfolded proteins; ii) transcriptional regulation, leading the abnormal expression of several genes (Chou et al., 2008; Evert et al., 2006) ; iii) axonal transport, due to the accumulation of ataxin-3 aggregates; iv) intracellular Ca^{2+} homeostasis (Chen et al., 2008); and v) mitochondrial function (Laco et al., 2012; Ramos et al., 2015) (Figure 1.3).

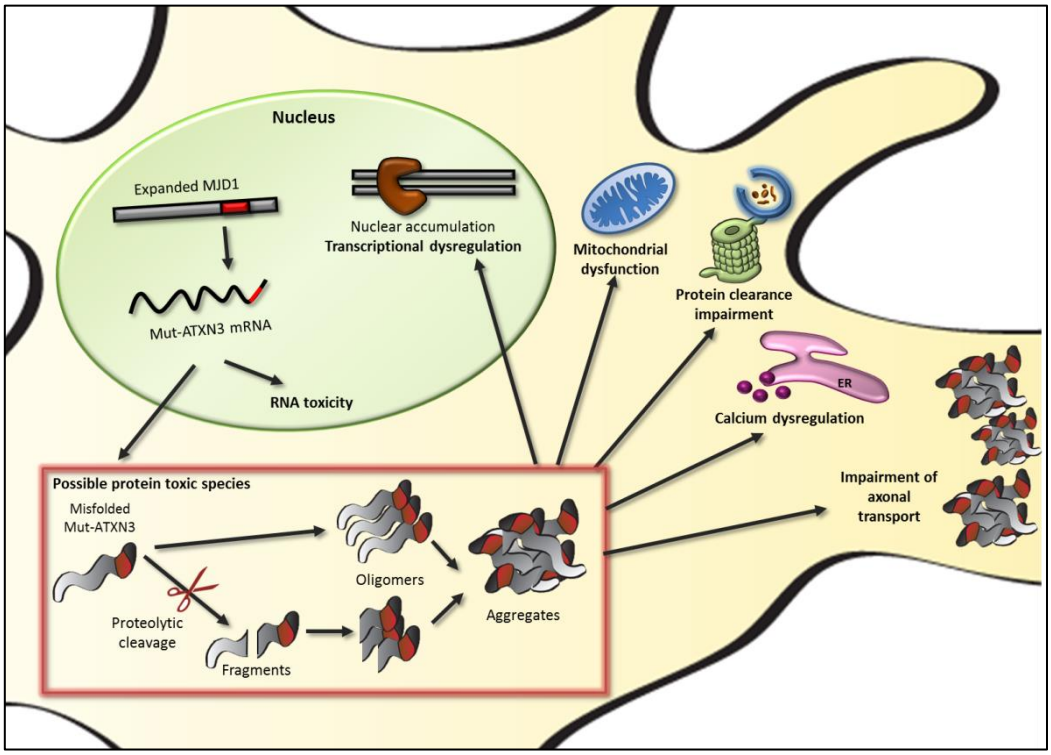

Figure 1.3: Schematic representation of possible pathogenic mechanisms in MJD. In the nucleus, the expanded MJD1 gene with CAG repeats in red is transcribed into mutant-ataxin-3 (Mut-ATXN3) mRNA, which may itself contribute to toxicity. Then, this transcript originates a mutant form of ataxin-3, with a polyglutamine tract (in red), which is prone to misfolding and can be proteolytically cleaved, giving rise to C-terminal fragments. Full-length and cleaved forms of ataxin-3 originates soluble monomers, oligomers or large insoluble aggregates. All these species (red box) might cause toxicity by different mechanisms: impairment of protein clearance systems, compromised axonal transport, dysregulation of calcium homeostasis and mitochondrial dysfunction. When translocated to the nucleus, these toxic species can also induce transcriptional alterations. All of these events contribute to neuronal dysfunction and degeneration.

RNA toxicity

Increasing evidence indicates that the pathogenic effects in PolyQ disorders are not uniquely caused by misfolded proteins, but also by the CAG expanded RNA. In fact, some CAG repeat diseases are caused by expansions on untranslated regions (e.g. SCA12), validating this hypothesis (Holmes et al., 1999).

This question was firstly addressed when Li et al. have described RNA toxicity as a major contributor to neurodegeneration in a MJD *Drosophila* model. The authors tested the expression of an untranslated CAG repeat of pathogenic length in neurons, having observed significant degeneration and ultimately death (Li et al., 2008). Subsequently, experiments in *C. elegans* and transgenic mice supported this conclusion, since untranslated CAGs repeats proved to be toxic, causing behavioral deficits (Hsu et al., 2011; Wang et al., 2011).

Following these reports, further investigation has been focusing on the RNA pathogenic mechanisms. *In silico* and *in vitro* experiments have shown that CAG-containing mRNAs form a hairpin structure, whose stability increases with CAG repeat number (de Mezer et al., 2011; Sobczak and Krzyzosiak, 2005). Concerning the mechanisms behind RNA-mediated toxicity, numerous hypotheses have been proposed including: i) the sequestration of important cellular molecules; ii) silencing of CTG repeat-containing mRNAs, iii) translational dysregulation of polyCAG mRNAs (reviewed in (Nalavade et al., 2013)).

The most well-studied mechanism consists on the recruitment of Muscleblind (MBNL1), a protein involved in alternative splicing of specific mRNAs. According to several reports, CAG expanded transcripts are able to sequester this protein and induce splicing defects (Mykowska et al., 2011; Wang et al., 2011). Very recently, Sathasivam et al. have demonstrated that aberrant splicing might affect the disease causing gene itself, consequently generating a pathogenic protein fragment, as reported for Huntigton's Disease (Sathasivam et al., 2013). Moreover, the sequestration of another factor: nucleolin might affect ribosome formation, consequently causing apoptosis (Tsoi et al., 2012).

On the other hand, hairpins generated from RNAs with expanded CAG repeats resemble double stranded RNA structures, possibly being cleaved by Dicer. Consequently, the resulting short RNA molecules might target complementary transcripts and downregulate CTG repeat-containing genes, as already reported in Huntington cellular models (Banez-Coronel et al., 2012). Finally, RNA toxicity might also be explained by an increase in the translation of expanded CAG repeat mRNAs (Krauss et al., 2013), further aggravating pathology.

Altogether, these findings suggest that mutant mRNA might have a fundamental role in the pathogenesis of MJD and should be considered as a therapeutic target.

1.1.5. Rodent models of MJD

Animal models of MJD have been crucial to clarify disease pathogenesis and test therapeutic approaches. Several invertebrate models of ataxin-3 overexpression in *Drosophila* and *C. elegans* have provided important discoveries in the field and allowed the screening of potential therapeutic molecules and genetic modifiers of MJD (Teixeira-Castro et al., 2011; Warrick et al., 2005). However, rodent models have been the elected ones for preclinical studies.

The great majority of MJD rodent models consist of transgenic animals expressing human mutant ataxin-3. For most of them, the transgene corresponds to a complementary DNA (cDNA) encoding a particular isoform of ataxin-3 under the control of a foreign promoter. They mostly differ on: i) the number of CAG repetitions, ii) the selected promoter, iii) the copy number of integrated transgenes, and iv) the transgene *per se*, which might correspond to full length or truncated ataxin-3.

Distinct models are based on the expression of full-length mutant ataxin-3 selectively in the CNS, triggered by the mouse prion protein or rat huntingtin promoter, ultimately causing aggregate accumulation throughout the mouse brain and motor impairments (Bichelmeier et al., 2007; Boy et al., 2010; Chou et al., 2008; Goti et al., 2004). Alternatively, Silva-Fernandes and collaborators aimed to mimic ataxin-3 ubiquitous distribution by using the cytomegalovirus (CMV) promoter, consequently inducing motor deficits and inclusion formation (in the CMVMJD135 mouse model) (Silva-Fernandes et al., 2010; Silva-Fernandes et al., 2014). In conclusion, all these models are characterized by full-length mutant ataxin-3 expression in several brain regions, recapitulating important MJD features.

In contrast, the first-developed MJD model, established by Ikeda et al., explored the selective expression of a C-terminal fragment of mutant ataxin-3 with 79 CAG repeats (79Q-ataxin-3) in Purkinje cells. This successfully resulted in neurodegeneration and ataxic phenotype (Ikeda et al., 1996). Subsequently, the same group (Torashima et al., 2008) tested a similar approach, but decreasing the number of CAGs to 69. This truncated form of mutant ataxin-3, when expressed specifically in Purkinje cells due to the L7 promoter, induced a very severe phenotype. Accordingly, polyQ69 mice exhibited a marked accumulation of aggregates accompanied by atrophy in the cerebellum, as well as serious loss of motor coordination starting at an early age (3 weeks). This model has been extensively used in preclinical studies since it is time and cost-effective, while mimicking a late stage of disease. The main limitations of polyQ69 mice include: i) the restricted expression to a particular neuronal subtype and brain region and ii) the symptoms severity and early onset, which might hamper the therapeutic impact of some approaches.

The fact that all these models express a unique ataxin-3 isoform driven by an exogenous promoter has been considered a major drawback. Therefore, Cemal et al. used the MJD1 gene instead of a particular cDNA molecule to generate a novel MJD model (Cemal et al., 2002). The authors used yeast artificial chromosome (YAC) constructs carrying the full-length MJD1 gene with 84 CAGs (MJD84.2). Therefore, different ataxin-3 isoforms can be expressed under the control of the normal endogenous regulatory regions. Consequently, MJD84.2 mice exhibited neuropathological

and behavioral changes with an early onset (4 weeks), explaining the great potential of this model for preclinical studies.

On the other hand, the Tet-off model developed by Boy et al. has been useful to clarify the reversibility of MJD symptoms (Boy et al., 2009). This was the first conditional model for the disease and proved that switching off mutant ataxin-3 expression might revert MJD associated phenotype and pathology.

Alternatively, acute models of MJD have been particularly important to study disease pathogenesis in specific brain regions. In this context, lentiviral vectors encoding human mutant ataxin-3 have been injected in the striatum and cerebellum of rodents, leading to neuropathological changes and behavioral alterations (Alves et al., 2008b; Nobrega et al., 2013a).

Finally, the generation of knock-in models was an important addition to the collection of MJD models, as they represent a genetically and physiologically accurate model of the disease. Ramani et al. introduced a 82 CAG repeat expansion into the endogenous murine ataxin-3 (Atxn3) locus, resulting in aggregate accumulation in several brain regions, but no phenotypic alterations (Ramani et al., 2015). Additionally, Switonski et al. generated the first humanized knock-in model, by replacing the 3' fragment of mouse Atxn3 gene with the equivalent human coding sequence containing a 91 CAG expansion. This model presented ataxin-3 inclusions, neuroinflammation and degeneration, followed by late deficits in motor coordination (Switonski et al., 2015).

In conclusion, a high variety of MJD rodent models have been generated so far and contributed to important discoveries in the field (Table 1.1). While some are particularly useful to study disease pathogenesis, others display MJD characteristic symptoms, being extremely suitable to test therapeutic approaches.

Table 1.1: Summary of the principal MJD rodent models

Model type	Model name	Transgene	(CAG)n	Promoter (region)	Neuropathology	Phenotype (age)	Ref
Transgenic	Q71-B	Full-length cDNA (isoform 1a)	71	Mouse prion protein (CNS)	Intranuclear inclusions in pons, cerebellar nuclei, substantia nigra and spinal cord	Motor deficits (2-4 months), weight loss, premature death	(Goti et al., 2004)
	70.61 CAG	Full-length cDNA (isoform 3c)	70	Mouse prion protein (CNS)	Inclusion bodies in cortex, pons, hippocampus, cerebellar nuclei	Motor deficits (6-8weeks), premature death	(Bichelmeier et al., 2007)
	Ataxin-3-Q79	Full-length cDNA (isoform 1a)	79	Mouse prion protein (CNS)	Intranuclear inclusions in pontine and dentate neurons, substantia nigra	Motor deficits (5-6months)	(Chou et al., 2008)
	HDProm MJD148	Full-length cDNA (isoform 3c)	148	Rat huntingtin promoter (brain)	Small aggregates (25 months): brain stem, red nucleus, pontine nuclei and cerebellum; Degeneration of Purkinje cells	Motor deficits (1 year)	(Boy et al., 2010)
	CMVMJD94	Full-length cDNA (isoform 3c)	94	CMV (ubiquitous)	Neuronal atrophy and astrogliosis, no inclusions	Motor deficits (4 months)	(Silva-Fernandes et al., 2010)
	CMV MJD135	Full-length cDNA (isoform 3c)	135	CMV (ubiquitous)	Inclusions in several brain regions, including pontine and dentate nuclei.	Motor deficits (16 weeks), weight reduction	(Silva-Fernandes et al., 2014)
	MJD79	Truncated cDNA	79	L7 (purkinje cells)	Cerebellar atrophy	Motor deficits (4 weeks)	(Ikeda et al., 1996)
	polyQ69	Truncated cDNA	69	L7 (purkinje cells)	Aggregates in Purkinje cells and DCN; Cerebellum atrophy	Motor deficits (3 weeks)	(Torashima et al., 2008)
	MJD84.2 (YAC)	Full-length MJD1 gene	84	Endogenous	Intranuclear inclusions in Purkinje cells, pontine and dentate neurons; Neurodegeneration	Motor deficits (4 weeks)	(Cemal et al., 2002)
	PrP/MJD77 (Tet-off)	Full-length cDNA (isoform 3c)	77	Hamster prion (brain)	Inclusions in cerebral cortex	Motor deficits (2 months)	(Boy et al., 2009)
Lentiviral-induced	Striatal LV	Full-length cDNA (isoform 1a)	72	PGK in lentivirus	Neuronal inclusions in the site of injection (striatum or substantia nigra)	Parkinson-like dysfunction (after injection into substantia nigra)	(Alves et al., 2008b)
	Cerebellar LV	Full-length cDNA (isoform 1a)	72	PGK in lentivirus	Inclusions in the cerebellum (site of injection)	Motor deficits (1 month after injection)	(Nobrega et al., 2013a)
Knock-in	Atxn3Q82	Insertion of CAG expansion into Atxn3 locus	82	-	Aggregates in DCN, brain stem, hippocampus, cortex and striatum	No behavioral alterations	(Ramani et al., 2015)
	Ki91 (Humanized)	Replacement of 3' fragment with human sequence	91	-	Inclusions in the cerebellum, cortex and hippocampus; Neuroinflammation; cerebellar neurodegeneration	Motor incoordination at a late stage (90 weeks)	(Switonski et al., 2015)

(CAG)n –number of CAG repeats; CMV – cytomegalovirus; PGK- phosphoglycerate kinase 1; CNS – Central Nervous System; DCN- deep cerebellar nuclei

1.1.6. Therapeutic strategies

The increasingly knowledge of MJD-associated pathogenic mechanisms (see Figure 1.3) has contributed to the development of new therapeutic approaches. Consequently, numerous preclinical studies in MJD rodent models have shown promising results, as summarized in Table 1.2. These therapeutic strategies can be generally divided into the following categories: a) reduction of mutant-ataxin3 mRNA levels (reviewed in the next chapter), b) prevention of mutant ataxin-3 proteolytic cleavage, c) activation of protein clearance, d) modulation of calcium homeostasis, e) transcriptional regulation and f) neuroprotection, as illustrated in Figure 1.4.

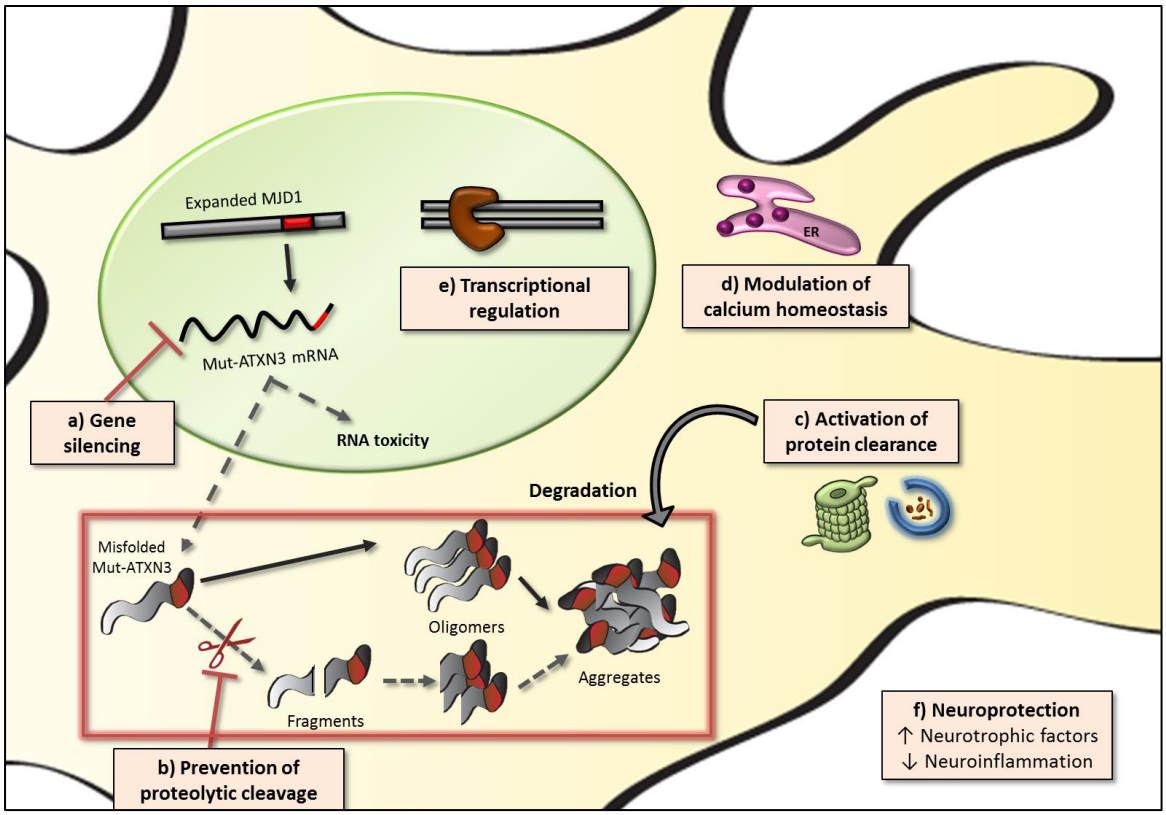

Figure 1.4: Schematic representation of the most common MJD therapeutic approaches. Numerous therapeutic strategies have been proposed for MJD, including: a) Gene silencing, which directly decreases the levels of mutant ataxin-3 mRNA; b) prevention of mutant ataxin-3 proteolytic cleavage, thus reducing the accumulation of C-terminal toxic fragments; c) Activation of protein clearance systems (ubiquitin-proteasome system and autophagy), to reduce the accumulation of misfolded proteins, such as mutant ataxin-3; d) Modulation of calcium homeostasis, in order to correct the defects induced by mutant ataxin-3; e) transcriptional regulation, leading to normalization of gene expression levels; f) neuroprotective effects, normally including an increase in neurotrophic factors and a neuroinflammation reduction.

Table 1.2 summarizes the principal therapeutic approaches tested until now in rodent models and the respective results.

Table 1.2: Summary of the principal preclinical studies for MJD in rodent models

Therapeutic Strategy	Therapeutic mechanism	Model	Therapeutic agent	Administration route	Results	Ref
Prevention of proteolytic cleavage	Calpain inhibition	Striatal LV	AAV2-calpastatin	Intraparenchymal (Striatum)	Neuropathology alleviation	(Simoes et al., 2012)
			BDA-410	Oral	Neuropathology and behavior improvements	(Simoes et al., 2014)
Activation of protein clearance	Autophagy activation	polyQ69/ Cerebellar LV	LV-beclin1	Intraparenchymal (Cerebellum)	Neuropathology and behavior improvements	(Nascimento-Ferreira et al., 2013)
		70.61 CAG	Temsirolimus	IP	Molecular, neuropathology and behavior improvements	(Menzies et al., 2010)
		CMVMJD 135	17-DMAG	IP	Neuropathology and behavior improvements	(Silva-Fernandes et al., 2014)
	UPS activation	polyQ69	LV-CRAG	Intraparenchymal (Cerebellum)	Neuropathology and behavior improvements	(Torashima et al., 2008)
			IDLV-CRAG			(Saida et al., 2014)
			AAV9-CRAG	Intravenous	Neuropathology alleviation	(Konno et al., 2014)
		ataxin-3-Q79	H1152	IP	Neuropathology alleviation	(Wang et al., 2013)
Modulation of calcium homeostasis	Ca2+ signaling stabilization	MJD84.2	Dantrolene	Oral	Neuropathology and behavior improvements	(Chen et al., 2008)
	Normalization of Purkinje cells firing activity	MJD84.2	SKA-31	IP	Electrophysiology and behavior improvements	(Shakkottai et al., 2011)
Prevention of Transcription Dysregulation	Reversion of histone hypoacetylation	ataxin-3-Q79	Sodium butyrate	IP	Molecular, electrophysiology neuropathology and behavior improvements	(Chou et al., 2011) (Chou et al., 2014)
Neuro protection	Control of glutamatergic transmission and prevention of calpain proteolysis	Striatal LV	Caffeine	Oral	Neuropathology alleviation	(Goncalves et al., 2013)
	UPS activation	ataxin-3-Q79	T1-11 JMF1907	Oral	Molecular, neuropathology and behavior alleviation	(Chou et al., 2015)
	Modulation of serotonine signalling	CMVMJD 135	Citalopram	Oral	Neuropathology and behavioral improvements	(Teixeira-Castro et al., 2015)
	Neurotransmission modulation, transcription regulation, neuroprotection	CMVMJD 135	Valproic acid	IP	Limited effects in the motor deficits. No neuropathology alleviation	(Esteves et al., 2015)
	Reduction of neuroinflammation, increase of neurotrophic factors	polyQ69	Transplantation of cerebellar neural stem cells	Intraparenchymal (Cerebellum)	Neuropathology and behavior improvements	(Mendonca et al., 2015)
	Autophagy activation, neurotrophic factors, reduction in neuroinflammation	Striatal LV/ polyQ69	AAV-NPY	Intraparenchymal (Striatum/ Cerebellum)	Neuropathology and behavior improvements	(Duarte-Neves et al., 2015)
	Reduction in neuroinflammation, autophagy activation	Striatal LV/ polyQ69	Caloric restriction, LV-SIRT1/ Resveratrol	Intraparenchymal (Striatum)/ IP	Neuropathology and behavior improvements	(Cunha-Santos et al., 2016)

UPS – ubiquitin-proteasome system; AAV - adeno-associated virus; BDA-410 - protease inhibitor; LV - lentivirus; 17-DMAG - Hsp90 inhibitor; CRAG - collapsin response mediator protein-associated molecule associated guanosine triphosphatase; IDLV - integrase-defective lentiviral vector; H1152 - ROCK inhibitor; SKA-31 - small-conductance calcium-activated potassium channel activator; T1-11 - adenosine A2A receptor agonist; JMF1907 - synthetic analogue of T1-11; NPY - Neuropeptide Y; SIRT1 – sirtuin-1; IP – intraperitoneal.

In summary, several approaches have been developed to treat MJD, with promising results in rodent models. However, the MJD pathogenic mechanism is extremely complex, involving different cellular systems, which are difficult to correct altogether with a unique therapeutic strategy. Most approaches tested so far target only one of the MJD-associated defects, such as impairments in protein clearance, transcription dysregulation or the accumulation of toxic fragments. As a consequence, they might not completely correct the disorder. Moreover, most approaches are not specific, leading to a generalized effect such as overall transcription downregulation, inhibition of proteolytic cleavage or stimulation of calcium signaling, for example. As a result, the treatment might also induce adverse effects. Moreover, all these strategies target the PolyQ-protein and downstream events, thereby not avoiding the toxic effects of mutant-ataxin3 mRNA.

Taken all of this into account, one of the most direct, specific and effective solutions to correct MJD would be to inhibit mutant ataxin-3 expression using RNA interference. By targeting the transcript, this intervention allows to act exactly at the beginning of pathogenesis, avoiding all the subsequent steps.

1.2. RNA interference (RNAi) as a potential treatment for MJD

The inhibition of mutant ataxin-3 expression holds great promise for MJD therapy, since it directly corrects the disorder cause. The successful results obtained so far with gene silencing in MJD and other CNS disorders demonstrates the great potential of this strategy. Thus, translation to the clinics greatly depends on the selection of the ideal RNAi molecule and delivery vector.

1.2.1. RNAi mechanism

RNA interference (RNAi) is an essential gene regulatory mechanism involved in several cellular processes, including: proliferation, differentiation, cell death and protection against viral infection and transposable elements (Carrington and Ambros, 2003). RNAi mediates gene silencing via small inhibitory RNAs capable of base pairing with specific mRNA sequences. In nature, this mechanism occurs primarily via microRNAs (miRNAs), with 19 to 25 nucleotides in length. miRNA generation process includes the following steps: i) primary miRNAs (pri-miRNAs) are transcribed from the genome, forming a hairpin structure; ii) upon expression, pri-miRNAs are cleaved by the nuclear Drosha–DGCR8 microprocessor complex, producing intermediate hairpin RNAs (60–70 nt), known as precursor miRNAs (pre-miRNAs); iii) Pre-miRNAs are then transported by Exportin-5 to the cytoplasm, where they are cleaved by a Dicer-containing complex. This last processing step removes the loop region, generating the mature miRNA duplex. The resulting duplex contains an antisense, or guide strand, and a sense, or passenger strand. The first one is then selectively

incorporated into the RNA-induced silencing complex (RISC) through a process called strand biasing. Activated RISC is able to induce gene silencing via two distinct modes, depending on the complementarity degree: i) perfect base-pairing results in target transcript cleavage, while ii) imperfect binding to target 3' untranslated region (UTR) induces translational repression and mRNA decay (reviewed in (Boudreau et al., 2011a) (Figure 1.5).

The increasing knowledge about RNAi mechanism has promoted the development of RNA interference as a tool to artificially silence specific genes and, consequently, treat several human disorders. This technology requires the introduction of designed inhibitory RNAs into cells, with the ability to activate RNAi endogenous machinery and consequently target certain mRNA molecules. There are different options regarding RNAi-based tools, including: synthetic small interfering RNA (siRNAs), which are directly introduced into the cytoplasm and loaded into RISC (Elbashir et al., 2001), but also artificial microRNAs (miRNAs) and short-hairpin RNAs (shRNAs), in which the silencing sequence is embedded into a hairpin structure (Paul et al., 2002; Zeng et al., 2002). The introduction of miRNAs and shRNAs into cells requires vector-based delivery and transcription in the nucleus, followed by RNAi machinery processing, starting at different points. While artificial miRNAs mimic pri-miRNAs, shRNAs enter the pathway in the same step as pre-miRNAs (Figure 1.5).

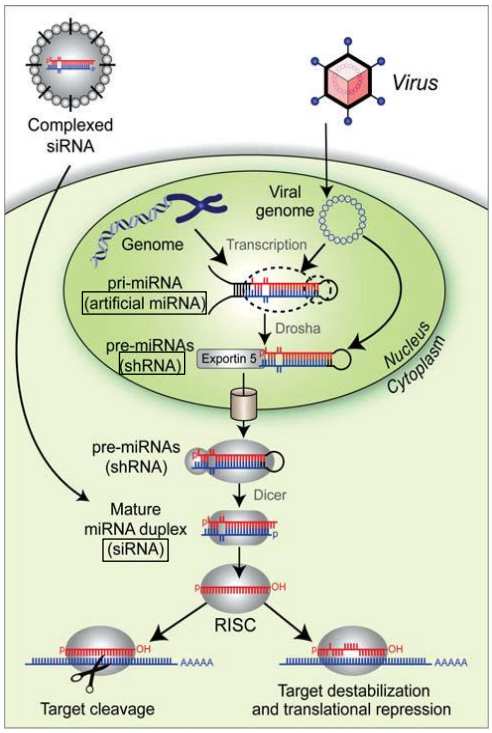

Figure 1.5: Schematic representation of the endogenous RNAi pathway and exogenous components that co-opt this pathway to achieve gene silencing. The RNAi pathway, normally triggered by endogenous microRNAs, is co-opted by exogenous RNAi tools, i.e. siRNAs, shRNAs and artificial microRNAs to induce gene silencing. They enter the pathway in different steps: i) siRNAs are introduced in the cytoplasm and directly loaded into RISC; ii) artificial miRNAs and shRNAs are delivered into the nucleus through expression vectors. Artificial microRNAs enter the pathway mimicking pri-miRNA, thus requiring Drosha processing, whereas shRNAs enter as pre-miRNAs, being directly exported to the cytoplasm after transcription. Adapted from (Boudreau et al., 2011a).

1.2.2. siRNA, shRNA and miRNA

Therapeutic gene silencing can be achieved using siRNAs, shRNAs or artificial microRNAs, which present different characteristics.

Despite the simplicity of siRNA effectors, their silencing effect is transient, consequently requiring repeated treatments. In a clinical setting, a stable and long-term action of RNAi constructs would be the ideal solution, allowing disease correction with a single treatment. This can be achieved using shRNAs or artificial microRNAs, which are introduced into the nucleus and expressed during a long period (Aagaard and Rossi, 2007).

The main differences between shRNAs and artificial miRNAs are related to their secondary structure and processing in the RNAi pathway. Following transcription, shRNAs are exported from the nucleus by Exportin-5 and, once in the cytoplasm, are cleaved by Dicer to generate mature duplexes. On the other hand, miRNAs require an additional step of excision by the Drosha-DGCR8 complex before translocation to the cytoplasm (Figure 1.5). Another difference between shRNA and artificial microRNA is the type of promoter normally used to trigger their expression. While shRNAs are usually expressed from polymerase III (pol III) promoters (Paddison et al., 2002), miRNAs can be efficiently expressed from polymerase II (pol II) promoters, thereby allowing time and tissue-specific expression (Shin et al., 2006). Until now, shRNA expression from pol III promoters has been the most commonly used RNAi tool. However, several studies reported toxic effects after shRNA delivery, which could be circumvented by embedding the silencing sequence into artificial miRNA scaffolds (Boudreau et al., 2009a; McBride et al., 2008).

shRNA-induced toxic effects were firstly reported by Grimm et al. after administering Adeno-associated viral vectors (AAV) encoding a battery of shRNAs into adult mouse liver. According to the results, the great majority of tested shRNAs induced liver damage, with almost half of them causing death within 2 months (Grimm et al., 2006). Subsequent studies in the CNS have reported shRNA-mediated toxicity after delivery to mouse striatum (Martin et al., 2011), (McBride et al., 2008) and cerebellum (Boudreau et al., 2009a), as well as rat ventromedial hypothalamus (van Gestel et al., 2014), substantia nigra (Khodr et al., 2011; Ulusoy et al., 2009) and red nucleus (Ehlert et al., 2010). In these reports, AAV-shRNA delivery has resulted in neurodegeneration, inflammation and behavioral alterations. Altogether, these findings indicated that shRNAs are the causative toxic agents, independently of their sequence and targets.

Consequently, several studies tried to clarify the mechanism behind these toxic effects, converging in the hypothesis that: i) shRNA molecules are expressed in high levels, leading to the buildup of precursor and processed forms, ii) this accumulation of inhibitory RNAs results in the saturation of crucial components from RNAi machinery, such as exportin-5 and/or proteins involved in RISC (Argonaute proteins); iii) the disruption of this system inhibits the activity of endogenous microRNAs, with important cellular functions, ultimately leading to cellular death (Boudreau et al., 2009a; Grimm et al., 2010; van Gestel et al., 2014). Additionally, the fact that Exportin-5 expression is relatively low in the brain (Yi et al., 2005) possibly explains why this organ is particularly prone to shRNA-induced toxicity. An alternate explanation would be off-targeting

silencing, which results in the downregulation of undesired targets with partial complementarity with the delivered shRNA construct, as proposed by Boudreau et al. (Boudreau et al., 2009a).

Regardless of the mechanism, it is extremely important to prevent adverse effects when using shRNAs as therapeutic molecules. One possible solution would be to reduce the vector dose, ideally finding a balance between efficiency and safety. Similarly to Grimm et al. reports in the liver (Grimm et al., 2006), Ulusoy et al. optimized vector dilution, successfully maintaining transgene knockdown efficiency and eliminating toxic effects in nigrostriatal projection neurons (Ulusoy et al., 2009) . On the contrary, by using lower vector doses, McBride et al. have observed a reduction on neuronal transduction, without any amelioration regarding neurotoxicity (McBride et al., 2008) . Alternatively, switching to a weak and tissue specific RNA Pol II promoter might have a positive impact on safety profile, in contrast to generally used potent RNA Pol III promoters (H1, U6). This strategy has already shown successful results in the liver (Giering et al., 2008), but involves several structural requirements to achieve the optimal configuration (Maczuga et al., 2012).

Therefore, the incorporation of shRNA sequences into microRNA backbones is emerging as the ideal solution to achieve safe gene silencing. In fact, artificial miRNAs have proved to be well-tolerated in the brain, since they do not saturate endogenous RNAi machinery. By directly comparing miRNA and shRNAs, Boudreau et al. showed improved silencing potency for shRNAs, accompanied by toxicity due to their higher expression levels (Boudreau et al., 2008). An alternative explanation would be a better transcript stability, which corroborates their novel finding that adding nucleotides to shRNA overhangs can decrease its expression levels, possibly mimicking what occurs in microRNAs. Finally, Castanotto et al. raised the idea that incorporation kinetics into RISC might be a major determinant of silencing power, competing strength and ultimately toxicity (Castanotto et al., 2007). Considering that miRNA molecules are subjected to an additional processing step, they might be incorporated more slowly into RISC when compared to shRNAs. In fact, cleavage by Drosha might act as a rate-limiting step for artificial microRNA, hindering the accumulation of excessive RNAi molecules and consequent machinery saturation.

In vivo studies performed by McBride and Boudreau et al. demonstrated that artificial microRNAs delivered into the mouse brain displayed an efficient silencing effect, combined with a safety profile, independently of the sequence and brain region. In fact, miR-treatment was able to alleviate toxicity when compared to animals injected with therapeutic shRNA, thus improving neuronal survival and reducing microglia activation (Boudreau et al., 2009a; McBride et al., 2008). Therefore, according to these reports, artificial microRNAs are able to attenuate neurotoxicity without compromising silencing efficacy, providing an ideal tool for gene silencing in the brain and potential therapeutic applications.

1.2.3. RNAi in neurodegenerative diseases

Gene silencing using RNAi has been proposed as a therapeutic strategy in several CNS disorders. This approach has proven to be particularly suitable for autosomal dominant diseases, since it directly corrects the genetic cause by silencing the mutant allele. Multiple studies have shown highly promising results in rodent models, as described in Table 1.3. Researchers have tested different RNAi molecules (siRNA, shRNA, miRNA), delivery vectors (lentivirus, adeno-associated virus, or direct administration of siRNAs) and routes of administration. Although shRNA has been the predominant RNAi molecule so far, recent studies have switched to artificial microRNAs. In what concerns the delivery route, direct injection into the brain parenchyma has been clearly the most predominant strategy, but intramuscular and intravenous injections have recently emerged as promising options.

Table 1.3: Summary of the principal studies using RNAi as therapeutic tool for CNS disorders with successful results in rodent models

Disease classification	Disease	mRNA target	RNAi tools	Allele specificity	Vectors	Administration routes	Ref
Motor neuron diseases	**ALS**	*SOD1*	shRNA miRNA	NAS AS (G93A)	LV AAV2 AAV9 rAAVrh10	Intramuscular Intraparenchymal Intra-CSF Intravenous	(Foust et al., 2013; Miller et al., 2005; Ralph et al., 2005; Raoul et al., 2005; Stoica et al., 2016; Thomsen et al., 2014; Wang et al., 2014; Xia et al., 2006)
Poly glutamine disorders	**HD**	*HTT*	siRNA shRNA miRNA	NAS AS (4 SNPs)	Adenovirus LV AAV1 AAV2/1 AAV9	Intraparenchymal Intra-CSF Intravenous	(Boudreau et al., 2009b; DiFiglia et al., 2007; Drouet et al., 2009; Drouet et al., 2014; Dufour et al., 2014; Franich et al., 2008; Harper et al., 2005; Huang et al., 2007; Machida et al., 2006; Stanek et al., 2014; Wang et al., 2005)
	SCA1	*ATXN1*	shRNA miRNA	NAS	AAV2/5 AAV2/1	Intraparenchymal	(Keiser et al., 2014; Keiser et al., 2013; Xia et al., 2004)
	MJD/ SCA3	*ATXN3*	siRNA shRNA miRNA	NAS AS (G987C)	LV AAV2/1 SNALPs	Intraparenchymal Intravenous	(Alves et al., 2008a; Conceicao et al., 2016b; Costa Mdo et al., 2013; Nobrega et al., 2014; Nobrega et al., 2013b; Rodriguez-Lebron et al., 2013)
	SCA7	*ATXN7*	miRNA	NAS	AAV2/1	Intraparenchymal	(Ramachandran et al., 2014)
Neuro degenerative disorders (familial forms)	**AD**	*CDK5* *APP* *BACE1*	shRNA miRNA	NAS AS (Swedish variant of APP)	LV AAV2 AAV2/5	Intraparenchymal	(Castro-Alvarez et al., 2015; Piedrahita et al., 2010; Rodriguez-Lebron et al., 2009; Singer et al., 2005; Yu et al., 2014)
	PD	*SNCA*	shRNA	NAS AS (A53T)	LV AAV2	Intraparenchymal	(Khodr et al., 2011; Sapru et al., 2006)

ALS- Amyotrophic lateral sclerosis; HD – Huntington's disease; SCA1/3/7 – Spinocerebellar Ataxia type 1/3/7; AD – Alzheimer's disease; PD – Parkinson's disease; SOD1 - superoxide dismutase 1; HTT – huntingtin; ATXN1/3/7 – ataxin 1/3/7; CDK5 - cyclin-dependent kinase 5; APP - amyloid precursor protein; BACE1-beta-secretase 1; SNCA - synuclein alpha; NAS – non-allele specific; AS – allele specific; SNP -single nucleotide polymorphisms; AAV – adeno-associated virus; LV – lentivirus vector; CSF – cerebrospinal fluid.

Non-allele specific (NAS) *versus* Allele-specific silencing

Therapeutic strategies involving gene suppression in dominantly inherited disorders might be designed to target both alleles or only the mutant form (Watson and Wood, 2012). Non-allele specific (NAS) silencing is technically easier, but should only be applied when the wild-type protein is non-essential or functionally redundant, in order to avoid deleterious effects. On the contrary, when the gene's normal function is indispensable, allele-specific (AS) approaches would be preferential. As described in Table 1.3, most results were achieved after NAS silencing, which proved to alleviate neuropathological and behavioral defects in familial forms of amyotrophic lateral sclerosis (ALS), Alzheimer disease and Parkinson's disease, as well as in PolyQ disorders.

A study performed by Xia et al. in a SCA1 mouse model was the first *in vivo* evidence for efficient RNAi-mediated gene silencing in PolyQ disorders (Xia et al., 2004). Subsequently, numerous NAS RNAi strategies have been employed in other spinocerebellar ataxias (mainly SCA1, SCA3 and SCA7) and in Huntington's disease. In the latter case, NAS strategies have shown successful results in different rodent models (Boudreau et al., 2009b; DiFiglia et al., 2007; Drouet et al., 2009; Dufour et al., 2014; Franich et al., 2008; Harper et al., 2005; Huang et al., 2007; Machida et al., 2006; Stanek et al., 2014; Wang et al., 2005). Translation to non-human primates (NHP) has already been explored by two studies, in which partial silencing of wild-type huntingtin (HTT) was well tolerated without adverse effects up to 6 months post-injection (Grondin et al., 2012; McBride et al., 2011). Similarly, Keiser et al. have directly administered AAV vectors encoding an artificial miRNA against ataxin-1 into NHP cerebellum, which resulted in broad distribution, efficient silencing and no toxic effects (Keiser et al., 2015). This data suggest that as long as a certain threshold level of wild-type expression is maintained, NAS might be a safe therapeutic approach. Nevertheless, determining this level for human disease could be particularly challenging.

Taken everything into account, allele-specific silencing is considered the safest approach for most dominantly inherited disorders in which wild type proteins exhibit crucial cellular roles. This strategy has already shown promising results *in vivo* as a therapeutic method for familial forms of ALS (Xia et al., 2006), Alzheimer's disease (Rodriguez-Lebron et al., 2009) and Parkinson's disease (Sapru et al., 2006), by targeting the point mutations that cause the disorders. However, this method is particularly challenging for PolyQ diseases, in which the causative mutation corresponds to a CAG expansion, since: i) RNAi molecules with less than 25 nucleotides are not able to efficiently discriminate between wild-type and expanded CAG tracts, and ii) this nucleotide repetition is present throughout the genome, potentially leading to off-target silencing (Scholefield and Wood, 2010). In this context, Hu et al. recently explored a miRNA-like mechanism, i.e. mismatched RNA duplexes, targeting the CAG expansion in mutant huntingtin. Interestingly, the authors achieved potent and highly selective silencing, possibly because the expanded CAG repeat offers multiple target sequences for RNAi binding, consequently facilitating translation inhibition (Hu et al., 2010). However, the low specificity of this strategy for the disease-causing gene might possibly induce adverse effects.

As an alternative, RNAi sequences might be directed at single nucleotide polymorphisms (SNPs) in linkage disequilibrium with CAG expanded alleles. The main limitation to this approach relates to the prevalence of disease-associated SNPs among patient populations (Boudreau et al., 2011a). Accordingly, AS silencing would be particularly useful when targeting SNPs present in the great majority of patients, as in the case of MJD (described in the following section). Another disorder that could benefit from this strategy is Huntington's disease, given the essential cellular roles of huntingtin (Dragatsis et al., 2000). Therefore, Drouet et al. developed shRNAs targeting several SNPs described for mutant HTT, which efficiently reduced neuropathology in a rat model (Drouet et al., 2014). Using a similar approach, Scholefield et al. have investigated particular SNPs present in mutant ataxin-7 and assessed the impact of allele specific silencing in a SCA7 cellular model and patient-derived fibroblasts, also with successful results (Scholefield et al., 2009; Scholefield et al., 2014).

1.2.4. RNAi in Machado-Joseph Disease

When using RNAi as a therapeutic approach for autosomal dominant disorders, selection between allele specific or non-specific methodology is a key factor. Considering the important cellular functions that have previously been described for ataxin-3 (see section 1.1.2), the lack of discrimination between wild-type (WT) and mutant (Mut) forms could be deleterious. This hypothesis has been recently addressed using different *in vitro* and *in vivo* models, with controversial results.

By silencing WT-ataxin-3 on human and mouse cell lines, Rodrigues et al. have detected an accumulation of ubiquitinated proteins, defects on cytoskeleton/adhesion and a marked increase in cell death (Rodrigues et al., 2010). In contrast, in ataxin-3 knock-out (KO) animal models, no major phenotypic alterations were detected. While the *C.elegans* model is characterized by transcription deregulation (Rodrigues et al., 2007), KO mice exhibit an accumulation of ubiquitinated proteins in the mouse brain and an increase in anxiety (Schmitt et al., 2007). Taken together, this data suggests the presence of a compensatory mechanism *in vivo* in the absence of ataxin-3 expression. In this way, proteins with similar roles would possible be activated, explaining why KO animals only present a mild phenotype.

According to these results, wild-type ataxin-3 is considered not to be crucial in a normal physiological situation, but could potentially be important in MJD disease context. Warrick et al. have proposed an important role for WT-ataxin-3 in polyQ pathogenesis modulation. The authors concluded that, in flies expressing mutant ataxin-3, co-expression of the wild-type form is able to alleviate neurodegeneration (Warrick et al., 2005). In this model, phenotypic amelioration was associated with WT-ataxin3 recruitment to nuclear inclusions and a consequent delay in their formation. Moreover, this protective effect was found to be dependent on ataxin-3 deubiquitinase activity and proteasome function. Consistent with this report, a gene dosage effect has been described for MJD, with homozygous patients showing an increased disease severity and earlier onset when compared to heterozygous subjects (Carvalho et al., 2008). This phenomenon

might reflect not only the presence of two mutant alleles, but also the partial loss of WT-ataxin-3 protective function.

In this context, Alves et al. have explored the role of WT-ataxin-3 in the MJD, but now using a rat model (Alves et al., 2010). Considering that WT protein modulates neuropathology in rodents in a similar way as described for *Drosophila*, then WT-ataxin-3 overexpression would result in pathology amelioration, whereas silencing this protein would aggravate the disease. However, the authors concluded that WT-ataxin-3 expression was not able to alleviate neuropathology in the MJD striatal lentiviral model. Subsequently, they proved that the opposite approach, i.e. silencing rat endogenous ataxin-3 in the same MJD model, was well-tolerated and has not exacerbated MJD-associated neuropathology. Finally, the authors generated a universal shRNA sequence that simultaneously targeted human and rat ataxin-3, mimicking a non-allele silencing methodology. This treatment efficiently reduced ubiquitinated ataxin-3 inclusions and promoted neuronal survival. Taken together, these findings suggest that silencing both mutant and wild-type ataxin-3 forms might be an efficient and safe approach in rodents. However, further studies would be necessary to validate the safety profile, particularly at long-term. Besides that, this is an artificial model which might not accurately translate what occurs in human patients. As a result, and considering the contradicting results achieved so far, allele-specific silencing might be a preferential option, since it allows the maintenance of ataxin-3 cellular functions.

Distinct RNAi strategies have been tested in MJD rodent models in the past years, with very successful results, as depicted in Table 1.4. Researchers have explored different methods (allele specificity/non-allele specificity), delivery vectors (liposomes, lentiviruses and AAVs), delivery routes (intracranial and intravenous injections) and silencing sequences (shRNA and microRNA constructs).

Table 1.4: Summary of preclinical studies exploring RNAi in rodent models of MJD

mRNA target	Allele specificity	RNAi tool	Vector	Administration route	Model	Results	Ref
ATXN3	NAS	shRNA	LV	Intraparenchymal (Striatum)	Striatal LV (rat)	Neuropathology alleviation	(Alves et al., 2010)
		miRNA	AAV2/1	Intraparenchymal (Cerebellum –DCN)	MJD84.2 (mouse)	Neuropathology alleviation; No behavior improvements	(Rodriguez-Lebron et al., 2013), (Costa Mdo et al., 2013)
	AS (G987C) rs12895357	shRNA	LV	Intraparenchymal (Striatum)	Striatal LV (rat)	Neuropathology alleviation	(Alves et al., 2008a)
				Intraparenchymal (Cerebellum)	PolyQ 69 (mouse)	Neuropathology and behavior improvements	(Nobrega et al., 2013b)
					Cerebellar LV (mouse)		(Nobrega et al., 2014)
		siRNA	RVG-9r SNALPs	Intravenous	PolyQ69/ Striatal LV (mouse)	Neuropathology and behavior improvements	(Conceicao et al., 2016b)

ATXN3 – ataxin-3; NAS – non-allele specific; AS – allele specific; AAV 2/1– adeno-associated virus 2/1; LV – lentivirus; RVG-9r SNALPs - Stable nucleic acid lipid particles with a short peptide derived from rabies virus glycoprotein; DCN - deep cerebellar nuclei.

Preclinical studies using non-allele specific silencing

Two parallel studies have explored the therapeutic impact of ataxin-3 non-allele specific silencing in MJD84.2 transgenic mice (Costa Mdo et al., 2013; Rodriguez-Lebron et al., 2013). For that purpose, the authors designed an artificial microRNA based on miRNA-124 sequence and targeting human ataxin-3 3'UTR region, which was subsequently packaged into AAV2/1 vectors, under the control of U6 promoter (rAAV-miR-ATXN3). Finally, these rAAV vectors were directly injected into the deep cerebellar nuclei (DCN) of 2 month- (Rodriguez-Lebron et al., 2013) or 6-8 –month-old (Costa Mdo et al., 2013) YAC-transgenic mice (MJD84.2), successfully transducing DCN neurons, but also Purkinje cells due to viral retrograde transport. Additionally, Costa et al. have reported efficient transduction in some brainstem and thalamic nuclei. rAAV-miR-ATXN3 treatment successfully reduced human ataxin-3 mRNA levels and attenuated its abnormal neuronal nuclear accumulation in the cerebellum. Moreover, the altered levels of certain microRNAs in the cerebellum, a characteristic of YAC-transgenic mice, were partially normalized when silencing mutant ataxin-3. However, rAAV-miR treatment was not able to alleviate MJD84.2 mice phenotypic and behavioral parameters, possibly due to the limited transduced region or the inability to revert neuronal dysfunction at advanced times of intervention (6-8 months). In conclusion, the therapeutic impact of rAAV-miR-ATXN3 injection could be maximized by increasing vector distribution throughout the brain and/or performing the injection at an earlier disease stage. Importantly, these studies observed a good safety profile for AAV administration, showing no off-target silencing effects or signs of neuroinflammation.

Preclinical studies using allele specific (AS) silencing

On the other hand, AS silencing might be preferential in MJD, by avoiding possible adverse effects related to WT-ataxin-3 silencing. The identification of a SNP in the CAG tract 3'end of *MJD1*, in linkage disequilibrium with the disease-causing expansion was a major breakthrough in the field (Gaspar et al., 1996). In 70% of MJD patients, *MJD1* mutant allele carries a cytosine at position 987, instead of the guanine nucleotide present in the wild-type gene (Gaspar et al., 2001). This observation opened the way to selective repression of mutant ataxin-3.

Therefore, Alves et al. have designed a shRNA construct targeting this SNP: sh-ATXN3-Mut(C), which was inserted into a lentiviral backbone, under the control of H1 promoter (Alves et al., 2008a). Firstly, the authors confirmed the efficiency and selectivity profile of this construct towards the mutant transcript *in vitro.* Subsequently, the same approach was tested in a rat model, by co-injecting lentiviral vectors encoding human mutant ataxin-3 (C) and shRNA (sh-ATXN3-Mut(C)) in the striatum. As a result, the authors observed a reduction in the number and size of ataxin-3 aggregates, accompanied by an increased neuronal survival, confirming the silencing efficiency of this allele-specific shRNA *in vivo*. Subsequently, Nobrega et al. have tested the impact of AS mutant ataxin-3 silencing in PolyQ69 transgenic mice (Nobrega et al., 2013b). For that, the authors used the same shRNA sequence (sh-ATXN3-Mut), since the SNP in mutant ataxin-3 is also present in the selected mouse model. Lentiviral vectors encoding this silencing construct

(LV-sh-ATXN3-Mut) were injected directly in the cerebellum of 3 week-old mice, mimicking a treatment after disease onset. Lentiviral vectors efficiently transduced around 60% of cerebellar cortex, consequently inducing neuropathological improvements. In fact, the treatment successfully reduced the number of mutant ataxin-3 inclusions, prevented neurodegeneration, rescued cerebellar atrophy and prevented neuronal arborization defects. Treated animals also exhibited a significantly better performance on behavioral tests. In conclusion, these results proved for the first time the therapeutic impact of allele-specific silencing of mutant ataxin-3 after disease onset. The same strategy was performed in the cerebellar lentiviral-based model, also with promising results (Nobrega et al., 2014).

Although successful in animal models, the intracranial injection of viral vectors involves an invasive procedure with possible side effects. Moreover, this delivery route promotes transgene expression in a limited brain region (Vite et al., 2003) , which could limit the therapeutic effect in humans. Therefore, vector spread throughout the brain would be an important optimization strategy.

Taking this into account, Conceiçao et al. have tested the delivery of the previously described silencing sequence, but through non-invasive administration of stable nucleic acid lipid particles. The fact that they were coupled with a peptide from rabies virus (RVG-9r SNALPs) conferred them the ability to cross the blood-brain barrier (BBB) (Conceicao et al., 2016b). RVG-9r SNALPs encapsulating siRNAs against mutant ataxin-3 were tested in transgenic mice expressing 69Q-truncated ataxin-3, through the administration of a total of 9 tail injections. This treatment resulted in some behavioral improvements and was able to attenuate cerebellum atrophy without apparent signs of toxicity (Conceicao et al., 2016a). This was an important step in the field of MJD gene therapy, constituting the first report of a successful gene silencing approach using non-viral vectors. However, the use of liposomes as delivery vectors is associated with a relatively low efficiency and the necessity to perform repeated injections throughout life.

To sum up, RNAi has been explored as a therapeutic approach for MJD, using different methods and delivery systems. Although with successful results, all of them presented some limitations, including: invasive procedures, low distribution throughout the cerebellum and brain or the need for repetitive injections. As a result, MJD therapy would benefit from a non-invasive treatment which could provide widespread and long-term transgene expression through a single administration – the aim of the present study.

1.2.5 Possible RNAi delivery vectors

Although siRNAs can be directly delivered to the CNS, they exhibit low stability and are degraded by nucleases *in vivo*, precluding the possible therapeutic effect of this method (Peer and Lieberman, 2011). To overcome this issue, siRNA chemical modifications to improve nuclease resistance might be introduced (Rettig and Behlke, 2012). As an alternative, RNAi molecules can be incorporated into delivery systems, classified as non-viral and viral vectors. An ideal delivery

system for RNAi to the CNS should: i) get access to the CNS and target the desirable cell type, ii) mediate an efficient delivery of RNAi molecules, leading to a robust and stable knockdown of the respective mRNA and iii) exhibit a good safety profile, with no toxic and immune responses. Moreover, RNAi delivery vectors should be easily produced at a large-scale to allow translation to the clinics.

Non-viral vectors

RNAi molecules can be incorporated into non-viral vectors such as liposomes, exosomes and polymeric nanoparticles, reviewed in (Posadas et al., 2010). These delivery systems display important advantages such as: i) the stable and safety profile, ii) the ability to cross the blood brain barrier and/or target specific cell types and tissues upon modifications; iii) simple and cost-effective production methods. However, they present a relatively low efficiency profile and mediate a transient effect, requiring repeated administrations, which in a long-term can trigger an immune response (Ramachandran et al., 2013).

Viral vectors

Recombinant viral vectors are considered the most efficient system to achieve long-term stable gene expression in the CNS, as depicted in tables 1.3 and 1.4. Over the years, several viral vector systems have been investigated for this purpose, such as: herpes simplex virus type 1, adenovirus, adeno-associated virus (AAV) and lentivirus (LV) (reviewed in (Choudhury et al., 2016b)).

AAV and lentivirus vectors have emerged as the vectors of choice for gene transfer to the CNS as they mediate efficient long-term gene expression with no apparent toxicity (Nobre and Almeida, 2011). Comparing both vectors, AAVs exhibit important advantages. Firstly, they are considered to be safer since the natural form is non-pathogenic (Berns and Linden, 1995), while lentiviruses derive from a highly pathogenic virus (HIV-1) (Naldini et al., 1996) and have to be modified in order to avoid genome integration (Sarkis et al., 2008). Moreover, the production of integrase-deficient LV vectors results in lower titers when comparing to AAV, which can easily be manufactured at a large scale (Choudhury et al., 2016b). Another difference consists on transgene expression levels, which are lower for LV, due to low copy numbers of transgene per cell (Ramachandran et al., 2013). Finally, LVs display a limited volumetric spread after direct infusion in the brain (500-700 µm from the site of infusion), possibly due to their large size preventing distribution through extracellular spaces in the brain (Cetin et al., 2006). In comparison, AAV smaller size allows a larger distribution (1-3 mm) (Kells et al., 2009). On the other hand, the main advantage of LVs against AAVs is their larger packaging capacity (up to 9kb), whereas AAVs display a limited insertion site (4.8 kb). Nevertheless, this would not be a determining factor for RNAi constructs, since AAV capacity is sufficient for their incorporation (Ramachandran et al., 2013). Taking everything into account, AAVs mediate a safe, widespread and robust transgene expression, thereby being considered the vector of election for RNAi delivery to the CNS.

1.3. Adeno-associated viruses (AAVs) as CNS delivery vectors

Adeno-associated viruses (AAVs) are currently the preferred vector for CNS gene delivery, since they exhibit long-term transgene expression in post-mitotic cells, neuronal tropism, low risk of insertional mutagenesis and diminished immune responses. Several clinical trials have already shown successful results, encouraging AAV administration as a therapeutic tool for other CNS disorders. The selection of a suitable serotype and administration routes are key factors to determine therapeutic efficiency.

1.3.1. Adeno-associated virus (AAV): the basics

AAV is a non-enveloped, small, linear single-stranded DNA-containing virus, originally described as a contaminant of adenovirus preparations. This virus belongs to the *Parvoviridae* family, particularly the genus *Dependovirus*, since it requires co-infection with a helper virus, such as adenovirus or herpesvirus, in order to replicate and complete its life cycle (Atchison et al., 1965). AAVs are classified as non-pathogenic viruses, which naturally infect humans with no disease association (Grossman et al., 1992).

AAV Genome

The 4.7 kb virus genome is composed of two open reading frames (ORFs): rep and cap, flanked by 145 bp inverted terminal repeats (ITRs) on the 5' and 3' ends, as illustrated in Figure 1.6. The *rep* ORF encodes four proteins: Rep 40, 52, 68 and 78, corresponding to spliced and unspliced products expressed using different promoters (P5 and P19). These Rep proteins, designated based on their molecular weight, are required for AAV replication, transcription, integration and encapsidation. On the other hand, the *cap* ORF leads to the production of three structural proteins: VP1, VP2 and VP3, which assemble in a ratio of 1:1:10 to form an icosahedral capsid of approximately 25 nm in diameter. The cap gene is transcribed from the P40 promoter and generates these three transcripts through alternative splicing and different start codons (Balakrishnan and Jayandharan, 2014). Finally, an alternative ORF in *cap* encodes assembly-activating protein (AAP), which interacts with proteins VP1-3, contributing to capsid assembly (Sonntag et al., 2010).

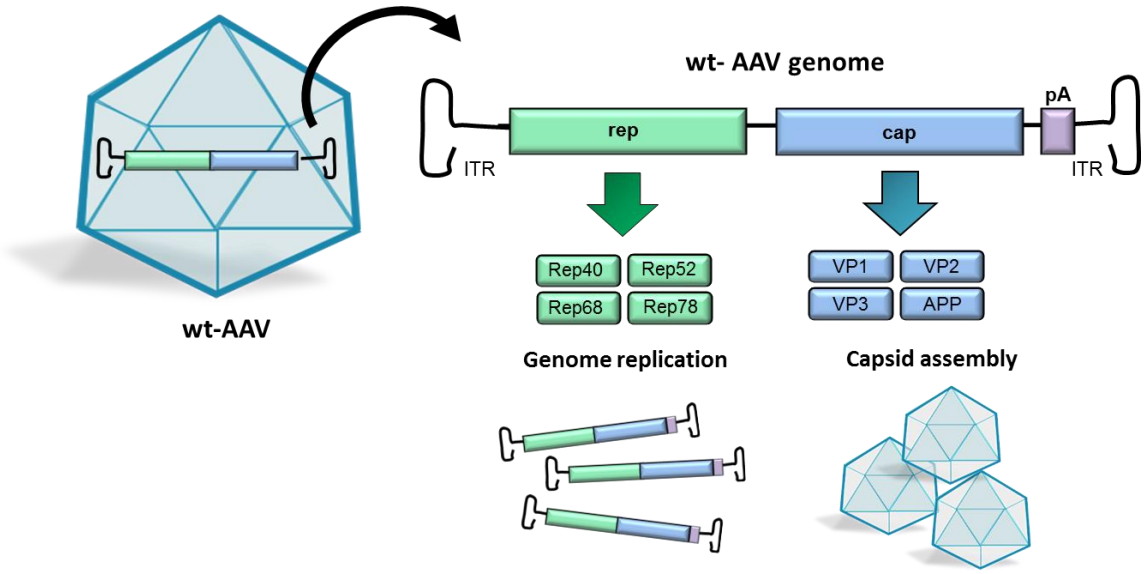

Figure 1.6 – Schematic representation of wild-type AAV, the respective genome and encoded proteins. Representation of the wild-type adeno-associated virus (WT-AAV) genome, containing two ORFs (rep and cap), a polyadenylation site (pA), and two inverted terminal repeats (ITRs). The rep ORF encodes Rep 40, 52, 68 and 78, which are required for AAV replication. The cap ORF generates proteins VP1-3, which assemble to form the AAV capsid. AAP (assembly-activating protein), which derives from an alternate ORF in cap, also contributes to capsid assembly.

AAV natural serotypes

Over the last years, twelve natural serotypes and more than 100 variants of AAVs have been isolated from humans and other primates (Gao et al., 2004). Different serotypes are defined by capsid protein motifs that are not recognized by the same neutralizing antibodies. Besides antigenicity, AAV serotypes present characteristic properties concerning capsid-receptor interactions. In fact, certain exposed capsid regions define interactions with the principal AAV receptors, which are cell surface glycans, and also with co-receptors. For example, AAV2 binds heparin sulfate proteoglycans, whereas AAV9 requires N-terminal galactose residues (Shen et al., 2011; Summerford and Samulski, 1998). These differences in receptor-affinity patterns are important in determining the preferential tissue tropism of AAV serotypes. For instance, AAV 8 and 9 preferentially target the liver (Inagaki et al., 2006), while AAV 4 exhibits a particularly efficient transduction in the eye (Weber et al., 2003). Table 1.5 summarizes the principal properties of AAV serotypes, including their origin, receptors and preferential tissue tropism.

Table 1.5: Principal properties of AAV1-9

Serotype	Origin	AAV receptors		Tissue tropism a)
		Primary Receptor	Co-receptor	
AAV1	NHP	α2,3/α2,6 *N*-linked SA	?	**SM, CNS**, heart, lung, eye, pancreas
AAV2	Human	HSPG	FGFR-1; HGFR;Integrin; LamR	**Kidney**, SM, CNS, liver, eye
AAV3	NHP	HSPG	FGFR-1; HGFR; integrin; LamR	SM, HCC
AAV4	NHP	α2,3 *O*-linked SA	?	**Eye**, CNS
AAV5	Human	α2,3 *N*-linked SA	PDGFR	**CNS, lung, eye,** SM
AAV6	Human	α2,3/α2,6 N-linked SA/ HSPG	EGFR	**SM (IV), heart**, lung
AAV7	NHP	?	?	**SM**, eye, CNS, liver
AAV8	NHP	?	LamR	**Liver, SM, CNS, eye, pancreas, heart**
AAV9	Human	N-linked Galactose	LamR	**Liver, lung, SM (IV), heart (IV), CNS (IV),** pancreas, eye, kidney (IV)

NHP - Non-human primates; SA – sialic acid; ? – Unknown; HGFR - hepatocyte growth factor receptor; LamR – Laminin Receptor; FGFR1 - fibroblast growth factor receptor 1; HSPG - Heparan sulfate proteoglycan; EGFR - epidermal growth factor receptor; PDGFR - platelet-derived growth factor receptor; SM- skeletal muscle; HCC- hepatocellular carcinoma; a) Preferential tissue tropism in mammals following local delivery. When indicated (IV), this tropism was also observed upon intravenous injection. The tissues for which each serotype is considered the preferential one are written in bold.

Adapted from: (Balakrishnan and Jayandharan, 2014; Lisowski et al., 2015; Miyake et al., 2012; Murlidharan et al., 2014; Nonnenmacher and Weber, 2012; Vandenberghe et al., 2009; Wu et al., 2006; Zincarelli et al., 2008).

1.3.2. Recombinant AAVs (rAAVs) for gene delivery

Production of rAAVs

The relative simplicity of the wild-type AAV genome facilitates the design of recombinant AAVs (rAAVs) as gene therapy vectors. The process of rAAV production generally involves transient triple transfection of HEK293 cells (illustrated in Figure 1.7). This method results in the production of rAAV vectors with a total packaging capacity of 4.7 kb (Dong et al., 2010), carrying the transgene of interest and no viral coding sequences.

AAV2 was the first to be developed into recombinant vectors for transgene delivery (Samulski et al., 1982). Recently, rAAVs originated from all 12 natural serotypes have been generated, showing different properties. Most of them have been developed by pseudotyping i.e. the cross packaging of the AAV genome (normally from AAV2) between various serotypes (Rabinowitz et al., 2002). Vector engineering has also been crucial so that AAVs acquire novel biomedically valuable properties through two main methods: rational design and directed evolution (reviewed in (Kotterman and Schaffer, 2014)).

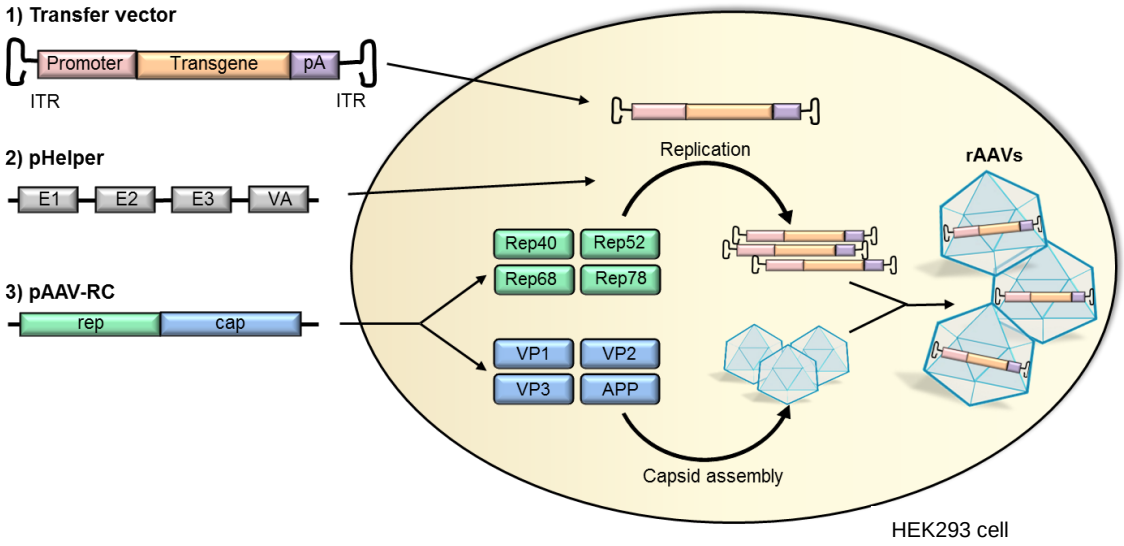

Figure 1.7 – Representation of recombinant AAV (rAAV) production process, through transient triple transfection of HEK293 cells. HEK293 cells are transfected using three plasmids: 1) the transfer vector, containing an ITR-flanked expression cassette consisting of a promoter, the transgene of interest and a poly-adenylation signal (PolyA) or a string of five thymidines to terminate transcription from pol II and pol III promoters, respectively (Xiao et al., 1997); 2) the helper plasmid (pHelper), containing adenoviral regions E1, E2, E3 and VA, which contribute to genome replication (Collaco et al., 1999) and 3) the pAAV-RC plasmid containing rep and cap genes that mediate genome replication and capsid assembly respectively. After replication and capsid assembly, the genome is packaged into an AAV capsid, resulting in new virus formation. *ITR – inverted terminal repeat; pA - poly(A) tail*

rAAV cellular transduction

Successful transduction by AAV vectors depends on cell surface receptor binding and several subsequent steps, such as: endocytic uptake, endosomal escape, nuclear entry, capsid uncoating, genome release, second strand synthesis and finally transcription (Balakrishnan and Jayandharan, 2014; Murlidharan et al., 2014), as illustrated in Figure 1.8). rAAV genome predominantly persists in the host cell as stable and circular extrachromosomal episomes (McCarty et al., 2004). Therefore, the frequency of integration into the host genome is extremely low.

rAAV cellular transduction greatly depends on host factors, which can positively or negatively affect vector efficiency (Mano et al., 2015). Curiously, a very recent study by Pillay et al. has identified a particular transmembrane protein (KIAA0319L) as an essential factor for AAV infection, independently of the serotype (Pillay et al., 2016). Therefore, the authors designated this protein as a universal AAV receptor. Moreover, Cervelli et al. has identified an inhibitory action for DNA-damage-response proteins in rAAV transduction. Upon nuclear entry, rAAV DNA was found to accumulate in discrete foci, in close proximity to foci containing these host proteins, which then bind to incoming AAV genomes, thereby restricting rAAV transduction (Cervelli et al., 2008). On the other hand, cellular DNA recombination and repair components might induce a subsequent positive effect, contributing to rAAV circular episomal generation (Choi et al., 2006).

The fact that second-strand synthesis is necessary for AAV cellular transduction might induce a delay in transgene expression (around 2 weeks for maximum expression), conferring a disadvantage when compared to other vectors (Ferrari et al., 1996). Self-complementary AAV vectors (scAAV) overcome this limitation as they carry double-stranded DNA genomes that become transcriptionally active immediately upon decapsidation in the nucleus. Noteworthy, several studies have reported a significantly higher transduction efficiency for scAAVs when compared to ssAAVs (McCarty et al., 2003; McCarty et al., 2001) (e.g. 80-fold increase in the liver (Wu et al., 2008)). The double-stranded nature of the scAAV vector also means that transgene capacity is reduced to about 2.2kb (McCarty et al., 2001), which is roughly half of single-stranded AAV vectors.

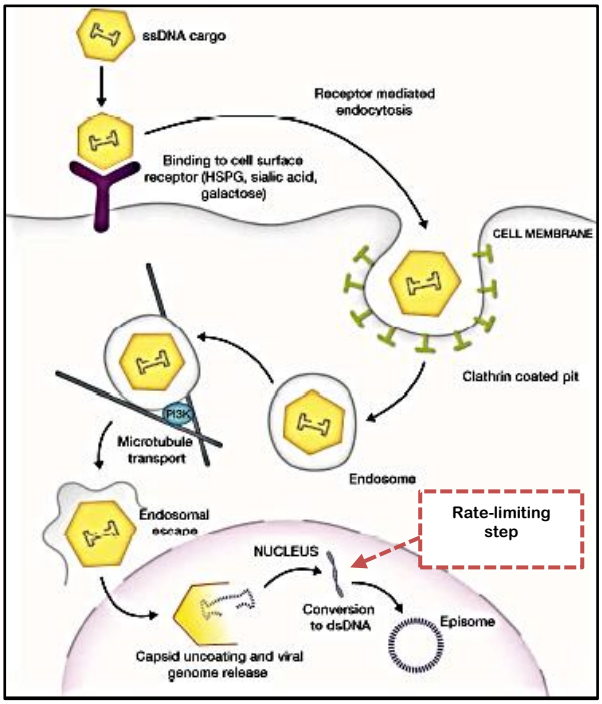

Figure 1.8: Representation of the principal steps involved in rAAV cellular transduction. Following interaction with the cell surface receptor, rAAV vectors get internalized and encapsulated in endosomes. Then, they enter the nucleus, leading to capsid uncoating, viral genome release and second strand DNA synthesis. This later process is considered a rate-limiting step, which can be bypassed when using self-complementary AAVs. Finally, rAAV genomes are maintained in the cell as extrachromosomal episomes. Adapted from: (Choudhury et al., 2016b)

1.3.3. rAAVs for CNS gene therapy

General advantages

Ideally, vectors for CNS gene delivery should present: i) an effective transduction and no off-target effects; ii) suitable transgene expression levels and duration, in order to induce a therapeutic effect in the absence of cellular toxicity; iii) lack of pathogenicity and immunogenicity, leading to no adverse responses to the treatment; and iv) large-scale efficient vector production, with high purity levels (Lentz et al., 2012).

Many AAV properties fit these requirements, explaining why this vector system is currently the most used in CNS preclinical and clinical studies. In fact, AAVs transduce both mitotic and post-mitotic cells. Additionally, most AAV serotypes present neuronal tropism, as indicated in Table 1.6, while some are also able to transduce other CNS cell types, such as astrocytes (Davidson et al., 2000). Another advantage of this system is the stable transgene expression in CNS for the lifespan of mice (Miyake et al., 2011), at least 8 years in non-human primates (Hadaczek et al., 2010) and 10 years in the human brain (Leone et al., 2012). This persistent gene expression in non-dividing cells explains why rAAVs are so suitable for gene therapy of CNS disorders, which are mostly chronic and affect post-mitotic cells.

In summary, AAV vectors offer the opportunity of permanently correcting a disease through a single administration. Furthermore, no significant adverse effects have been observed, since AAVs are non-pathogenic, leading to diminished inflammatory and immune responses (Bessis et al., 2004; Murrey et al., 2014). In addition, rAAV cell infection results mainly in episomal transgene expression, consequently reducing the risk of insertional mutagenesis (McCarty et al., 2004), an important safety concern for integrating viral vectors such as lentiviruses. Finally, efficient and scalable methods for rAAV production and purification provide encouragement for future investigation and clinical applications (Miyake et al., 2012).

rAAV CNS transduction

The ability of rAAVs to target the CNS has been extensively studied using different delivery routes. When injected directly into the brain parenchyma of adult rodents, AAV serotypes exhibit different CNS transduction efficiency and cellular tropism. Several comparative analyses have revealed that most of the serotypes are superior to AAV2, as they transduce larger CNS areas and present higher transgene expression levels upon intraparenchymal injection, such as AAV5, AAV7, AAV8 (Aschauer et al., 2013; Taymans et al., 2007) and particularly AAV9, which shows the highest vector distribution throughout the CNS (Cearley and Wolfe, 2006). Furthermore, the great majority of rAAV serotypes transduce almost exclusively neurons (Cearley and Wolfe, 2006). AAV4, on the contrary, preferentially targets ependymal cells, whereas AAV1 and AAV5 efficiently transduce both neurons and glial cells (Davidson et al., 2000; Wang et al., 2003).

One important pathway that might facilitate vector spread within the CNS is axonal transport, following a retrograde and/or anterograde direction. In this way, viral vectors are transported across synaptic connections, ultimately transducing spatially distinct neuronal subpopulations. AAV9, for instance, undergoes both anterograde and retrograde transport, which might contribute to its wide distribution throughout the CNS (Castle et al., 2014). This feature has recently been observed in non-human primate brain (Green et al., 2016).

Finally, Zhang and Yang et al. (Yang et al., 2014a; Zhang et al., 2011) evaluated CNS transduction after intravenous injection in neonatal and adult mice respectively. Based on the results obtained in newborn animals, the different serotypes can be ranked according to their performance in the

following order: 1) AAV9, which displays the greatest CNS transduction efficiency; 2) AAV 1, 6, 7, 8 which show moderate transduction levels and 3) AAV2 and 5, for which the authors only observed small populations of transduced cells. Following this type of administration, AAV serotypes are able to transduce both neurons and astrocytes (Miyake et al., 2011; Zhang et al., 2011).

To summarize, Table 1.6 provides a direct comparison between the most commonly used rAAVs (rAAV 1-9), their ability to target the CNS after intraparenchymal/intravenous injections, as well as their ability to undergo axonal transport.

Table 1.6: Principal properties of rAAV1-9 as CNS delivery vectors

Serotype	CNS transduction				
	Upon intraparenchymal injection in adult mice		Upon IV injection in neonatal mice		Axonal transport
	Level of transduction	Cellular tropism	Level of transduction	Cellular Tropism	
AAV1	++	Neurons + glia	+	Neurons + glia	R
AAV2	+	Neurons	-	-	A
AAV3	?	?	?	?	?
AAV4	+	Ependymal cells	?	?	?
AAV5	+++	Neurons + glia	-	-	R
AAV6	++	?	+	Neurons + glia	R
AAV7	+++	Neurons	+	Neurons + glia	?
AAV8	+++	Neurons	+	Neurons + glia	A, R
AAV9	+++	Neurons	++	Neurons + glia	A, R

IV- intravenous; - : no significant transduction; + : low levels; ++ : moderate levels; +++ : high levels; A - anterograde transport; R - retrograde transport.
Adapted from: (Aschauer et al., 2013; Burger et al., 2004; Cearley and Wolfe, 2006; Davidson et al., 2000; Miyake et al., 2011; Taymans et al., 2007; Yang et al., 2014a; Zhang et al., 2011)

rAAVs in CNS clinical studies

Due to their unique properties, AAVs have been extensively investigated in the context of human gene therapy. Accordingly, the first commercially available gene therapy product in Europe (2012) was an AAV1-based strategy for lipoprotein lipase deficiency (Glybera). Moreover, several clinical trials already reported stable FIX (coagulation factor IX) expression in hemophilia B patients following AAV-based therapy (High et al., 2014). These encouraging results opened the way to extensive investigation regarding the therapeutic impact of rAAVs in other diseases, namely affecting the CNS.

As depicted in Table 1.7, AAV administration has been tested for a wide range of CNS disorders. Considering all the clinical trials performed so far, intraparenchymal AAV2 injection is still the most commonly used method, although other serotypes (AAVrh.10, AAV1, AAV5 and AAV9) and delivery routes (intravenous and intramuscular) are now emerging as potential alternatives.

Table 1.7 – Summary of clinical trials for CNS disorders using rAAVs

Disease classification	Disease	Serotype	Route and local of administration	Transgene (cDNA)	Clinical Trial (Phase)	Identifier
Motor neuron diseases	**Spinal Muscular Atrophy type 1 (SMA)**	AAV9	Intravenous	*SMN*	Phase I	NCT02122952
Lysosomal storage disorders	**Batten Disease**	AAV2	Intraparenchymal (Cortex)	*CLN2*	Phase I	NCT00151216
		AAVrh.10	Intraparenchymal	*CLN2*	Phase I and II	NCT01414985 NCT01161576
	MPSIIIB (Sanfilippo syndrome B)	AAV5	Intraparenchymal	*NAGLU*	Phase I and II	ISRCTN19853672 http://www.isrctn.com
Glycogen storage disorders	**Pompe disease**	AAV9	Intramuscular (Tibialis anterior muscle)	*GAA*	Phase I	NCT02240407
		AAV1	Intramuscular (Intradiaphragmatic)	*GAA*	Phase I and II	NCT00976352
Idiopathic Neuro degenerative disorders	**Alzheimer's disease**	AAV2	Intraparenchymal (Basal forebrain)	*NGF*	Phase I and II	NCT00087789 NCT00876863
	Parkinson's disease	AAV2	Intraparenchymal (Subthalamic nucleus)	*GAD*	Phase I and II	NCT00195143 NCT00643890 NCT01301573
		AAV2	Intraparenchymal (Putamen)	*NTN*	Phase I and II	NCT00252850 NCT00400634 NCT00985517
		AAV2	Intraparenchymal (Putamen)	*GDNF*	Phase I	NCT01621581
		AAV2	Intraparenchymal (Striatum)	*AADC*	Phase I and II	NCT00229736 NCT02418598 NCT01973543
Monoamine neurotransmitter disorders	**Aromatic L-amino Acid Decarboxylase (AADC) Deficiency**	AAV2	Intraparenchymal (Putamen)	*AADC*	Phase I and II	NCT01395641
Leuko-Dystrophies	**Canavan disease**	AAV2	Intraparenchymal (Frontal, periventricular and occipital lobes)	*ASPA*	Phase I	(McPhee et al., 2006)

SMN - Survival of Motor Neuron; CLN2 - Tripeptidyl Peptidase-I; NAGLU - α-N-acetylglucosaminidase; GAA - Acid alpha-glucosidase; NGF - Nerve Growth Factor; GAD - Glutamate decarboxylase; NTN - Neurturin; GDNF - Glial Derived Neurotrophic Factor; AADC - Aromatic L-Amino Acid Decarboxylase; ASPA- Aspartoacylase.
Data obtained from clinicaltrials.gov (on 24- 07-2016).

1.3.4. Routes of rAAV administration to the CNS

Intraparenchymal injection has been the most commonly used route of administration of AAV vectors to the CNS in the majority of clinical studies (Table 1.7). The direct delivery into the brain parenchyma circumvents the blood-brain barrier, but leads to poor vector spread (1-3 mm), and as a result transgene expression is limited to the site of injection (Vite et al., 2003). This is an important limitation for many neurodegenerative disorders that affect large regions of the CNS, such as lysosomal storage disorders, Alzheimer's disease and MJD. Additionally, each injection requires a craniotomy and general anesthesia, associated with the risk of hemorrhaging and pathogen contamination. Accordingly, a clinical study for Parkinson's disease (NCT00400634) has reported serious side effects related to this surgical procedure (Marks et al., 2010).

Taking this into account, the ideal alternative would correspond to a non-invasive procedure that enables widespread vector distribution in the CNS. A possible solution is to infuse AAV vectors into the cerebrospinal fluid (CSF). This can be done through intracerebroventricular (ICV), intra-

cisterna magna (ICM) or lumbar intrathecal injections (IT), as illustrated in Figure 1.9, with the latter being the least invasive and consequently the most attractive for clinical applications. Moreover, intramuscular injection is considered a suitable approach to motor neuron diseases treatment. In fact, some AAV vectors can be taken up by nerve terminals and undergo retrograde transport to motor neurons soma in the spinal cord (Benkhelifa-Ziyyat et al., 2013). Finally, intravascular injection is also a promising alternative, being generally divided into intra-arterial (e.g. intracarotid or intrafemoral) and intravenous (IV) routes, as depicted in Figure 1.9.

Huda et al. have directly compared three distinct AAV delivery routes: intraparenchymal, intra-CSF (intra cisterna-magna) and intravascular (intravenous). Taken all together, the authors demonstrated that intraparenchymal administration is the preferred route to achieve strong but localized transgene expression. When comparing intra-CSF with intravenous injections, they concluded that intrathecal injection resulted in overall higher transgene expression levels, but in a more restricted CNS region. Therefore, although requiring higher doses, intravenous injection would be preferential to achieve widespread vector distribution (Huda et al., 2014). Additionally, this delivery route exhibits the great advantage of being minimally invasive and therefore considered the ideal one for clinical trials. Nevertheless, intravascular AAV administration efficiency greatly depends on vector ability to cross the blood-brain barrier (BBB).

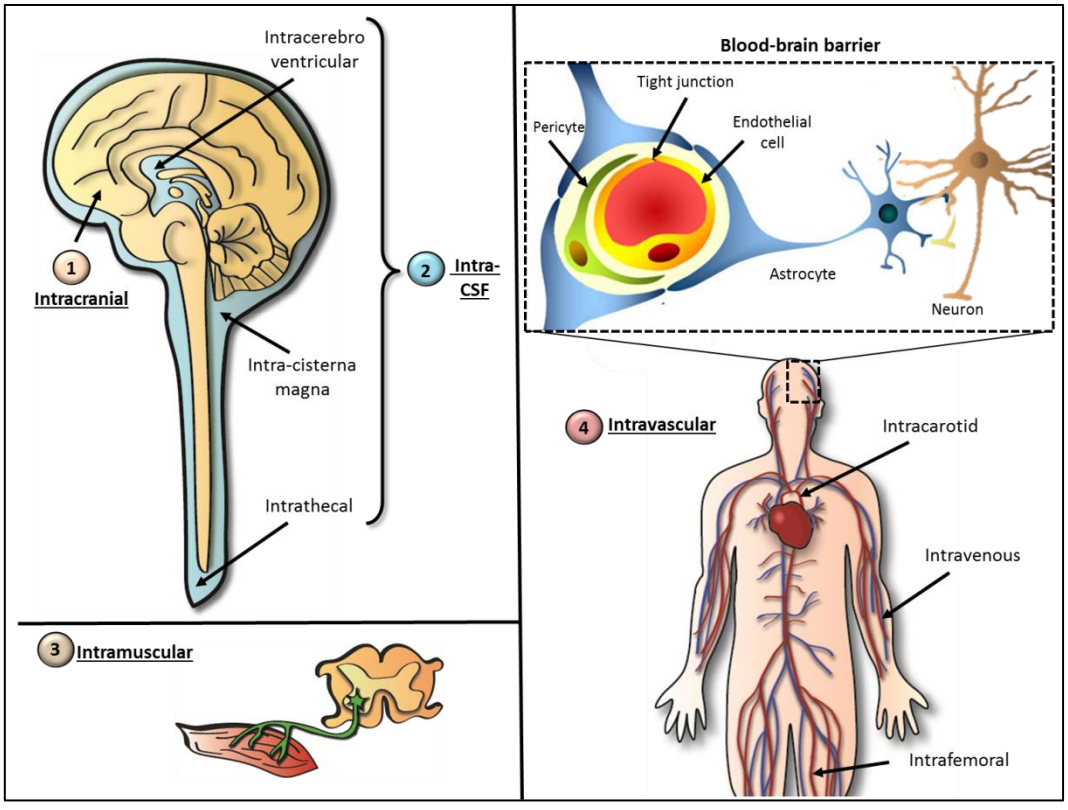

Figure 1.9 – Possible routes of rAAV administration to the CNS. 1) Intraparenchymal injection; 2) Administration into the CSF: intrathecal, intra-cisterna magna and intracerebroventricular injections; 3) Intramuscular administration; 4) Intravascular delivery: intravenous, intracarotid and intrafemoral administration. In order to get access to the CNS, intravascular injected vectors have to circumvent the blood-brain barrier. Adapted from: (Abbott, 2013)

1.3.5. The blood-brain barrier (BBB) as an obstacle to intravascular delivery

The blood-brain barrier (BBB) is an essential interface between blood circulation and the central nervous system. This barrier is formed by the endothelial cells lining brain microvessels as well as the surrounding pericytes and astrocytic end feet (Figure 1.9). BBB's normal function is crucial to maintain brain homeostasis, since it mediates the selective transport of essential molecules, while protecting from potentially harmful compounds. Accordingly, the tight junctions between endothelial cells form an efficient physical barrier, restricting paracellular transport. Additionally, the presence of specific transport systems, enzymes and receptors further limits traffic across BBB (Abbott, 2013; Abbott et al., 2006).

By acting as a highly selective barrier, BBB precludes drug transport from the blood to the CNS. Therefore, recent research has developed new methods to circumvent this barrier and enhance rAAV delivery to the brain after intravascular administration. Transient BBB permeabilization through osmotic disruption (e.g. using mannitol) (Burger et al., 2005; McCarty et al., 2009) and focused ultrasound in combination with microbubbles (FUS) (Hsu et al., 2013; Marquet et al., 2014) have already shown successful results. Nevertheless, both pharmacological and physical strategies used to disrupt the BBB may induce adverse effects and hamper future clinical progresses (Berger et al., 1995; van Hengel et al., 1997). As a result, the ideal alternative would be to use a delivery route with the natural ability to cross the BBB, maintaining the integrity of this barrier.

1.4. Non-invasive gene delivery to the CNS using AAV9

Despite all the advantages of systemic AAV delivery, this method has been hindered by the fact that most serotypes cannot circumvent the BBB. As indicated in Table 1.6, intravenous administration does not induce an efficient CNS transduction for most of the known serotypes.

Therefore, the discovery that a particular serotype, AAV9, has the natural ability to bypass the BBB has expanded the applications of intravenous AAV administration in CNS gene therapy. Importantly, this characteristic has already been shown in different animal models and time points, although with distinct cellular tropisms. Numerous preclinical studies have explored AAV9 IV injection in CNS disorders with successful results, suggesting a similar approach for MJD.

1.4.1. AAV9 ability to cross the BBB

Foust and Duque et al. firstly demonstrated that AAV9 circumvents the BBB in both neonatal and adult mice, leading to widespread CNS gene expression (Duque et al., 2009; Foust et al., 2009). The mechanism AAV9 uses to cross the BBB is still unknown. However, according to Manfredsson, besides binding to terminal N-linked galactose receptors, AAV9 might interact with protein transporters, which normally mediate the movement of several molecules from the blood to the

brain (e.g. monocarboxylate transporter 1 for lactate (MCT1) or glucose transporter GLUT1) (Manfredsson et al., 2009), explaining its BBB-crossing ability.

Although this property is not restricted to AAV9 (Zhang et al., 2011) (Yang et al., 2014a), this serotype has been the most widely studied vector for IV delivery, since it induces higher transgene expression levels and more widespread transduction throughout the CNS than other candidates. During the course of this work, two particular studies have focused on the optimization of these features (Choudhury et al., 2016a; Deverman et al., 2016) by introducing alterations in the AAV9 capsid and generating new rAAV variants with superior CNS transduction levels following systemic administration. These findings indicate that AAV9 characteristics are extremely advantageous for non-invasive CNS delivery and could still be optimized in the future.

1.4.2. Neonatal versus adult IV injection

Although able to cross the BBB independently of the animal age, AAV9 exhibits different transduction profiles in the CNS after IV administration to newborn or adult subjects.

Several studies have investigated AAV9 CNS cellular tropism in rodents after intravenous injection and showed different profiles depending on the animal age. When intravenously administered to nenonatal mice, AAV9 vectors have consistently shown: efficient transduction of neurons and astrocytes in multiple brain regions and a significant preference for motor neurons (MNs) in the spinal cord (Foust et al., 2009; Miyake et al., 2011; Rahim et al., 2011; Wang et al., 2010). On the other hand, for IV injection performed in adult rodents, rAAV9 has shown a predominant astroglial transduction in the CNS (Foust et al., 2009). Nevertheless, significant transgene expression can still be achieved in spinal cord MNs (Duque et al., 2009) and several neuronal populations in the brain (Gray et al., 2011). Although the literature shows no clear consensus in what concerns AAV9 ability to target neurons in adult mice, all studies point towards the same conclusion: neuronal transduction efficiency declines with age. Accordingly, earlier stages of development (postnatal days 1-10) are considered the most suitable periods to induce therapeutic effects directed to mouse neurons.

Similar studies have been performed in other animal models. For instance, Duque et al. have reported efficient transduction of spinal cord MNs in neonate and adult cats, following AAV9-IV injection (Duque et al., 2009). The percentage of AAV9-positive cells also proved to decrease when the injection is performed at later stages.

Subsequently, several authors assessed whether the same outcome occurs in non-human primates (NHPs). In this context, it has been shown that AAV9 bypasses the BBB and efficiently transduce neurons after IV delivery to neonatal rhesus macaques (Foust et al., 2010). Moreover, reports from Dehay and Gray consistently matched the results obtained in mice: widespread neuronal transduction in the brain following injections at P1, in contrast to glial preference when administration is performed in juvenile NHPs (Dehay et al., 2012; Gray et al., 2011).

In summary, the previously described studies were a major breakthrough in the field since: i) they consistently corroborated the possibility of CNS gene transfer through a non-invasive systemic delivery route and ii) they revealed AAV9 natural tropism to CNS upon IV injection using different models (rodents, cats and non-human primates) and administration times.

1.4.3. Preclinical studies for CNS using AAV9 IV administration

The discovery of AAV9 ability to cross BBB was the starting point for an extensive investigation regarding its therapeutic effect in the CNS after intravenous administration, as depicted in Table 1.8. A wide range of neurological disorders have been proved to benefit from this treatment, which can be useful to: i) restore a faulty gene, as in the case of of lysosomal storage disorders and Spinal Muscular Atrophy type 1; ii) to introduce a disease-modifying gene that might alleviate neuropathology, as investigated for Alzheimer's disease; iii) to silence the disease-causing gene, as reported for Huntington's disease and amyotrophic lateral sclerosis.

The results reported for Spinal Muscular Atrophy type 1 (SMA1) have been extremely important in the field. Several studies have investigated the impact of rAAV9 encoding *SMN1* (survival of motor neuron 1), particularly through systemic administration in neonatal transgenic mice. Firstly reported by Foust et al., this therapy resulted in significant improvements regarding motor function, neuromuscular physiology and life span, by increasing SMN levels in the spinal cord, brain and muscles. However, the therapy had maximal benefit in a particular developmental period, showing little effects when the injection was performed at postnatal day 10 (Foust et al., 2010). Contemporary studies confirmed the beneficial effects of rAAV9-SMN1 delivery in SMA neonatal mice (Dominguez et al., 2011; Valori et al., 2010). Notably, subsequent experiments exploring rAAV9 ability to transduce spinal cord MNs and other tissues in large animal models after systemic administration have provided confidence for translation to human patients (Bevan et al., 2011; Foust et al., 2010). All of these studies culminated in the first clinical trial approved for the test of rAAV9 in neurodegenerative disorders (NCT02122952) (see Table 1.7). This Phase I dose escalation study (10^{13}-10^{14} vg/kg) is currently recruiting type 1 SMA patients, namely infants with less than 9 months. The main goal is to test the efficiency and safety of a single rAAV9-SMN intravenous delivery. This revolutionary step might be crucial to evaluate the therapeutic impact directly on humans and define ideal viral doses for future treatments.

Focusing on the gene silencing approaches, important results have been reported particularly for Amyotrophic Lateral Sclerosis (ALS) and Huntington's disease. Accordingly, Foust et. al have developed rAAV9 vectors encoding a shRNA against SOD1 as a potential therapeutic tool for familial ALS. Following intravenous administration of this vector into two distinct ALS mouse models, at different time points (P1, P21, P85, P215), the authors reported a delay in disease onset, prolonged survival and motor function improvements. Interestingly, beneficial effects were observed even when treatment was initiated after disease onset, although the best results corresponded to earliest intervention (P1) (Foust et al., 2013).

Similarly, Dufour et al. have tested the impact of rAAV9 vectors encoding an artificial microRNA against huntingtin as a potential treatment for Huntington's disease. Following intrajugular vein injection into 3 week-old transgenic mice, the authors observed a significant silencing effect in several affected brain regions as well as peripheral tissues. Consequently, this treatment successfully prevented neuropathological signs, such as inclusion bodies formation, neuronal death and striatal and cortical atrophy. Moreover, rAAV9-miR treatment had a positive impact on body weight. However, no behavioral improvements were reported, suggesting that i) this vector dose (7.5×10^{10} per gram body weight (vg/gram bw)) was not sufficient to prevent motor defects or that ii) the treatment should be performed at an earlier age, to maximize rAAV9 neuronal tropism (Dufour et al., 2014).

Overall, these findings demonstrate the versatility of rAAV9-IV injection in CNS gene therapy, as it induces positive effects using different therapeutic strategies and injection time points. In particular, the positive outcomes reported after RNAi delivery greatly encourage the exploitation of this therapeutic option in other CNS disorders, such as MJD.

Table 1.9 – Description of preclinical studies using AAV9 IV injection for CNS gene therapy.

Disease class	Disease	Genetic cause (Neuropathology)	Animal model Age	Time of injection	Transgene	Result	Ref
Motor neuron diseases	**SMA1**	**Mutations in *SMN1*** (MN death)	**Mouse** Neonatal	P1	*SMN*	Survival of MN, rescue of neuromuscular physiology and life span	(Dominguez et al., 2011; Foust et al., 2010; Glascock et al., 2012; Valori et al., 2010)
			Mouse Neonatal	P1	**shRNA-PTEN**	Phenotype improvement and survival extension	(Little et al., 2015)
	SMARD1	**Mutations in *IGHMBP2*** (MN death)	**Mouse** Neonatal	P1	*IGHMBP2*	Motor improvements, NM physiology normalization. Life span extension	(Nizzardo et al., 2015)
	ALS	**Familial: Mutations in *SOD1*** (MN death)	**Mouse** Neonatal Juvenile	P1, P21, P85	**shRNA-SOD1**	Delay of disease onset, behavioral improvements and survival extension	(Foust et al., 2013)
			Mouse Adult	P215		Slow disease progression, survival extension	
		Sporadic: ADAR2 downregulation (MN death)	**Mouse** Adult	9–15 Weeks	*ADAR2* (SynI)	Prevention of motor dysfunction and neuronal death. Behavior improvements	(Yamashita et al., 2013)
PolyQ diseases	**HD**	**Mutation in *HTT*** (Inclusions and neurodegeneration)	**Mouse** Juvenile	3 weeks	**miRNA-HTT**	Prevention of CNS and peripheral pathology, decrease in weight loss. No behavioral improvements	(Dufour et al., 2014)
	MJD	**Mutation in *MJD1/ATXN3*** (Inclusions and neurodegeneration)	**Mouse** Neonatal	P1-2	*CRAG* (MSCV)	Prevention of mutant ataxin-3 aggregation, improved dendritic differentiation	(Konno et al., 2014)
Neuro-developmental disorders	**Rett Syndrome**	**Mutations in *MECP2*** (Neuro-development problems)	**Mouse** Juvenile	4-5weeks	*MECP2*	Modest effect in survival and synaptic defects	
			Mouse Adult	10-12 months		Rescue of behavioral and cellular deficits	(Garg et al., 2013)
Lysosomal storage disorders	**MPSIIIA**	**Mutations in *SGSH*** (CNS and peripheral problems)	**Mouse** Adult	2 months	*SGSH*	Reduction in neuroinflammation and lifespan extension	(Ruzo et al., 2012)
	MPSIIIB	**Mutations in NAGLU** (CNS and peripheral problems)	**Mouse** Juvenile	4–6 weeks	*NAGLU*	Amelioration of neuropathology. Improvement in behavior and longevity	(Fu et al., 2011)
	MPS VII	**Mutations in *GUSB*** (CNS and peripheral problems)	**Dog**	P3	*GUSB*	Reduction in GAGs accumulation and inflammation	(Gurda et al., 2015)
	GM1	***GLB1* mutations** (Neurodegeneration in the CNS)	**Mouse** Juvenile	6 weeks	*GLB1*	Phenotypic amelioration and extension in lifespan	(Weismann et al., 2015)
	Sandhoff disease	**Mutations in HEXB** (Neurodegeneration in the CNS)	**Mouse** Neonatal	P1-P2	*HEXB*	Improvements in motor activity and longevity.	(Walia et al., 2015)
			Mouse Adult	6 weeks			
	MSD	**Mutations in *SUMF1*** (CNS and peripheral problems)	**Mouse** Neonatal	P1-2	*SUMF1*	Decrease of inflammation and behavioral improvements	(Spampanato et al., 2011)
	MLD	**Mutations in *ASA*** (Myelin degradation)	**Mouse** Neonatal	P0-P1	*ASA*	Correction of neuropathology. Behavioral improvements	(Miyake et al., 2014)
Peroxisomal disoders	**X-ALD**	**Mutations in *ABCD1*** (VLCFA increase, neurodegeneration)	**Mouse** Juvenile	6-8 weeks	*ABCD1*	Decrease in CNS VLCFA accumulation	(Gong et al., 2015)
Idiopathic diseases	**AD**	Accumulation of amyloid-β in the brain	**Mouse** Adult	7–9 months	*NEP* (SynI)	Decrease in Aβ accumulation and alleviation of cognitive dysfunction	(Iwata et al., 2013)

SMA1 – Spinal Muscular Atrophy type 1; SMARD - Spinal Muscular Atrophy with respiratory distress type 1; ALS – Amyotrophic Lateral Sclerosis; HD – Huntington's disease; MJD – Machado-Joseph disease; MPS – Mucopolysaccharidosis; GM1 - GM1-gangliosidosis; MSD - Multiple sulfatase deficiency; MLD - metachromatic leukodystrophy; X-ALD - X-linked Adrenoleukodystrophy; AD – Alzheimer's disease; CNS – central nervous system; SMN- survival of motor neuron; IGHMBP2 - Immunoglobulin Mu Binding Protein 2; SOD1 - superoxide dismutase 1; ADAR2 - RNA-editing enzyme adenosine deaminase acting on RNA2; HTT – huntingtin; MJD1/ATXN3- ataxin-3; MECP2 - methyl-CpG binding protein 2; SGSH - N-sulphoglucosamine sulphohydrolase (sulfamidase); NAGLU - α-N-acetylglucosaminidase; GUSB - Beta-glucuronidase; GLB1 - galactosidase beta 1; HEXB - beta-hexosaminidase; SUMF1 - sulfatase modifying factor 1 gene; ASA- arylsulfatase; ABCD1- ATP-binding cassette transporter. VLCFA - Very Long Chain Fatty Acids; PTEN - phosphatase and tensin homolog; SynI - synapsin I promoter; CRAG - collapsin response mediator protein-associated molecule associated guanosine triphosphatase; MSCV - Murine stem cell virus promoter; NEP – Neprilysin; MN – motor neuron; NM – neuromuscular; GAG – glycosaminoglycan.

1.4.4. Preclinical studies for MJD using AAV9 IV administration

The unique study exploring rAAV9 IV injection for MJD therapy, performed by Konno et al., has not tested a silencing approach, but instead promoted mutant ataxin-3 clearance (Konno et al., 2014). For that purpose, the authors used a single-stranded rAAV9 vector encoding CRAG, a protein known to induce proteasome degradation. In this case, the transgene was expressed under the control of MSCV promoter (murine stem cell virus), which presents strong transcriptional activity in Purkinje Cells (PCs). Viral vectors were intravenously injected in polyQ69 transgenic newborn mice (P1/2) through the jugular vein. This treatment successfully prevented important MJD-associated neuropathological signs. Accordingly, rAAV9-CRAG transduced PCs exhibited: i) a decrease in mutant ataxin-3 aggregates in number and size, ii) an arrangement into monolayers, iii) improvements in dendritic length and arborization, and iv) correction of electrophysiology and signaling defects. Nevertheless, behavioral parameters have not been evaluated in this study. Moreover, the authors only reported robust rAAV9 transduction in a single cerebellar lobule (lobule 10) in MJD transgenic mice, in contrast to the normal widespread distribution achieved in wild-type subjects. These differences in vector distribution might be possibly explained by poor vascularization in the cerebellar cortex of MJD transgenic mice, as confirmed by low VEGF (vascular endothelial growth factor) expression levels.

In summary, the fact that transduction was restricted to a single cerebellar lobule was identified as the major limitation in this study. Nevertheless, Konno's work was considered a major step in MJD preclinical investigation, since it was the only one until now using: i) AAV9 as a therapeutic vector for MJD and ii) viral delivery to the blood stream instead of direct administration in the brain parenchyma.

Taking everything into account, further investigation into MJD therapy should exploit rAAV9 IV injection, due to its important advantages when comparing to the commonly used intraparenchymal injection. Moreover, AAV9 delivery of RNAi constructs to the CNS has already shown promising results in other CNS disorders, suggesting a similar strategy for MJD.

1.5. Objectives

The lack of available treatment for Machado-Joseph disease (MJD) demands further investigation towards possible therapeutic approaches, particularly based on RNA interference (RNAi) using viral vectors. Previous studies have already shown the positive impact of ataxin-3 silencing *in vivo*, but involved invasive procedures and targeted limited brain regions.

Taking all of this into account, the main goal of this project was to develop a non-invasive viral-based gene therapy for MJD. For that purpose, we generated an AAV9-mediated system encoding an artificial microRNA against mutant ataxin-3 (miR-ATXN3) and tested it in a transgenic mouse model of MD.

The specific objectives of this study were (outlined) as follows:

- to validate the designed artificial microRNA construct *in vitro*, by evaluating ataxin-3 knockdown efficiency and specificity;
- to generate recombinant AAV9 vectors encoding miR-ATXN3 (rAAV9-miR-ATXN3);
- in order to investigate the potential therapeutic impact of this strategy, systemically inject rAAV9-miR-ATXN3 into neonatal MJD transgenic mice, to:
    - Analyze rAAV9 distribution throughout the MJD mouse brain after intravenous injection;
    - Evaluate the efficiency of rAAV9-mediated cerebellar transduction;
    - Explore the effects of rAAV9 administration on MJD-associated motor and balance impairments;
    - Investigate the impact of rAAV9-miR-ATXN3 treatment in MJD neuropathological changes.

2. Materials and Methods

2.1. *In vitro* studies

shRNA lentiviral plasmids and lentiviral vector production

shRNA lentiviral plasmids have previously been produced by our group, as already described (Alves et al., 2008a; de Almeida et al., 2001). Briefly, shRNAs against mutant ataxin-3 (sh-ATXN3), i.e. targeting the SNP present in most MJD patients (C987- rs12895357) have been inserted into the 3'LTR of a lentiviral vector containing the H1 promoter.

Lentiviral vectors encoding human wild-type (LV-WT-ATXN3) and mutant ataxin-3 (LV-Mut-ATXN3), with 27Q and 72Q respectively, have previously been generated by our group in HEK293T cells with a four-plasmid system, as already described (de Almeida et al., 2001). The lentiviral particles were resuspended in 1% bovine serum albumin (BSA) in phosphate-buffered saline (PBS). The viral particle content of batches was determined by assessing HIV-1 p24 antigen levels (RETROtek, Gentaur, Paris, France). Viral stocks were stored at -80°C until use.

miRNA-based RNAi plasmids

Based on the specific silencing sequence that our group has previously shown to efficiently abrogate Machado-Joseph disease (Alves et al., 2008a; Conceicao et al., 2016b; Nobrega et al., 2014; Nobrega et al., 2013b), we designed a miR155-based artificial miRNA against mutant ATXN3 mRNA (miR-ATXN3) (Figure 2.1A). A control miRNA, whose sequence does not silence any mammalian mRNA was also designed (miR-Control). Both artificial miRNAs were subsequently cloned into a self-complementary adeno-associated virus serotype 2 backbone (scAAV2-U6-miRempty-CBA-eGFP plasmid), kindly provided by Miguel Sena-Esteves (UMass Medical School, Gene Therapy Center, Worcester, MA). This plasmid includes the enhanced green fluorescent reporter gene (EGFP) and artificial miR is driven by U6 promoter (Figure 2.1B).

Mouse neural crest-derived cell line (Neuro2a cells) culture

Mouse neural crest-derived cell line (Neuro2a cells) were obtained from the American Type Culture Collection cell biology bank (CCL-131) and maintained in DMEM medium supplemented with 10% fetal bovine serum, 100 U/ml penicillin and 100 mg/ml streptomycin (Gibco) (complete medium) at 37 °C in 5% CO2/air atmosphere.

Neuro2a cells infection

To obtain neuronal cell lines stably expressing mutant/wild type ataxin-3, Neuro2a cells were infected with lentiviral vectors encoding for full-length human mutant ataxin-3 (72Q) or the wild-type form (27Q), as previously described (Nascimento-Ferreira et al., 2011). Briefly, Neuro2a cells were incubated with the respective vectors at the ratio of 10 ng of p24 antigen/10^5 cells, in the presence of polybrene.

Neuro2a cells transfection

On the day before transfection, Neuro2a cells previously infected with wild-type or mutant ataxin-3 were plated in a twelve-well plate (180.000 cells/well). Cells were transfected with the respective plasmids: LV-sh-ATXN3, AAV-miR-ATXN3 and AAV-miR-Control, using Polyethylenimine (PEI) linear, Mw 40,000 (Polysciences, Inc., Warrington, PA, USA), as transfection reagent. Briefly, DNA:PEI complex formation was induced by mixing 10 µL of DMEM, 4 µL of PEI (1mg/ml) and 800ng of DNA. Following a 10 minute incubation at room temperature, 500 µL of DMEM complete medium were added to the mixture. Finally, Neuro2a cells were incubated with 500 µL of transfection solution per well, after removing half of the medium. Forty-eight hours after transfection, Neuro2a cells were washed with PBS1X, treated with trypsin, collected by centrifugation and stored at - 80°C.

RNA extraction, DNase treatment and cDNA synthesis

Total RNA was isolated using Nucleospin RNA Kit (Macherey Nagel, Düren, Germany) according to the manufacturer's instructions. Briefly, after cell lysis, the total RNA was adsorbed to a silica matrix, washed with the recommended buffers and eluted with RNase-free water by centrifugation. Total amount of RNA was quantified by optical density (OD) using a Nanodrop 2000 Spectrophotometer (Thermo Scientific, Waltham, USA) and the purity was evaluated by measuring the ratio of OD at 260 and 280 nm.

In order to avoid genomic DNA contamination and co-amplification, DNase treatment was performed using Qiagen RNase-Free DNase Set (Qiagen, Hilden, Germany), according to the manufacturer's instructions. Briefly, the final volume of reaction was 6 µL, containing 0.6 µL of DNase buffer, 0.25 µL of DNase and 500 ng of RNA. After a 30 minute incubation at 37 °C, 0.5 µL of 20 mM EDTA pH=8 were added to stop the reaction. The final step was a 65°C incubation for 10 minutes.

cDNA was then obtained by conversion of 420 ng of total RNA using the iScript Select cDNA Synthesis Kit (Bio-Rad, Hercules, USA) according to the manufacturer's instructions. The complete mix, with a total volume of 10 µL, was prepared using 2 µL of reaction mix (5x), 0.5 µL of iScript reverse transcriptase and the appropriate volume of RNA template and nuclease-free water. The complete reaction mix was incubated 5 minutes at 25°C, followed by 30 minutes at 42°C and 5 minutes at 85°C. After reverse transcriptase reaction, the mixtures were stored at −20°C.

Quantitative real-time PCR (qPCR)

All qPCRs were performed in an Applied Biosystems StepOnePlus Real-Time PCR system (Life technologies, USA) using 96-well microtiter plates and the SsoAdvanced SYBR Green Supermix (Bio-Rad, Hercules, USA), according to the manufacturer's instructions.

Reactions were performed in a 20 µL of final volume reaction mixture containing 10 µL of SsoAdvanced SYBR Green Supermix (Bio-Rad, Hercules, USA), 10 ng of DNA template and 500 nM of previously validated specific primers for human ataxin-3, mouse ataxin-3, mouse

glyceraldehyde 3-phosphate dehydrogenase (GAPDH) and mouse hypoxanthine guanine phosphoribosyl transferase (HPRT) according to MIQE guidelines. The PCR protocol was initiated by a denaturation program (95 °C for 30 seconds), followed by 40 cycles of two steps: denaturation at 95°C for 5 seconds and annealing/extension at 56°C for 10 seconds. The melting curve protocol started after amplification cycles, through a gradual temperature increase, from 65 to 95°C, with a heating rate of 0.5 °C/5s.

The cycle threshold values (Ct) were determined automatically by the StepOnePlus software (Life technologies, USA). For each gene, standard curves were obtained and quantitative PCR efficiency was determined by the software. The mRNA relative quantification with respect to control samples was determined by the Pfaff method. Ideal reference genes were determined using the GenEx software.

2.2. *In vivo* studies

Production of Adeno-associated viral serotype 9 (AAV9) vectors

AAV9 vectors have been kindly provided by Miguel Sena-Esteves (UMass Medical School, Gene Therapy Center, Worcester, MA). Briefly, vector stock was prepared by triple transfection of HEK293T cells with calcium phosphate precipitation of vector constructs (AAV-miR-ATXN3 and AAV-miR-Control), pFΔ6 (adenoviral helper plasmid) and AAV9 rep/cap plasmid, as previously described (Zolotukhin et al., 1999), leading to the production of rAAV9-miR-ATXN3 and rAAV9-miR-Control (Figure 2.1C). AAV9 vectors were then purified by iodixanol gradient centrifugation, followed by concentration and dialysis as previously described (Choudhury et al., 2016a). The vector titer was determined by quantitative real-time PCR (qPCR) with specific primers and probe for bovine growth hormone polyA element (pBGH).

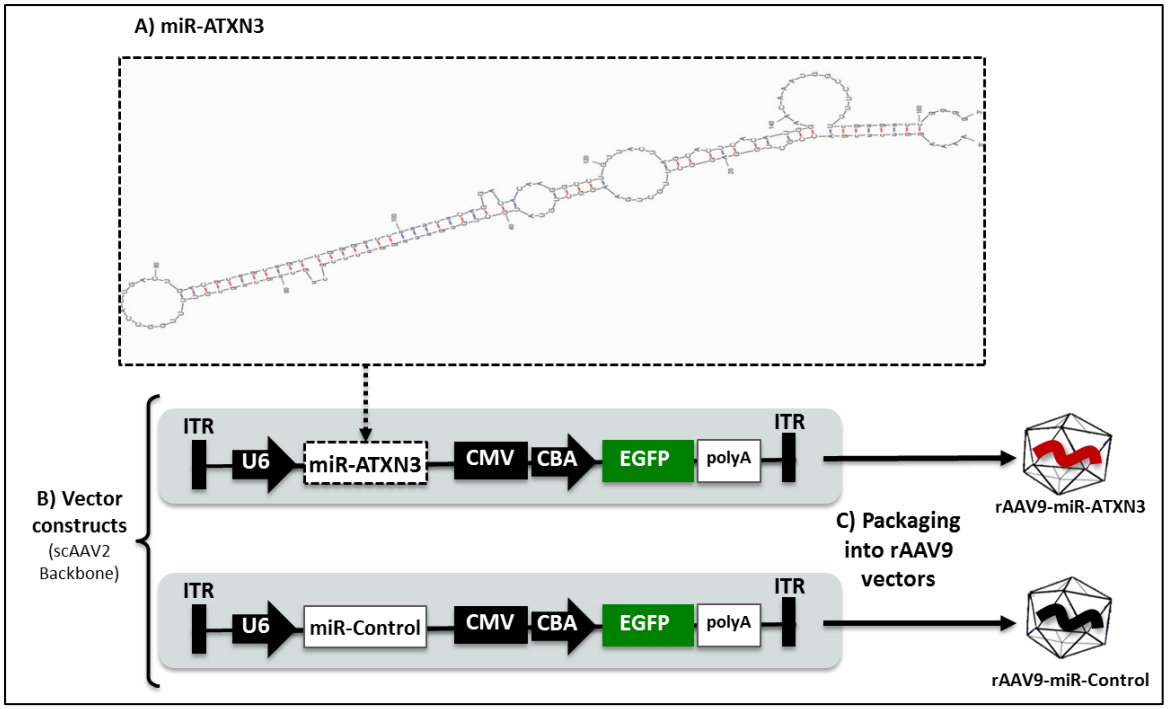

Figure 2.1: Representation of RNAi vectors targeting mutant ataxin-3. A) An artificial microRNA construct (miR-ATXN3) was designed based on the silencing sequences that our group has previously shown to specifically silence mutant ataxin-3 (Alves et al., 2008); B) miR-ATXN3 was inserted into an scAAV2 plasmid vector backbone, under the control of the U6 promoter and with enhanced green fluorescent reporter gene (EGFP). A control miRNA, whose sequence does not silence any mammalian RNA was also designed (miR-Control) and inserted into the same scAAV2 backbone. C) Both artificial miRs were subsequently packaged into recombinant AAV9 vectors, leading to the production of rAAV9-miR-ATXN3 and rAAV9-miR-Control. *CMV, Cytomegalovirus enhancer; CBA, Chicken beta-actin promoter; EGFP, Enhanced green fluorescent protein; ITR, Inverted terminal repeats.*

Animals

PolyQ69-transgenic MJD mice were used in the present study. This model expresses N-terminal-truncated human ataxin-3 with a 69 polyglutamine tract specifically in cerebellar Purkinje cells, under the control of L7 promoter (Torashima et al., 2008). Moreover, the mutant protein exhibits a haemagglutinin (HA) epitope at the amino terminus. Importantly, the transgene contains the previously identified SNP downstream of the CAG expansion (Gaspar et al., 2001), therefore showing complementary with miR-ATXN3 sequence, as depicted in Figure 2.2. Transgenic mice are characterized by an accumulation of mutant ataxin-3 in Purkinje cell layer and deep cerebellar nuclei and a pronounced cerebellar atrophy. They exhibit a severe ataxic phenotype starting at postnatal day 21.

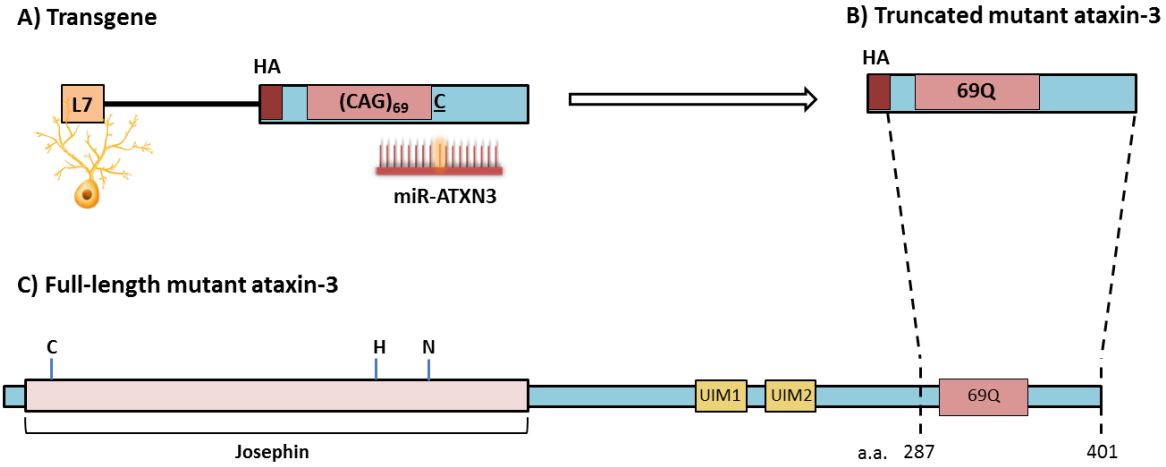

Figure 2.2: Schematic representation of: A) cDNA construct used to generate polyQ69 mice, which contains: the L7 promoter, an HA epitope, a 69 CAG expansion and the SNP (a cytosine downstream of trinucleotide repetitions). Therefore, this construct shows complementary with miR-ATXN3; B) the truncated mutant ataxin-3 expressed in transgenic mice, with 69 glutamines and an HA epitope. This protein lacks the 286 N-terminal aminoacid residues present in full-length ataxin-3, represented in C).

The transgenic mice colony (C57BL/6 background) was maintained at the animal house facility of the Centre for Neuroscience and Cell Biology (CNC) by backcrossing heterozygous males with C57BL/6 females. Animals were housed in a temperature-controlled room maintained on a 12 h light/12h dark cycle. Food and water were provided *ad libitum*. Genotyping was performed by PCR at 4 weeks of age.

The experiments were carried out in accordance with the European Community Council Directive (86/609/EEC) for the care and use of laboratory animals. The researchers received adequate training (FELASA certified course) and certification to perform the experiments from Portuguese authorities (Direcção Geral de Veterinária).

Experimental design

The present study used 19 female heterozygous MJD mice, injected at postnatal day 1 (P1), with AAV9 encoding miR-ATXN3 (n=8) and AAV9 encoding miR-Control (n=11).

Control and treated MJD mice were then evaluated based on their behavioral performance and neuropathological alterations. A battery of behavioral tests was performed at 35, 55 and 85 days. Mice were sacrificed at postnatal day 95 (P95), followed by brain pathology analysis.

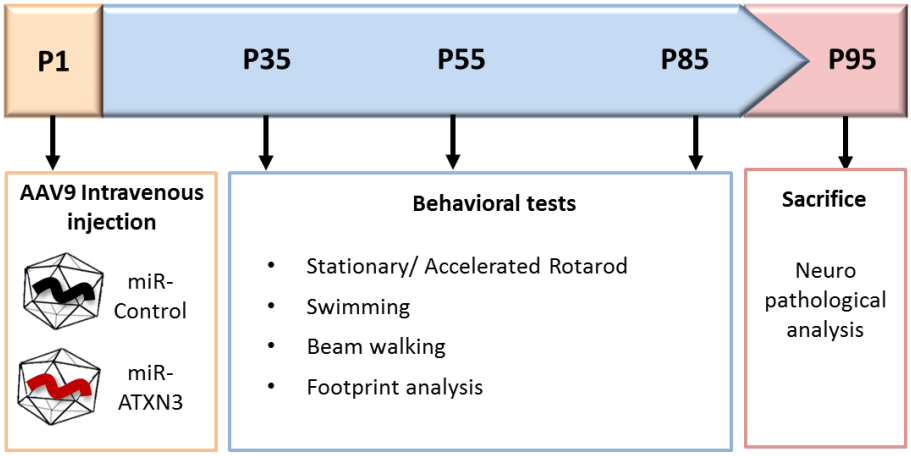

Figure 2.3: Experimental plan, divided into three important tasks: 1) AAV9 intravenous injection at PN1; 2) Behavioral assessment at 3 different time points and 3) neuropathological analysis.

AAV9 neonatal injection

Intravenous injections were performed in the facial vein of newborn MJD mice and wild-type littermates (P1). In our optimized protocol, we firstly anesthetized the neonates using a bed of ice during approximately 1 minute. After that, we injected a total of $3.5x10^{11}$ vg of AAV9 vectors, in a total volume of 50 µL, into the facial vein using a 30-gauge syringe (Hamilton, Reno, NV, USA). A correct injection was verified by noting blanching of the vein.

Behavioral testing

MJD transgenic mice performed a battery of behavioral tests at 35, 55 and 85 days of age, in the same dark and quiet room with controlled temperature, after one hour of acclimatization.

- **Rotarod**

The rotarod apparatus (Letica Scientific Instruments, Panlab) was used in order to evaluate MJD mice motor coordination and balance, by measuring their latency to fall (in seconds). The performance was analyzed at stationary rotarod, using a constant speed of 5 rpm and at accelerated rotarod, in which the velocity gradually increased from 4 to 40 rpm, both for a maximum of 5 minutes. For each time point (35, 55 and 85 days), the test was performed at three consecutive days, with a total of four trials per day. Between subsequent trials, mice had a resting period of at least 20 minutes. For statistical analysis, the mean latency to fall for each time point was calculated considering all consecutive days and trials.

In order to evaluate possible toxicity due to the treatment, a group of wild-type mice subjected to rAAV9-miR-ATXN3 (n=5) and rAAV9-miR-Control (n=5) IV injection also performed rotarod tests. In this case, the test was performed only in the last time point (85 days) at two consecutive days, with a total of four trials per day. For statistical analysis, the mean latency to fall was calculated considering the second day.

- **Swimming**

MJD mice limb coordination was also evaluated through swimming performance in a glass tank (70 cm long, 12.5 cm wide and with 19.5 cm height-walls). The pool presents one visible platform at the end and was filled with water until its level (8.5 cm). Mice were then placed at one end of the tank and were encouraged to swim to the escape platform at the opposite extremity. For each time point, animals performed four trials, swimming across the tank twice per trial and with at least 20 minutes of rest between trials. Their performance was video recorded, in order to measure the time required to swim the whole distance and climb the platform with their four paws. Statistical analysis was based on the mean scores of trials 2, 3 and 4.

- **Beam walking**

MJD mice motor coordination and balance were assessed by evaluating their ability to cross a series of elevated beams. Long wood beams were placed horizontally, 20 cm above a padded surface with both ends mounted on a support. For each time point, mice performed two consecutive trials on each beam, progressing from the easiest to the most difficult one: i) 18-mm square wide, ii) 9-mm square wide and iii) 9-mm round diameter beams. For all of them, mice had to traverse 40 cm to reach an enclosed safety platform. The latency to cross the beam and the motor performance were recorded and scored according to a predefined rating scale (Mendonca et al., 2015).

- **Footprint**

MJD mice footprint patterns were analyzed in order to compare different gait parameters. After coating fore and hind paws with non-toxic red and blue paints respectively, the animals were encouraged to walk in a straight line on a 50 cm long, 10 cm wide, paper-covered corridor into an enclosed box. For each time point, five consecutive steps in each side, preferentially at the middle of the run, were selected for analysis. Stride length values were measured, corresponding to the distance between subsequent left and right forelimbs and hindlimbs. The hind and front base width were determined by measuring the distance between right and left hind and front paws, respectively. In order to assess step alternation uniformity, the overlap was measured as the distance between the fore- and hind-paw from the same side. For each time point, the mean value obtained for the selected five consecutive steps was used for statistical analysis.

2.3. Histological processing

Tissue preparation

After an overdose of pentobarbital, mice were intracardiacally perfused with cold PBS 1X followed by fixation with 4% cold paraformaldehyde (PFA 4%). The brains were then removed and post-fixed in 4% paraformaldehyde for 24h at 4 °C and cryoprotected by incubation in 25% sucrose/PBS for 48 h at 4 °C.

For each animal, 96 sagittal sections of 30 µm were cut throughout one brain hemisphere using a cryostat (LEICA CM3050S, Germany) at −20°C. They were then collected and stored in two 48-well plates, as free-floating sections in PBS 1X supplemented with 0.05% sodium azide at 4°C.

Immunohistochemistry

The immunohistochemistry protocol was performed as previously reported (Alves et al., 2010). For each animal, eight sagittal sections with an intersection distance of 240 µm were selected.

The procedure started with endogenous peroxidase inhibition by incubating the sections in PBS1X containing 0.1% Phenylhydrazine (Merck, USA), for 30 minutes at 37°C. Subsequently, tissue blocking and permeabilization were performed in 0.1% Triton X-100 10% NGS (normal goat serum, Gibco) prepared in PBS1X, for 1 hour at room temperature. Sections were then incubated overnight at 4°C with the primary antibody Rabbit anti-GFP (Invitrogen), previously prepared on blocking solution at the appropriate dilution (1:1000). After three washings, brain slices were incubated in anti-rabbit biotinylated secondary antibody (Vector Laboratories) diluted in blocking solution (1:250), at room temperature for 2 h. Subsequently, free-floating sections were rinsed and treated with Vectastain ABC kit (Vector Laboratories) during 30 minutes at room temperature, inducing the formation of Avidin/Biotinylated peroxidase complexes. The signal was then developed by incubating slices with the peroxidase substrate: 3,3'-diaminobenzidine tetrahydrochloride (DAB Substrate Kit, Vector Laboratories). The reaction was stopped after achieving optimal staining, by washing the sections in PBS1X. Brain sections were subsequently mounted on gelation-coated slides, dehydrated in an ascending ethanol series (75, 95 and 100%), cleared with xylene and finally coverslipped using Eukitt mounting medium (Sigma-Aldrich).

Images of sagittal brain sections subjected to GFP immunohistochemistry were obtained in Zeiss Axio Imager Z2 microscope. Whole-brain images were acquired with an EC Plan-Neofluar 5×/0.16 objective, whereas images of particular regions were obtained with a Plan-Apochromat 20×/0.8 objective.

Immunofluorescence

Fluorescence immunohistochemical procedure was performed as previously described (Mendonca et al., 2015). For each animal, eight sagittal sections with an intersection distance of 240 µm were selected.

Briefly, the protocol started with a blocking and permeabilization step, in which free-floating sections were kept in 0.1% Triton X-100 in PBS1X supplemented with 10% NGS (normal goat serum, Gibco), for 1 h at room temperature. Brain slices were then incubated overnight at 4°C with the following primary antibodies diluted in blocking solution (10% NGS, 0.1% Triton X-100 in PBS): Mouse anti-HA (1:1000, Invivo Gen) and Rabbit anti-GFP (1:1000, Invitrogen). Following three washing steps in PBS1X, free-floating sections were incubated 2h at room temperature in fluorophore-coupled secondary antibodies prepared in blocking solution at the appropriate dilution: anti-mouse and anti-rabbit conjugated to Alexa Fluor 594 and 488 (1:200, Life technologies), respectively. After three rising steps in PBS1X, nuclear staining was performed using DAPI (4',6-diamidino-2-phenylindole). Subsequently, brain sections were washed, mounted on gelatin-coated microscope slides and finally coverslipped on Dako fluorescence mounting medium (S3023).

Cresyl Violet staining

Cresyl Violet staining was performed using eight sagittal sections with an intersection distance of 240 µm per animal. Selected brain sections were pre-mounted on gelatin-coated slides and dried at room temperature. After being washed in water, sections were subjected to dehydration (using ethanol 96% and 100%), defatting (using xylene substitute) and rehydration (using ethanol 75% and water). Then, slides were immersed in cresyl violet for 5 minutes, in order to stain the Nissl substance present in the neuronal bodies. Finally, sections were washed in water, differentiated in 70% ethanol and dehydrated by passing through 96% and 100% ethanol solutions. Following a clearing step in xylene, sections were mounted with Eukitt (Sigma-Aldrich).

Immunofluorescence quantitative analysis

Following GFP and HA immunofluorescence, specific sagittal sections were selected to acquire images of the whole cerebellum.

Serial z-stack images (interval= 0.9 µm) were captured by a confocal microscope (Zeiss Cell Observer Spinning Disk Microscope). Images were acquired with a Plan-Apochromat 20×/0.8 objective, using solid state lasers lines (561 nm or 488) for excitation.

- **Quantification of GFP mean and integrated intensity**

Quantification of mean and integrated GFP fluorescence intensity was performed in 3 specific sagittal sections from treated animals (cut in a sagittal plane 0.48, 0.72 and 0.96 mm lateral to the midline: Sagittal diagrams 105, 107 and 109 in (Franklin and Paxinos)). Images of the whole

cerebellum were acquired using confocal microscopy, as already described. Then, maximum intensity projections were obtained for each section, using Zen Black 2012 software.

Mean GFP fluorescence intensity was determined to quantify the viral transduction level in specific cerebellar lobules. For each section, mean GFP fluorescence intensity was determined by the Zen software and calculated after background subtraction. Final values correspond to the average intensity, considering the three analyzed sections per animal.

Integrated GFP fluorescence intensity was determined for cerebellar lobules altogether, in order to compare total viral transduction levels in different animals. In this case, mean GFP fluorescence intensity was determined including all cerebellar lobules and this value was multiplied by the respective area, to calculate integrated fluorescence intensity. Final values correspond to the average integrated intensity, considering the three analyzed sections per animal.

- **Quantitative analysis of haemagglutinin-tagged (HA) aggregates**

Three specific sections per animal were selected to quantify the number of aggregates in lobules 10, 9 and 6 (sagittal planes 0.48, 0.72 and 0.96 mm lateral to the midline for lobules 9 and 10; sagittal planes 0.72, 0.96 and 1.68 mm lateral to the midline for lobule 6, according to (Franklin and Paxinos)).

Images were acquired using a confocal microscope, as previously described. Average intensity projections were obtained for each section, using Zen Black 2012 software. After manual quantification of the number of aggregates in each lobule, the value was normalized with the respective lobular area, determined in the Zen software. Final values correspond to the average number of aggregates/mm^2 in the three selected sections per animal. Both treated and control groups were included in this analysis.

Quantification of molecular layer thickness

Three specific sections per animal were selected to quantify molecular layer thickness in lobules 10, 9 and 6, following cresyl violet staining (sagittal planes 0.48, 0.72 and 0.96 mm lateral to the midline for lobules 9 and 10; sagittal planes 0.72, 0.96 and 1.68 mm lateral to the midline for lobule 6, according to (Franklin and Paxinos)).

Images of the whole cerebellum were obtained in Zeiss Axio Imager Z2 microscope with a Plan-Apochromat 20×/0.8 objective and analyzed with Zen Blue software.

For each section, molecular layer thickness was calculated separately in lobules 10, 9 and 6, using three measurements in predefined specific regions. Final values correspond to the mean molecular layer thickness in the respective lobule, considering the three selected sections per animal. Both treated and control groups were included in this analysis.

2.4. Statistical analysis

Statistical analysis was performed using Prism GraphPad software. Data are presented as mean ± standard error of mean (SEM) and outliers were removed according to Grubb's test (alpha=0.05). Unpaired Student's t-test was performed to compare control and treated groups, whereas One-way ANOVA test was used for multiple comparisons. Correlations between parameters were determined according to Pearson's correlation coefficient. Significance was determined according to the following criteria: $p>0.05$= not significant (ns); *$p<0.05$, **$p<0.01$ ***$p<0.001$ and ****$p<0.0001$.

3. Results

3.1. miR-ATXN3 specifically reduces mutant ataxin-3 mRNA levels *in vitro*

In this project, we selected a short-hairpin RNA silencing sequence which has already proved to be efficient in selective knockdown of human mutant ataxin-3, while maintaining the levels of the wild-type form (sh-ATXN3) (Alves et al., 2008a). However, due to the recognized toxicity of shRNAs in the brain (McBride et al., 2008), in the present study this sequence was incorporated into a miR-155 scaffold, generating an artificial microRNA (miR-ATXN3). In parallel, a control sequence, which does not silence any mammalian mRNA, was also used and incorporated into a miR-155 scaffold (miR-Control). Both artificial miRNAs were cloned into a self-complementary AAV2 backbone under the control of U6 promoter and with EGFP as reporter gene (AAV-plasmids) (Figure 2.1).

In order to confirm whether silencing capacity and specificity are maintained in this novel silencing construct, miR-ATXN3 AAV-plasmid was transfected in a mouse neural crest-derived cell line (Neuro2a) stably expressing: i) human mutant ataxin-3 (72Q) or ii) human wild-type ataxin-3 (27Q). We used miR-Control AAV plasmid as the negative control and a lentiviral plasmid encoding sh-ATXN3 as a positive control.

According to quantitative real-time PCR (qPCR) results, both miR-ATXN3 and sh-ATXN3 induced a significant reduction of human ataxin-3 mRNA levels in Neuro2a cells expressing the mutant form (42.03% ± 6.26% and 63.34% ± 5.66%, respectively) (Figure 3.1A). In contrast, in Neuro2a cells infected with wild-type ataxin-3, no significant alterations in mRNA levels were detected after transfection with miR-ATXN3 plasmids (Figure 3.1B). These results indicate that this new miR-based construct retains the silencing ability and selectivity previously reported by our group for the shRNA construct.

Moreover, no alterations in the levels of endogenous mouse ataxin-3 mRNA were detected (Supplementary Figure 1), proving that the silencing effect is specific for human ataxin-3.

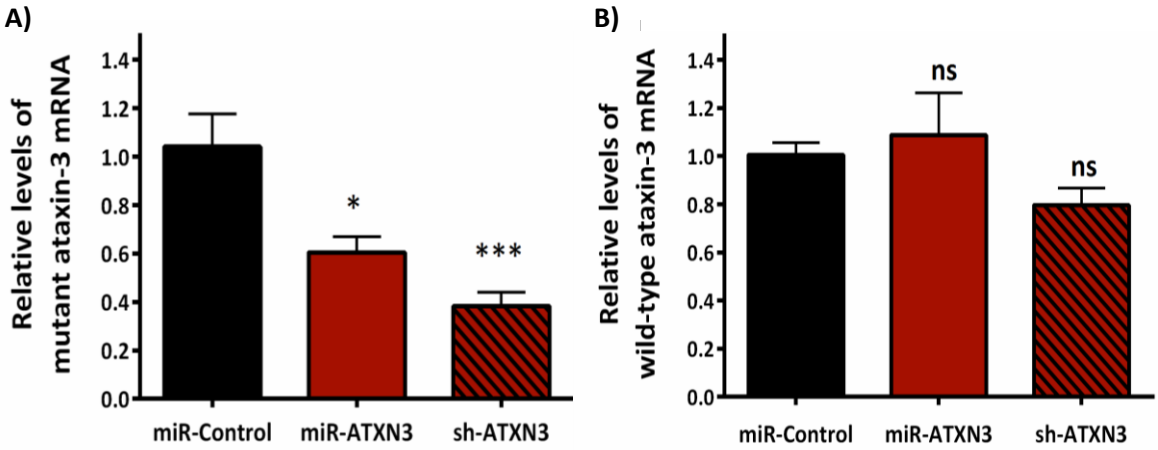

Figure 3.1: miR-ATXN3 mediates an efficient and allele-specific silencing of mutant ataxin-3 *in vitro*. Neuro2a cells (mouse neural crest-derived cell line) infected with lentiviral vectors encoding for A) human mutant ataxin-3 (72Q) or B) human wild-type ataxin-3 (27Q) were transfected with plasmids encoding miR-Control, miR-ATXN3 and sh-ATXN3. Relative expression levels of human ataxin-3 mRNA were determined by quantitative real-time PCR. Results are expressed as the mean relative mRNA level ± SEM (n=5).

Internal controls for normalization were selected according to GenEx analysis, corresponding to: mouse ataxin-3 and Glyceraldehyde 3-phosphate dehydrogenase (GAPDH) mRNA levels in A), and mouse GAPDH and hypoxanthine guanine phosphoribosyl transferase (HPRT) mRNA levels in B). Statistical analysis was performed by Ordinary One-way ANOVA (*p<0.05, ***p<0.001, ns= not significant).

3.2. rAAV9 vectors are able to cross the blood-brain barrier and transduce the CNS in wild-type and MJD transgenic mice when intravenously injected at postnatal day one (P1)

Since the aim of our project was to explore the therapeutic potential of rAAV9 vectors encoding miR-ATXN3 in MJD, miR-ATXN3 and miR-Control AAV plasmids were packaged into rAAV9 capsids (Figure 2.1). Then, rAAV9-miR-ATXN3 and rAAV9-miR-Control were intravenously (IV) administered to female neonatal polyQ69 transgenic MJD mice litters (including wild-type and transgenic animals) (Torashima et al., 2008) through intrafacial vein injections. For therapeutic purposes, we focused our attention in transgenic MJD mice, which were divided into two groups: i) miR-ATXN3 and ii) miR-Control.

In order to get therapeutic impact, IV-injected rAAV9 vectors have to circumvent the blood-brain barrier (BBB) and efficiently transduce the brain. As a result, we started by studying rAAV9 distribution in transgenic mouse brain, after sacrifice at 95 days old. For that purpose, we performed an Immunohistochemistry in sagittal brain sections using an antibody against green fluorescent protein (GFP), the reporter gene present in the AAV-plasmids (Figure 3.2). Besides analyzing sections from rAAV9-injected transgenic mice, we also used a non-injected MJD mouse as a negative control and a rAAV9-injected wild-type (WT) mouse to compare rAAV9 distribution.

The pattern of GFP expression was very similar in the transgenic mice, both in the control and treated groups, subjected to rAAV9 IV injection. The vector proved to efficiently spread throughout the brain, with particularly strong GFP expression in the hippocampus, cerebellum, pontine nuclei, medulla and spinal cord (Figure 3.2). Other efficiently transduced areas included the olfactory bulb, striatum and cortex (Supplementary Figure 2). The main difference observed between transgenic and wild-type animals corresponds to cerebellar GFP expression. In fact, MJD animals exhibit a weaker and spatially limited GFP signal, when comparing to the robust transgene expression in the whole cerebellum of WT mice. These observations might be explained by cerebellar vascularization defects in transgenic animals, which have already been reported for this model (Konno et al., 2014).

A) Tg

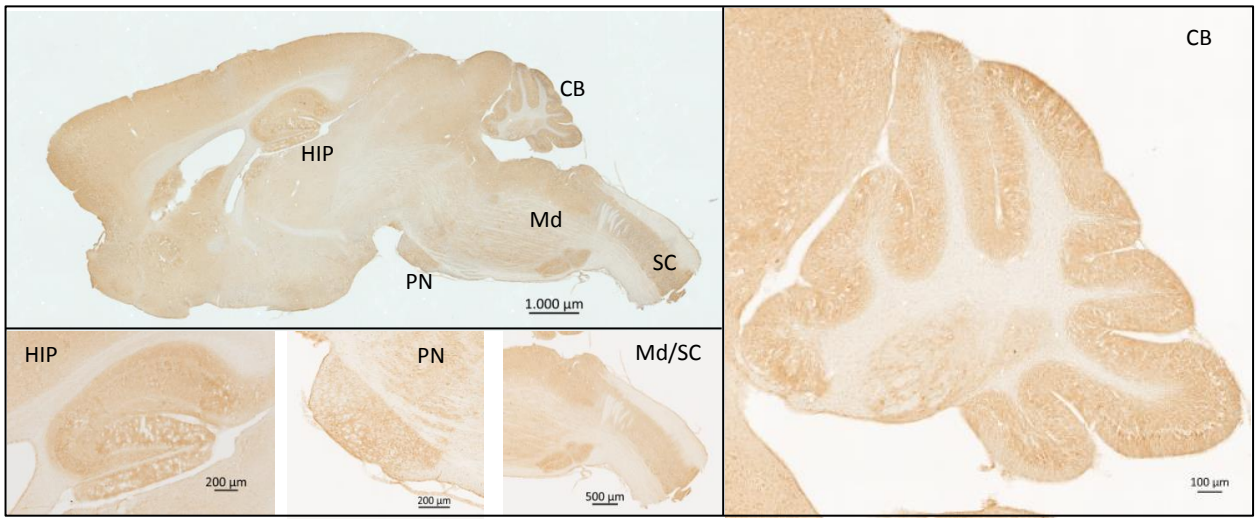

B) Tg inj

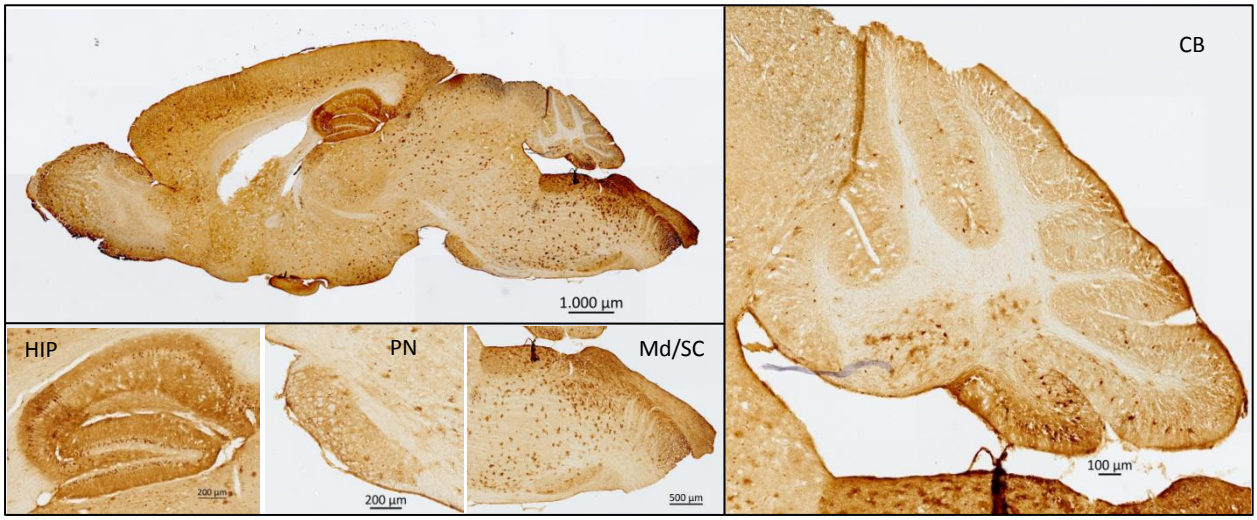

C) WT inj

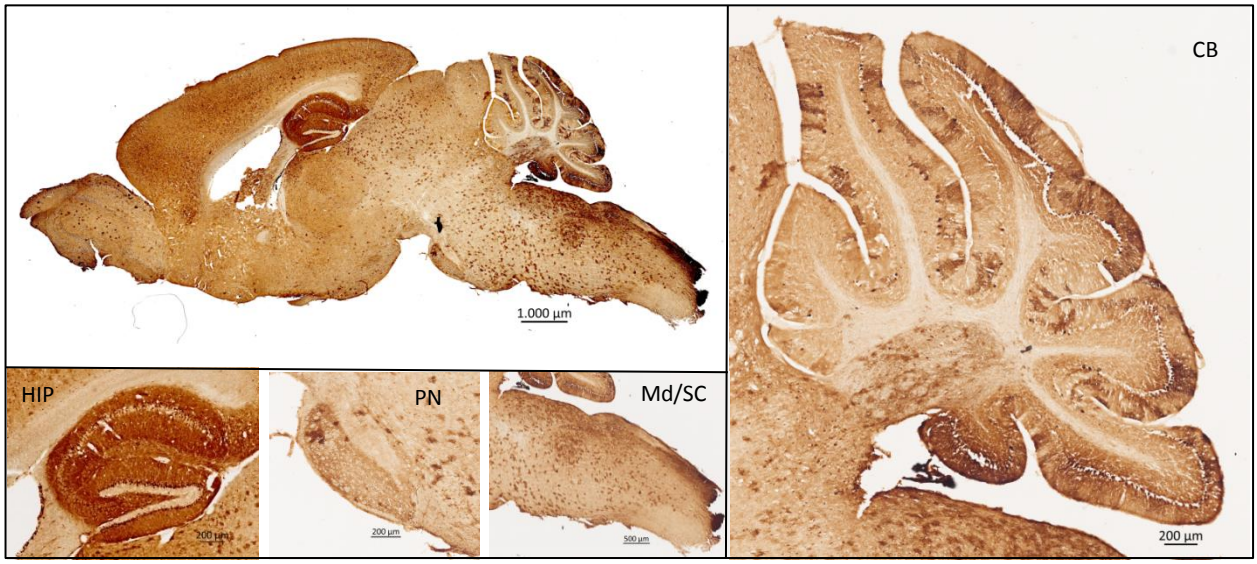

Figure 3.2: Intravenously injected rAAV9 vectors mediate an efficient transduction throughout the brain of wild-type and transgenic MJD mice.

Representative images of GFP immunohistochemistry (in brown) in the brains of 3-month-old mice: A) a non-injected transgenic mouse; B) a transgenic mouse subjected to rAAV9-miR-ATXN3 IV injection at postnatal day 1; C) a wild-type mouse subjected to the same procedure. Images show rAAV9 transduction of the whole brain, cerebellum (CB), hippocampus (HIP), pontine nuclei (PN) and medulla/spinal cord (Md/SC), obtained with 5x and 20x objectives.

3.3. rAAV9 vectors efficiently transduce specific regions of transgenic mouse cerebella

For this work, we used polyQ69 MJD transgenic mice as the experimental model. These animals express a truncated form of human ataxin-3, with 69 glutamine repeats and an N-terminal haemagglutinin (HA) epitope, driven specifically in cerebellar Purkinje cells by the L7 promoter (Torashima et al., 2008) (Figure 2.2). For this reason, the therapeutic action of rAAV9-miR-ATXN3 greatly depends on vector ability to transduce the cerebellum, particularly this cellular subtype. Therefore, we analyzed in further detail the distribution of GFP signal in this region, after immunohistochemical processing.

As represented in Figure 3.3, GFP expression was not equally distributed throughout the cerebellum, being particularly evident in cerebellar lobule 10, followed by the deep cerebellar nuclei (DCN) and lobule 9. Transduced isolated neurons were also detected in lobules 6 and 7 and in the remaining lobules, although to a less extent. Importantly, choroid plexus cells of fourth ventricle also exhibited a marked GFP expression. This pattern of GFP distribution was observed for all transgenic animals subjected to rAAV9 IV injection, including the control and treated groups.

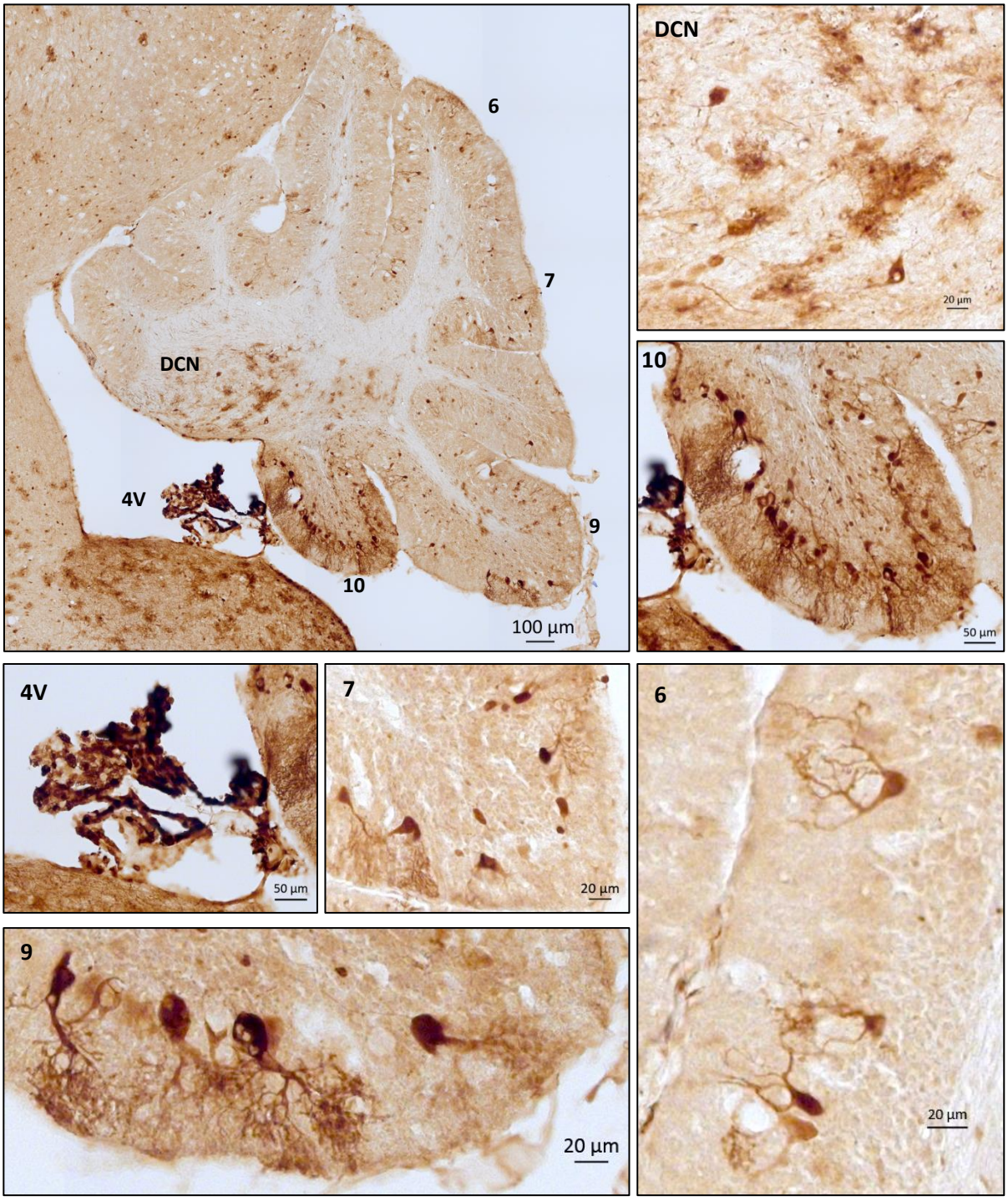

Figure 3.3: rAAV9 vectors exhibit an efficient transduction of transgenic mouse cerebella. Representative images of GFP visible immunohistochemistry (in brown) in the cerebellum of a 3-month-old mouse subjected to rAAV9-miR-ATXN3 neonatal IV injection. Images were obtained with a 20x objective and show cerebellar regions with particularly efficient transduction including: deep cerebellar nuclei (DCN), lobules 10, 9, 7 and 6 and choroid plexus cells of the fourth ventricle (4V).

In order to quantitatively compare transgene expression levels in different cerebellar lobules of rAAV9-miR-ATXN3 treated mice, we performed a fluorescence immunohistochemistry using an antibody against GFP. Then we calculated the normalized mean intensity of GFP fluorescence in three distinct cerebellar regions: a) lobules 1–5, b) lobules 6–8, and c) lobules 9–10 (Figure 3.4). The first two regions presented similar values, while in lobules 9 and 10 the mean intensity was significantly higher (approximate 4-fold increase). Altogether, these results suggest that IV-injected rAAV9 vectors preferentially transduce the nodular zone of the cerebellum (posterior lobule 9 and lobule 10), next to the fourth ventricle.

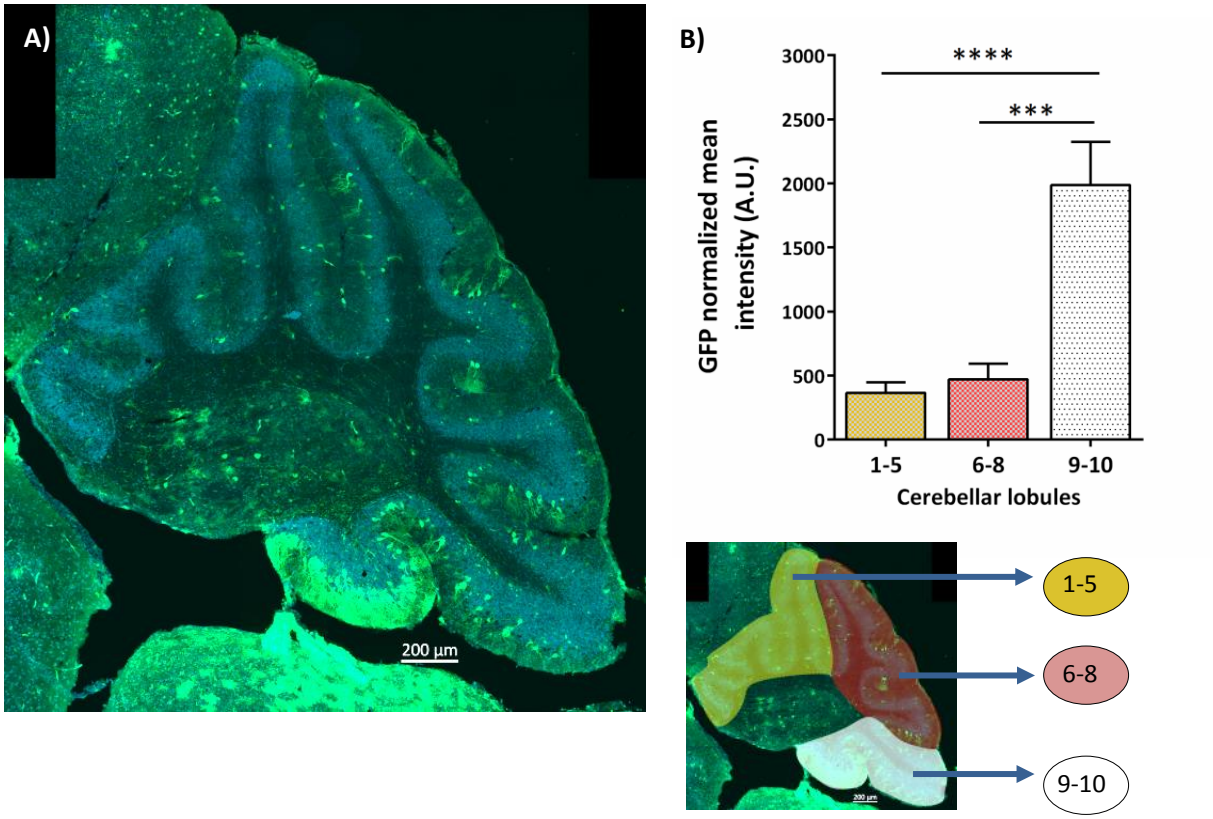

Figure 3.4: rAAV9 exhibits distinct transduction efficiencies in different cerebellar lobules. A) Representative image of GFP fluorescence immunohistochemistry (in green) and DAPI staining (in blue) in the cerebellum of transgenic mice subjected to rAAV9-miR-ATXN3 injection. Images were obtained in a confocal microscope with a 20x objective. B) Comparison of GFP normalized mean intensity (A. U. = arbitrary units) in three distinct cerebellar regions: lobules 1–5 (in yellow), 6–8, (red) and 9–10 (white). Analysis was performed using three consecutive sections from rAAV9-miR-ATXN3 treated mice (n=8). Results are expressed as the mean value ± SEM. Statistical analysis was performed by using the Ordinary One-way ANOVA (***p<0.001, ****p< 0.0001).

Finally, we assessed whether rAAV9 targets the cell population mainly affected in this mouse model, i.e. the Purkinje cells that express mutant ataxin-3 (Figure 3.5). For that, we performed a co-immunofluorescence labeling both GFP and Haemagglutinin (HA). As expected, HA signal was detected in the Purkinje cell layer, in which mutant ataxin-3 was distributed throughout the soma with a diffuse staining and in the form of aggregates. Moreover, mutant ataxin-3 aggregates were also detected in the axon terminals of Purkinje cells, in deep cerebellar nuclei (DCN). When comparing the distribution of GFP and HA signals, we observed a co-localization in the Purkinje cell layer and in the DCN, the two major regions of mutant ataxin-3 accumulation. This pattern was similar for all rAAV9-IV injected mice, including control and treated groups.

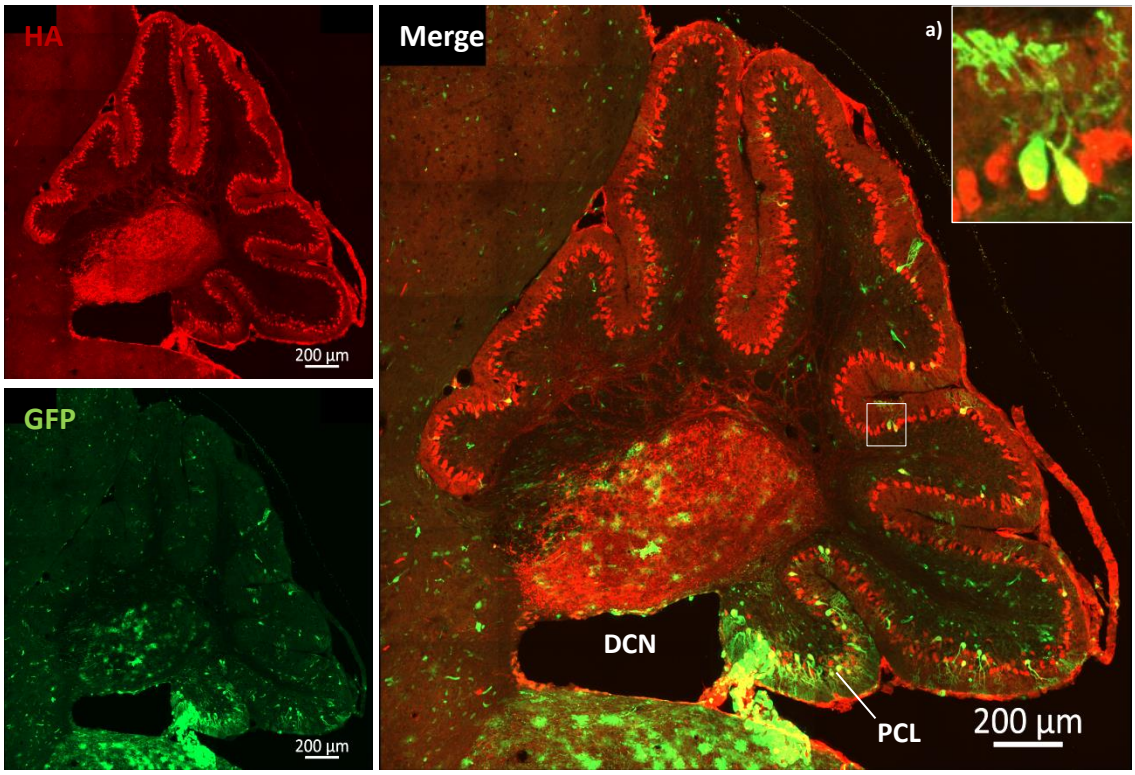

Figure 3.5: rAAV9 targets the main regions of mutant ataxin-3 accumulation in transgenic mouse cerebella. Representative images showing immunofluorescence for HA (in red) and GFP (in green) in the cerebellum of a transgenic mouse subjected to rAAV9-miR-ATXN3 injection at P1. Images were obtained in a confocal microscope with a 20x objective. a) Representative image of rAAV9-positive Purkinje cells, showing co-localization of HA and GFP signals. *DCN – deep cerebellar nuclei; PCL – Purkinje cell layer*

3.4. rAAV9-miR-ATXN3 intravenous administration into neonatal transgenic mice alleviates motor impairments

In the present study we investigated whether rAAV9-miR ATXN3 injection would alleviate MJD-associated behavioral deficits. The most common MJD symptoms include impairments in motor coordination and balance, as well as ataxic gait (D'Abreu et al., 2010). PolyQ69 transgenic mice successfully mimic these features, showing an extremely severe ataxic phenotype with an early onset (P21) (Conceicao et al., 2016b; Cunha-Santos et al., 2016; Duarte-Neves et al., 2015; Konno et al., 2014; Mendonca et al., 2015; Nascimento-Ferreira et al., 2013; Nobrega et al., 2014; Torashima et al., 2008). These behavioral impairments occur due to Purkinje cell dysfunction, a neuronal subpopulation with important roles in motor coordination and learning. In fact, Purkinje cells are vulnerable and easily damaged leading to impaired motor control ability (Sarna and Hawkes, 2003).

In order to explore the impact of rAAV9-miR-ATXN3 treatment on transgenic mice behavior, both treated and control animals were subjected to a battery of tests at three different ages: 35, 55 and 85 days. These tests included stationary and accelerated rotarod, as well as beam walking test, since they are appropriate to assess balance and motor coordination. Additionally, the swimming test allowed further evaluation of motor performance and strength. On the other hand, footprint analysis allowed us to evaluate MJD-associated gait deficits.

Rotarod performance was determined as the mean latency time to fall when mice walk in a rotarod apparatus both at constant and accelerated velocities. The treatment proved to have beneficial effects at all time points and for both paradigms (Figure 3.6). The most consistent results were obtained at 85 days, since this improvement was statistically significant for both stationary and accelerated rotarod (1.7 and 1.5 fold increase in latency time to fall, respectively).

Importantly, rAAV9-injected wild-type animals were also evaluated based on their stationary and accelerated rotarod performances at 85 days to assess whether this treatment is well-tolerated. No differences were detected for the rotarod performance of wild-type mice injected with rAAV9-miR-Control or rAAV9-miR-ATXN3 (Supplementary Figure 3). These findings indicate that the therapeutic sequence does not induce major toxic effects.

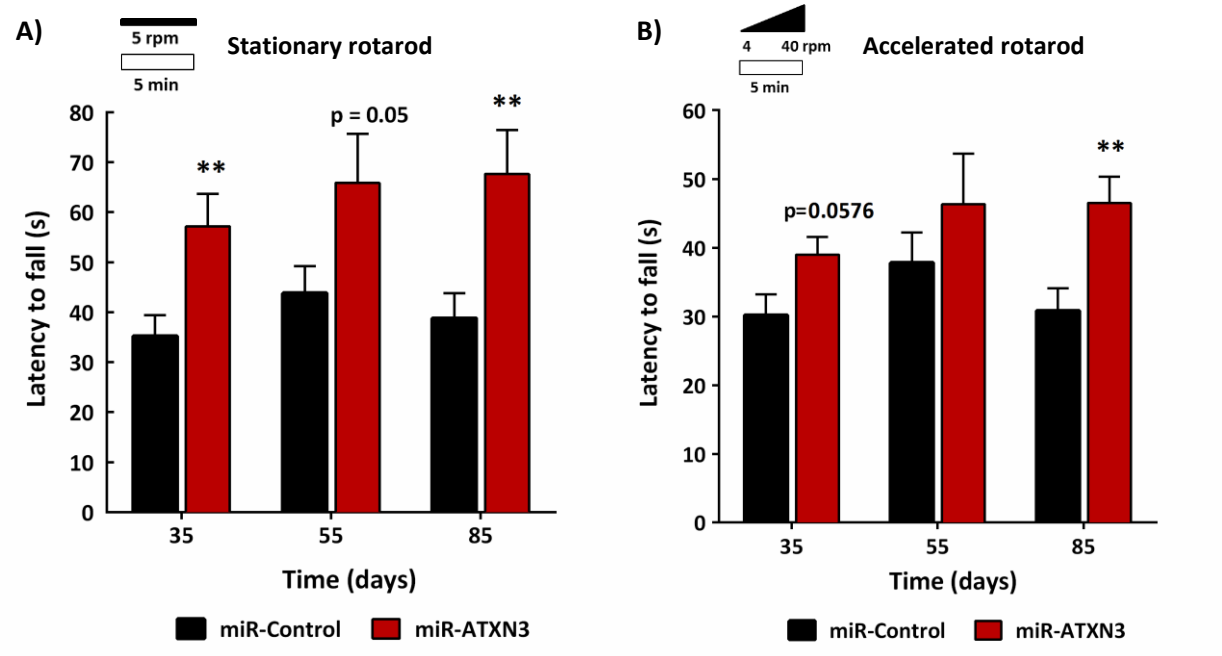

Figure 3.6: Silencing mutant ataxin-3 improves rotarod performance in MJD transgenic mice. A) Rotarod performance at constant velocity (5 r.p.m). B) Rotarod performance at accelerated velocity. Data are presented as mean latency time to fall ±SEM for control mice (miR-Control, n = 11) and mice injected with rAAV9-miR-ATXN3 (n = 8). Statistical analysis was performed using the unpaired Student's t-test (**p<0.01).

In the swimming test, mice were placed at one extremity of a water-filled glass tank and were encouraged to swim across the pool and climb a platform. The time required for each animal to swim the whole distance and climb the platform was recorded. According to the results, treated animals showed a better performance at 55 days (Figure 3.7A).

In the beam-walking test, mice crossed a i) 18-mm square wide, ii) 9-mm square wide and a iii) 9-mm diameter round elevated beam. Animals were evaluated based on the time they took to complete the walk and on their motor coordination. Performance was scored according to a predefined rating scale (Mendonca et al., 2015), in which higher scores indicate a better balance and coordination. According to this analysis, no differences between the control and treated groups were detected for the 18-mm and 9-mm square wide beams (Supplementary Figure 4). Nevertheless, animals exhibited distinct performances on the 9-mm diameter round beam, which is considered the most difficult to cross (Figure 3.7B). In the control group, a progressive reduction in the performance score along time was observed, while treated mice retained their ability to traverse the beam. As a result, animals injected with rAAV9-miR-ATXN3 presented a significantly better performance in the beam-walking test at the last time point (2.2 fold increase in mean score).

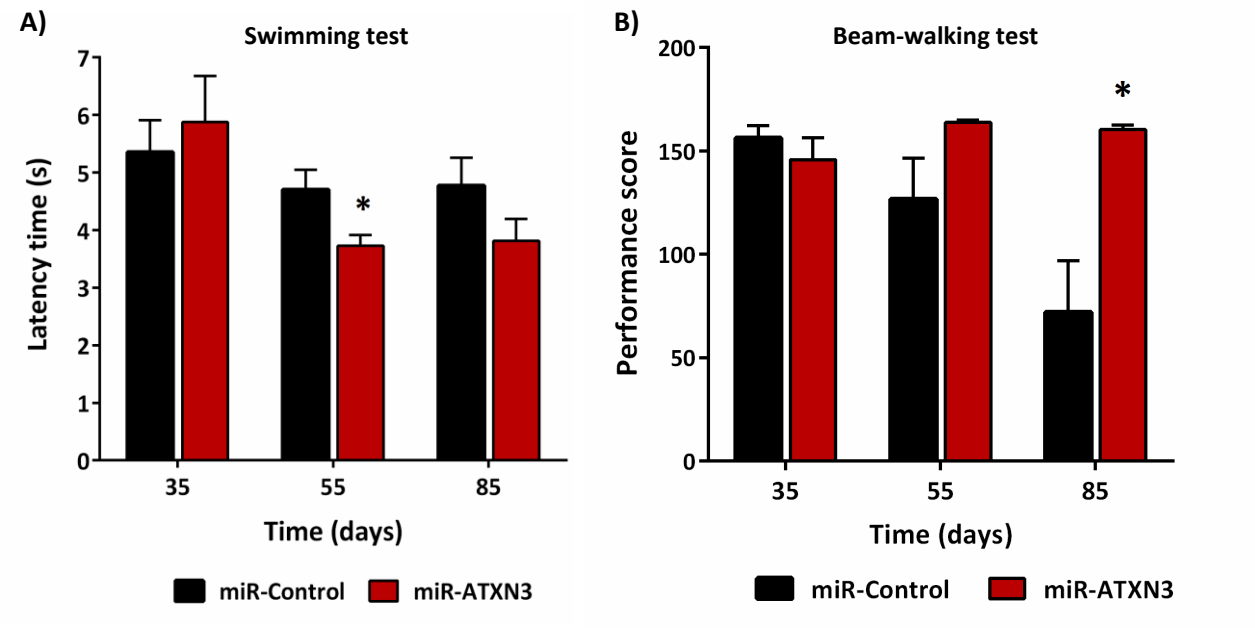

Figure 3.7: rAAV9-miR-ATXN3 treatment improves swimming and beam-walking performances in MJD transgenic mice. A) Animals were evaluated based on the time they took to swim across a pool and climb the platform. Data are presented as mean latency time ±SEM. B) Animals were evaluated based on their performance when walking on a 9-mm round beam. Considering the total time to cross the beam and the motor coordination, each animal received a score (Mendonca et al., 2015). Data are presented as mean performance score ±SEM. For both tests, statistical analysis was performed using the unpaired Student's t-test (*$p<0.05$), comparing the performance of control mice (miR-Control, n = 11) and mice injected with rAAV9-miR-ATXN3 (n = 8).

In order to assess whether the treatment was able to attenuate MJD characteristic limb and gait ataxia, we analyzed the footprint pattern of both experimental groups. Ataxic gait is normally characterized by: i) an increased stride width; ii) a shorter stride length and iii) an increased overlap distance, which reflects less uniformity of step alternation. Analysis of gait patterns from treated animals, when compared to the control group revealed several improvements at different time points, mainly: a significant decrease in hind and front base width, at 55 and 35 days, respectively. Additionally, at the last time point (85 days), a significant reduction in footprint overlap distance was detected (Figure 3.8). No alterations were observed for stride length (Supplementary Figure 5).

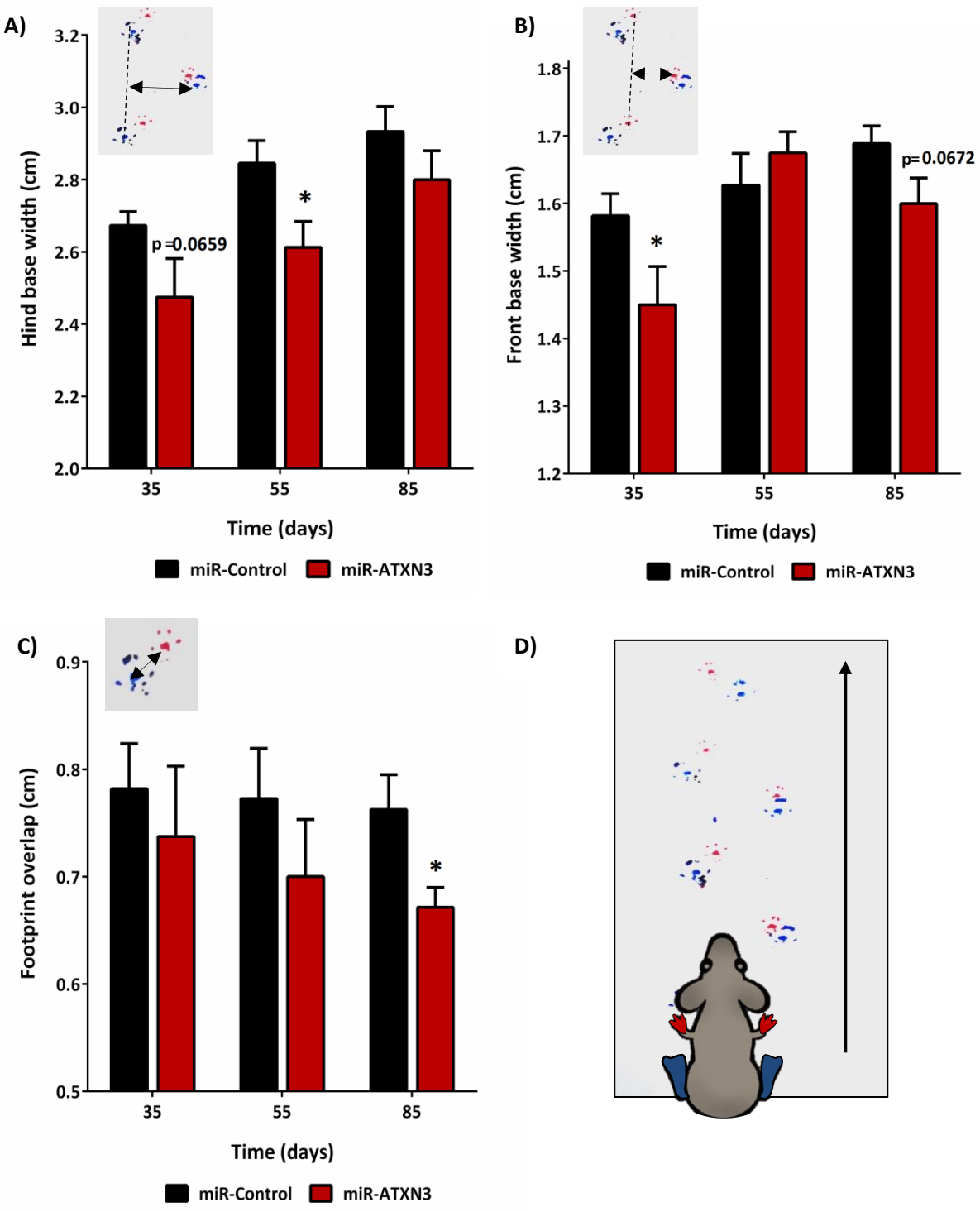

Figure 3.8: rAAV9-miR-ATXN3 treatment improves gait ataxia in MJD transgenic mice. Gait pattern was analyzed my measuring: A) hind base width, B) front base width and C) footprint overlap (cm). Data are presented as the mean distance ±SEM for control mice (miR-Control, n = 11) and mice injected with rAAV9-miR-ATXN3 (n = 8). Statistical analysis was performed using the unpaired Student's t-test (*p<0.05). D) Representation of footprint test, showing the front and hind paws colored in red and in blue, respectively.

3.5. rAAV9-miR-ATXN3 treatment alleviates MJD-associated neuropathology

Importantly, we evaluated the impact of rAAV9-miR-ATXN3 injection on MJD-associated neuropathological changes. One of the major hallmarks of MJD consists on the accumulation of mutant ataxin-3 aggregates, which reflects disease progression (Hayashi et al., 2003). In the selected mouse model, these aggregates are formed in Purkinje cells starting at P40 and markedly increasing in number and size along time (Torashima et al., 2008).

Therefore, we performed an immunofluorescence for haemagglutinin (HA) in sagittal sections from treated and control MJD mice, since this tag is present in the N-terminal of mutant ataxin-3. Then, we quantified the number of mutant ataxin-3 aggregates per area in cerebellar lobules 10 and 9, since they correspond to the region with higher transduction levels. In order to conclude the impact of rAAV9 treatment in regions with low transduction efficiency, we also analyzed lobule 6. According to our results, rAAV9-miR-ATXN3 treatment reduced aggregation in all three analyzed lobules (35%, 18% and 20% decrease in lobules 10, 9 and 6, respectively), thereby contributing to neuropathology attenuation (Figure 3.9).

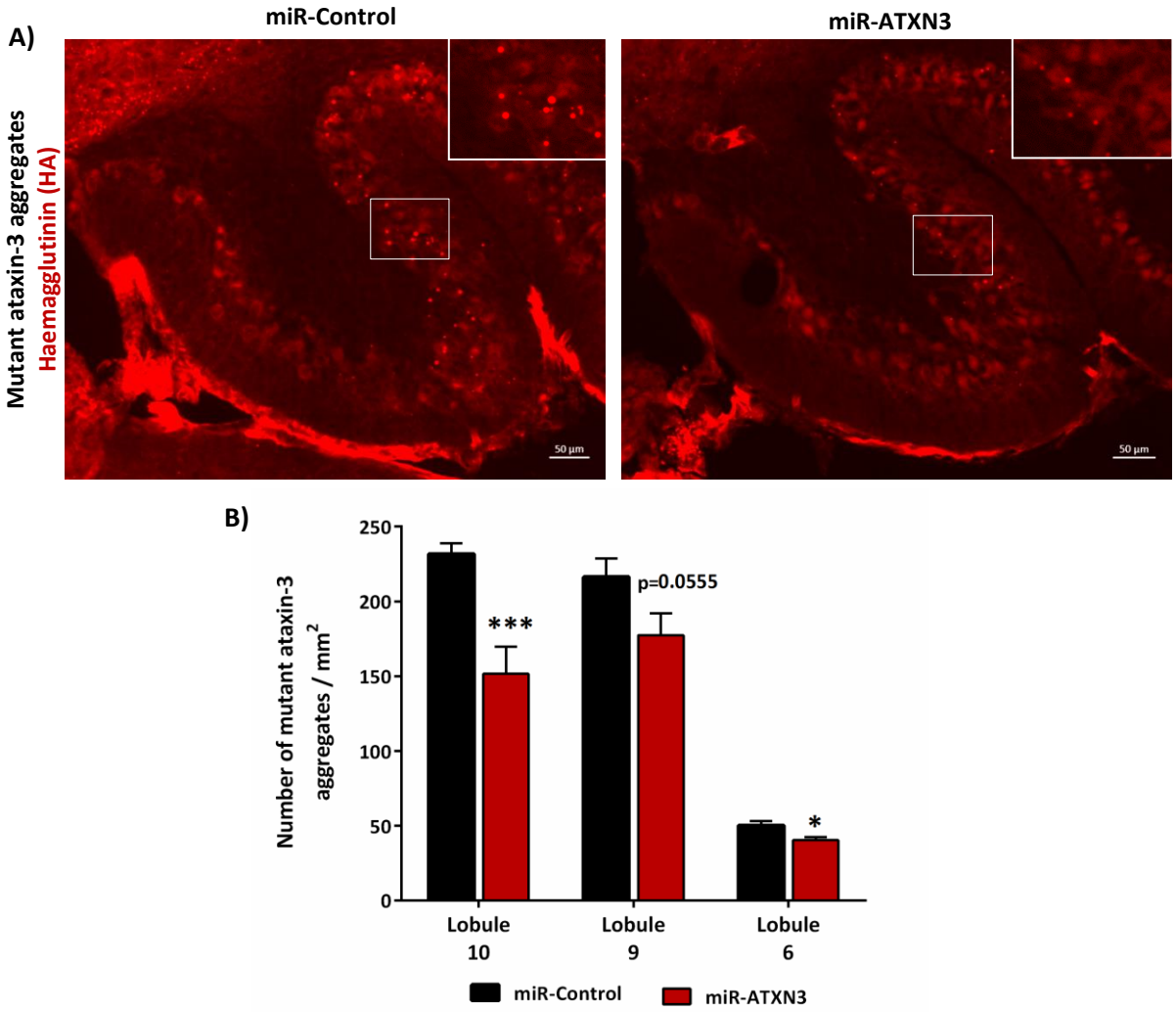

Figure 3.9: rAAV9-miR-ATXN3 treatment efficiently reduces the number of mutant ataxin-3 aggregates.

A) Representative images of immunofluorescence labeling mutant ataxin-3 (HA in red) in the lobule 10 of control (miR-Control) and treated (miR-ATXN3) transgenic mice. Images were obtained in a confocal microscope with a 20x objective. B) Quantification of mutant ataxin-3 aggregates per area in lobules 10, 9 and 6. Values correspond to the mean ± SEM using three specific sections for each animal (miR-Control, n=11; miR-ATXN3, n=8). Statistical analysis was performed using the unpaired Student's t-test (*p<0.05, ***p<0.001).

Another important feature in MJD patients includes cerebellar atrophy, which occurs as a consequence of neurodegeneration in this region and normally presents a correlation with clinical symptoms (Camargos et al., 2011). In this particular mouse model, a marked cerebellar atrophy is detected as early as 3 weeks of age (Torashima et al., 2008). Accordingly, degeneration or functional/morphological alternations in Purkinje cells might affect other cerebellar regions due to the strong interconnection between distinct cellular types. In particular, Q69 transgenic mice are characterized by a poor dendritic arborization in Purkinje cells, consequently reducing the molecular layer thickness (Cunha-Santos et al., 2016; Konno et al., 2014; Nascimento-Ferreira et al., 2013; Nobrega et al., 2014; Torashima et al., 2008). Therefore, we performed the cresyl violet staining in sagittal sections from both experimental groups, in order to distinguish the cerebellar layers (Figure 3.10). By analyzing the molecular layer, we found a significant larger thickness in lobules 10 and 9 of miR-ATXN3 treated mice (21% and 15% respectively), as well as a tendency in lobule 6 (13%). Altogether these findings indicate that silencing mutant ataxin-3 through a rAAV9 IV injection into neonatal mice induces beneficial effects in the cerebellum, ameliorating some of MJD-associated neuropathological changes.

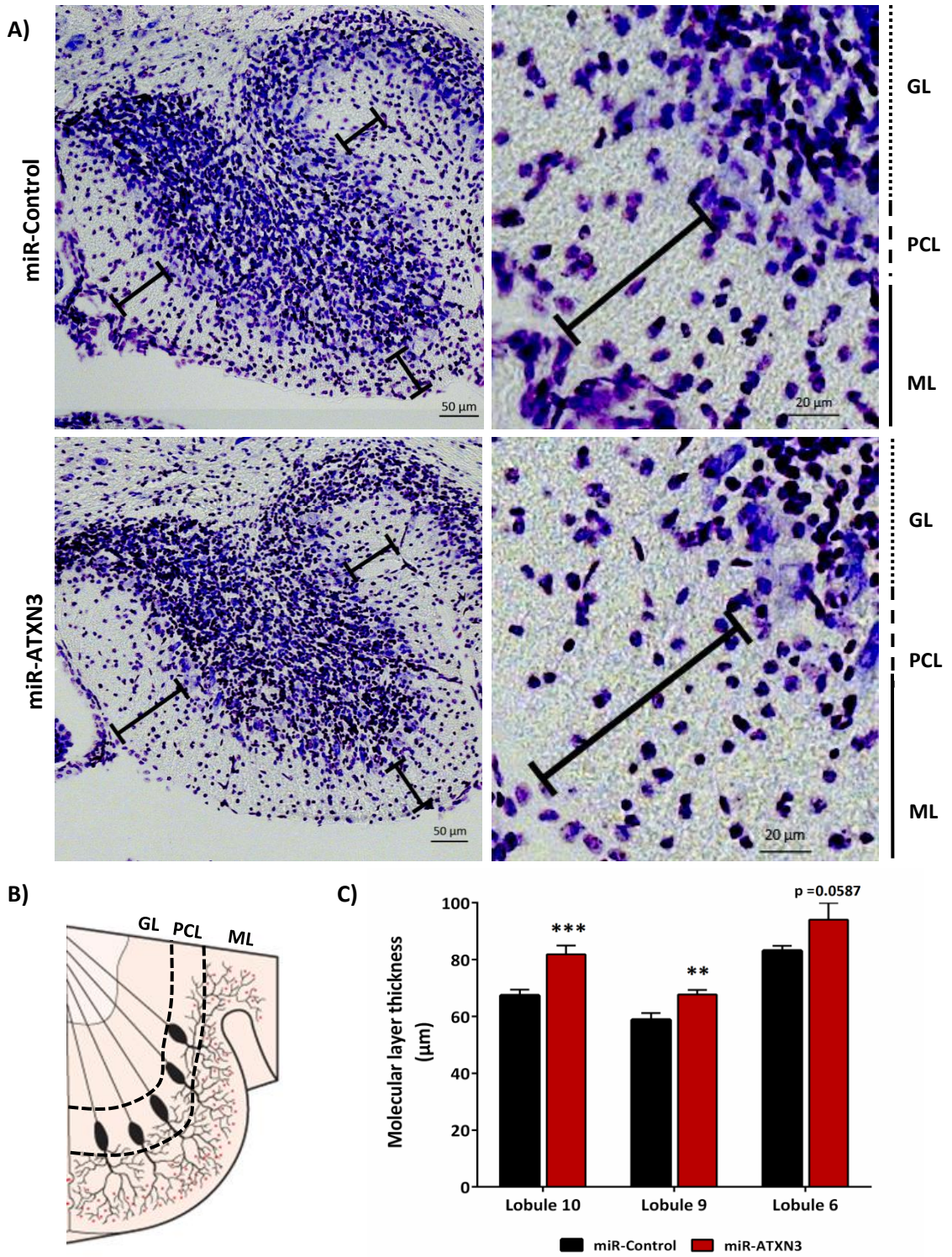

Figure 3.10: rAAV9-miR-ATXN3 treatment efficiently preserves molecular layer thickness. A) Representative images of cresyl violet staining in the lobule 10 of treated and control transgenic mice, obtained with a 20x objective. Right panels show in further detail the molecular layer (ML) thickness. (PCL – Purkinje cell layer; GL – Granular layer). B) Schematic representation of cerebellar layers, showing the extension of Purkinje cell dendrites into the molecular layer. C) Quantification of molecular layer thickness in lobules 10, 9 and 6. Values correspond to the mean ± SEM of three specific sections for each animal (miR-Control, n=11; miR-ATXN3, n=8). Statistical analysis was performed using the unpaired Student's t-test (**p<0.01, ***p<0.001).

3.6. Different rAAV9 transduction levels correlate with neuropathological and behavioral parameters in treated mice

Finally, we assessed whether the therapeutic effect in treated mice is dependent on the levels of rAAV9 cerebellar transduction. The fact that particular animals presented a more evident behavioral improvement or neuropathology attenuation could be explained by a higher vector dose transducing Purkinje cells.

For that purpose, we analyzed GFP mean fluorescence on lobules 10 and 9, as well as the number of aggregates per area in the respective region. We found an inverse correlation between these two parameters, leading to the conclusion that higher transduction levels on lobules 10 and 9 are accompanied by an improvement in aggregate clearance (Figure 3.11A). However, the same relation could not be established for lobule 6 (Supplementary Figure 6), indicating that benefic effects on this particular region might depend on other parameters.

Moreover, we assessed whether mice with superior cerebellar transduction correspond to the ones with better motor performance. In this context, we found a positive relation between GFP integrated intensity in all cerebellar lobules and average performance in accelerated rotarod (Figure 3.11B).

Taking all of this into account, we concluded that the variability observed in treated animals for behavioral tests and neuropathological signs can be caused by different transduction efficiencies. In summary, rAAV9-miR-ATXN3 injection induces a dose-dependent response, since higher vector concentrations in the cerebellum correspond to a more powerful therapeutic effect.

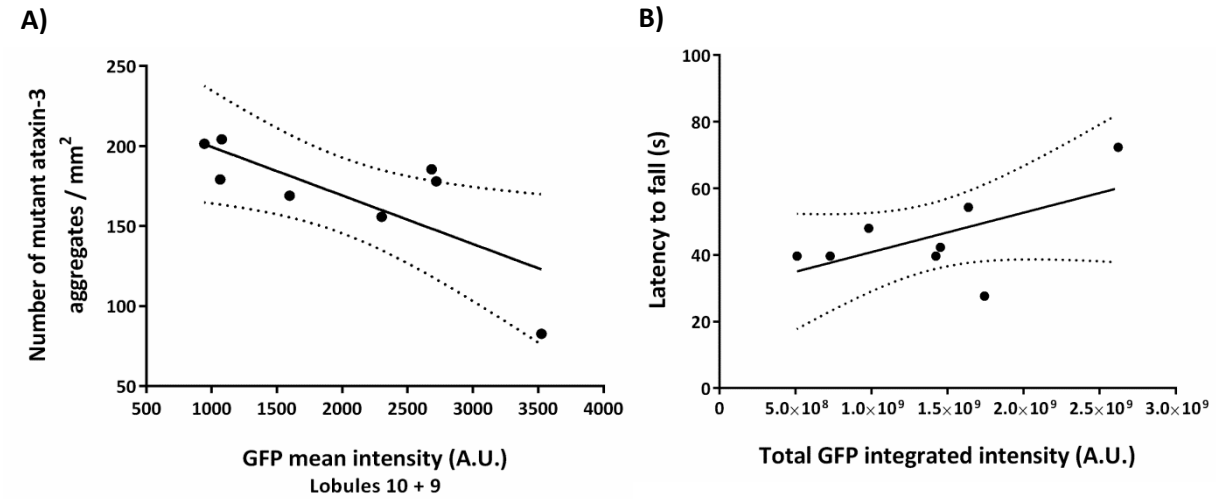

Figure 3.11: Different rAAV9 transduction levels correlate with neuropathological and behavioral parameters in treated mice. A) Linear regression graph between GFP mean intensity in lobules 9 and 10 (A.U.= arbitrary units) and number of aggregates/mm^2 in the same region for rAAV9-miR-ATXN3 treated animals (n=8) (p=0.0309, R^2=0.5675). B) Linear regression graph between GFP integrated intensity in all cerebellar lobules (A.U.= arbitrary units) and mean latency to fall in accelerated rotarod for rAAV9-miR-ATXN3 treated animals (n=8), considering all time points (35, 55 and 85 days). According to residual analysis, one animal was considered an outlier for the predicted linear regression model. Analysis was performed without this animal (p=0.0123, R^2=0.7457). Statistical analysis was performed using Pearson's correlation (two-tailed p value). Dotted lines represent the 95% confidence intervals.

4. Discussion

Machado-Joseph disease (MJD) is an incurable and fatal neurodegenerative disorder, for which RNA interference (RNAi) represents the most direct therapeutic strategy. Our group has shown successful results following intraparenchymal injection of lentivirus encoding silencing sequences specifically targeting mutant ataxin-3 (Alves et al., 2008a; Nobrega et al., 2014; Nobrega et al., 2013b). However, this delivery route constitutes an invasive procedure associated with severe adverse effects (Marks et al., 2010). Moreover, intraparenchymal administration results in limited vector dispersion throughout the brain, thereby not targeting all regions affected in MJD. Taking all of this into account, in this project we developed a novel non-invasive viral gene therapy for MJD. For that purpose, we used a silencing sequence based on the short-hairpin RNA (shRNA) construct previously designed by our group, which mediates mutant ataxin-3 allele specific knockdown (sh-ATXN3) (Alves et al., 2008a). In this case, we selected adeno-associated viral vector serotype 9 (AAV9) as the delivery vector, since this particular serotype efficiently crosses the blood-brain barrier (BBB), enabling intravenous administration (Duque et al., 2009; Foust et al., 2009).

RNAi is considered a highly promising approach to correct genetic disorders. However, its therapeutic impact and safety profile greatly depend on the selected silencing construct. Recent investigation has shown a potential toxic effect when delivering shRNAs to rodent brains, due to RNAi machinery saturation (Boudreau et al., 2009a; McBride et al., 2008). These adverse responses might be circumvented by inserting the silencing sequence into a microRNA backbone (miR). Based on that, the first step of this project consisted on the incorporation of the validated sh-ATXN3 sequence into a microRNA-155 backbone, leading to the production of miR-ATXN3 (Figure 2.1).

Subsequently, we evaluated miR-ATXN3 silencing efficiency *in vitro* using a mouse neural crest-derived cell line (Neuro2a) infected with lentiviral vectors encoding for human mutant ataxin-3 (LV-Mut-ATXN3). Transfection with miR-ATXN3 resulted in a 42.03% ± 6.26% reduction in mutant ataxin-3 mRNA levels, close to what occurs in the presence of sh-ATXN3 (Figure 3.1A). Therefore, we concluded that knockdown ability is maintained following construct incorporation into a microRNA backbone.

On the other hand, given that wild-type ataxin-3 displays important cellular roles, allele specific silencing is considered the ideal option for MJD. In fact, ATXN3 normally participates in protein quality control and transcription regulation, explaining why its downregulation could have deleterious effects in MJD patients (Rodrigues et al., 2007; Schmitt et al., 2007). Based on that, as mentioned before, we used an allele-specific silencing strategy that allows the discrimination between mutant and wild-type transcripts, thereby maintaining ataxin-3 normal function. As shown in figure 3.1B, expression of miR-ATXN3 did not modify wild-type human ataxin-3 levels in Neuro2a cells previously infected with lentiviral vectors encodings for WT-ATXN3. This observation confirmed that our miRNA-based strategy is also allele specific, a significant advantage when translating this therapeutic approach to human patients.

Based on these results, recombinant self-complementary AAV9 vectors (rAAV9) encoding miR-ATXN3 (rAAV9-miR-ATXN3) or a control miR sequence (rAAV9-miR-Control) were produced (Figure 2.1). We selected an AAV vector since it is considered the preferred platform for CNS gene delivery, given its efficient neuronal transduction, long-term transgene expression and safety profile (Ojala et al., 2015). In particular, AAV9 has the capacity to bypass the BBB in wild-type rodents, cats, and non-human primates, enabling intravenous injection (IV) (Duque et al., 2009; Foust et al., 2009; Foust et al., 2010). This minimally invasive procedure will also allow CNS widespread vector distribution, two important advantages when compared to the commonly used intracranial injection.

The ability of developed rAAV9 vectors to transpose the BBB and to transduce neurons upon intravenous injection was evaluated in a severely impaired transgenic mouse model of MJD (PolyQ69 transgenic mice) and in their wild-type littermates (Torashima et al., 2008). This transgenic mouse model expresses a truncated form of human ataxin-3 containing 69 glutamine repeats specifically in the cerebellar Purkinje cells and develops a severe and early-onset (P21) pathological phenotype. Moreover, this MJD transgenic mouse model allows the evaluation of allele-specific strategies, as the truncated human ataxin-3 carries the C variant (Gaspar et al., 2001) (Figure 2.2) present in 70% of the MJD patients.

In the present project, rAAV9-IV injection was performed in neonatal mice (P1), since neuronal transduction has proved to be superior during this period in rodents (Foust et al., 2009) (see section 1.4.2). When analyzing rAAV9 distribution 3 months after injection, we observed efficient transduction throughout the CNS, including regions normally affected in MJD such as the cerebellum, brainstem, spinal cord and striatum. In particular, the pontine nuclei, which are a major site of degeneration in MJD, showed great transgene expression (Figure 3.2). Additionally, the cerebral cortex, olfactory bulb and hippocampus also showed efficient transduction. This is the first study exploring rAAV9 distribution throughout the CNS following IV injection in this particular MJD mouse model, which proves to be similar to transduction patterns in wild-type subjects. Importantly, the large rAAV9 dispersion in the brain suggests that, when translating this strategy to other MJD models (Bichelmeier et al., 2007; Boy et al., 2010; Cemal et al., 2002; Chou et al., 2008; Goti et al., 2004; Silva-Fernandes et al., 2010; Silva-Fernandes et al., 2014) or human patients, vectors could target most of the affected regions, correcting the disease throughout the CNS.

Given that human mutant ataxin-3 expression is restricted to the cerebellar Purkinje cells (PCs) in this mouse model, we focused our attention to this neuronal population. PCs display an essential role in motor coordination and learning (Ito, 2002). They localize in the cerebellar cortex and receive input from climbing fibers (brainstem) and mossy fibers (thalamus, brainstem, spinal cord). Following information integration, PCs provide inhibitory output to the deep cerebellar nuclei (DCN), which then connect with motor-associated regions. When analyzing rAAV9-mediated cerebellar transduction (Figures 3.3 and 3.5), we observed marked transgene expression in Purkinje cells, enabling a direct silencing effect in this neuronal population. Moreover, choroid plexus epithelial cells and the DCN have also shown high transduction levels (Figure 3.3). This latter

finding indicates that AAV vectors might be retrogradely transported from the DCN to the PCs, contributing to therapeutic impact, as previously described (Keiser et al., 2014). Furthermore, DCN rAAV9 transduction might be beneficial in MJD patients and other mouse models (Bichelmeier et al., 2007; Boy et al., 2010; Cemal et al., 2002; Chou et al., 2008; Goti et al., 2004; Silva-Fernandes et al., 2014), since this region is severely affected in the disease context.

Interestingly, we concluded that rAAV9 was not equally distributed throughout the cerebellum, showing a particularly efficient transduction in lobules 10 and 9. This region showed 4 times higher transgene expression levels than other cerebellar lobules, in which some isolated rAAV9-positive Purkinje cells have been detected (Figure 3.4). Wild-type animals, on the contrary, presented vector efficient distribution throughout the whole cerebellum. These results are in accordance to Konno's reports regarding rAAV9 distribution pattern in polyQ69 transgenic MJD mice (Konno et al., 2014). These authors concluded that the limited rAAV9 dispersion is caused by defects in cerebellar vascularization. Accordingly, vascular endothelial growth factor (VEGF) expression and protein levels in the cerebellum have found to be decreased in this particular MJD model.

The preferential lobule 10 transduction, previously reported for transgenic and wild-type animals (Huda et al., 2014; Konno et al., 2014) might occur due to a better vascularization in this region or likely due to its proximity with the choroid plexus of fourth ventricle. The choroid plexus (CP) is composed by a monolayer of epithelial cells, which are responsible for cerebrospinal fluid (CSF) production and constitute a barrier between blood and CSF – the blood-CSF barrier (BCSFB) (Kaur et al., 2016). Therefore, blood-circulating rAAV9 vectors reaching the choroid plexus might eventually circumvent BCSFB and pass to the CSF. Since lobule 10 is close to the choroid plexus and in the path of CSF flow, rAAV9 access to PCs would preferentially occur in this cerebellar region.

Following rAAV9 biodistribution studies, we evaluated the potential therapeutic impact of these vectors. For that purpose, we compared the treated and control experimental groups, which received a P1 intravenous injection of rAAV9 vectors encoding miR-ATXN3 or miR-Control, respectively.

Firstly, we assessed whether rAAV9-IV injection successfully resulted in a phenotypic alleviation. We selected suitable tests to evaluate the main MJD-associated impairments, mainly related to: motor coordination, balance and gait pattern. Behavioral tests were performed at 35 days, since at this age polyQ69 transgenic MJD mice already exhibit a severe ataxic phenotype. Then, the same parameters were evaluated at 55 and 85 days, to investigate the impact of this therapy on disease progression and to demonstrate whether mutant ataxin-3 silencing is maintained over time. Overall, treated animals showed a better performance in all behavioral tests, with significant results in rotarod, swimming, beam walking and footprint analysis, indicating a general improvement in motor skills (Figures 3.6-3.8). This is the first report of significant behavioral improvement following AAV-mediated ataxin-3 silencing. In fact, Costa et al. have not observed any phenotypic amelioration after AAV2/1-miR-ATXN3 injection in the cerebellum of another model, MJD84.2 transgenic mice (Costa Mdo et al., 2013). Moreover, this was also the first time

that rAAV9-IV injection demonstrated a positive behavioral impact in PolyQ disorders. In fact, Dufour et al. failed to induce motor amelioration in a Huntington's disease (HD) mouse model following IV injection of rAAV9-miR-HTT vectors at 3 weeks (Dufour et al., 2014). Altogether, this indicates a superior therapeutic impact for our strategy, possibly due to the selected serotype, delivery route and time of injection.

Subsequently, we evaluated MJD-associated neuropathological changes, namely the presence of aggregates and cerebellar atrophy. Our analysis was focused on lobules 10 and 9, which we predicted as the region with better therapeutic impact, and lobule 6, which was randomly selected to conclude whether the silencing effect also spreads throughout the rest of the cerebellum. Approximately 3 months after injection, we quantified the number of aggregates per area and the molecular layer thickness of all three lobules. We observed a marked reduction in aggregate accumulation, accompanied by a preservation of molecular layer thickness for all the regions in study. The most significant results were obtained for lobule 10, corresponding to a 35% decrease in the number of aggregates per area and a 21% larger molecular layer thickness in comparison to control animals (Figures 3.9 and 3.10). Therefore, we concluded that the treatment successfully resulted in mutant ataxin-3 silencing, similarly to other reports exploring AAV delivery of miRNA-ATXN3 constructs to the cerebellum (Costa Mdo et al., 2013; Rodriguez-Lebron et al., 2013). Besides reducing the accumulation of toxic species, rAAV9-miR-ATXN3 injection possibly improved neuronal arborization and function, explaining the alleviation in cerebellar atrophy. Importantly, the results obtained for lobule 6 demonstrate that the therapeutic impact also occurs in regions of relatively weak rAAV9 transduction. These findings show some similarities to previous reports exploring AAV9 IV injection in PolyQ disorders. For instance, Konno et al. have observed a reduction in the number of aggregates and an improvement in PC arborization following rAAV9-CRAG delivery into polyQ69 MJD mice, although limited to lobule 10 (Konno et al., 2014). In comparison to this study, we were able to induce a more widespread effect, given that neuropathological signs were also attenuated in other cerebellar lobules. Additionally, Dufour et al., have reported a decrease in aggregate accumulation and atrophy in specific brain regions of HD mice due to rAAV9-mediated huntingtin silencing, similarly to our observations (Dufour et al., 2014).

Altogether, our results demonstrate that mutant ataxin-3 silencing through rAAV9 IV injection is an efficient therapeutic approach in transgenic MJD mice, alleviating both behavioral and neuropathological impairments. Importantly, these positive effects were obtained in a very severe model with an early onset, which could already exhibit neurological and vascularization defects at the time of treatment. Therefore, we predict an even more significant impact if testing this strategy in other MJD models, which present a late and mild phenotype (Bichelmeier et al., 2007; Boy et al., 2010; Cemal et al., 2002; Chou et al., 2008; Goti et al., 2004; Silva-Fernandes et al., 2010; Silva-Fernandes et al., 2014).

Although the first observations regarding rAAV9 distribution suggested a localized therapeutic response only in lobule 10, a very generalized effect was detected in the whole cerebellum and mice behavior. One could speculate that lobule 10 highly efficient transduction could be sufficient

to induce improvements in beam walking test or rotarod, since this lobule is part of the vestibular system, being important for balance (Witter and De Zeeuw, 2015). However, only an overall beneficial effect could explain the general better performance of treated mice, especially in tests exploring motor coordination, strength and gait. One possible explanation is that transduced PCs in other lobules, although scarce, might be sufficient to induce positive effects in the respective region. This can occur through a neuroprotective action induced by rAAV9-positive PCs in the entire cerebellum, by releasing neurotrophic factors or inhibiting neuroinflammation, for example. Alternatively, transduced PCs might transfer miR-ATXN3 molecules to the neighboring cells. Accordingly, Rodriguez-Lebron et al. have observed an efficient silencing effect in neurons that are negative for the vector reporter gene (Rodriguez-Lebron et al., 2013). They explained this phenomenon, designated as the 'penumbra effect' through the possible transfer of miRs between different neurons. Therefore, transduced PCs might communicate with rAAV9-negative neurons using extracellular vesicles containing miR-ATXN3 (Higa et al., 2014; Pegtel et al., 2010). Using a similar mechanism, transduced cells in the DCN can also release miR-ATXN3 constructs, which are then delivered to PC projections. Finally, the fact that CP epithelial cells are themselves transduced by rAAV9 could eventually contribute to our findings. Accordingly, choroid plexus-directed gene therapy has been investigated in the context of lysosomal storage disorders, where it allows the continuous secretion of therapeutic proteins into CSF, leading to beneficial effects (Hironaka et al., 2015; Liu et al., 2005; Yamazaki et al., 2014). Similarly, CP epithelial cells can secrete miRNAs incorporated into extracellular vesicles (EV) (Burgos et al., 2013; Tietje et al., 2014). Based on that, it is possible that rAAV9-positive CP cells in the fourth ventricle can transfer miR-ATXN3-containing EVs to the CSF, which then exert their silencing action in the cerebellum. Graphical abstract summarizes the possible mechanisms underlying rAAV9-miR-ATXN3 therapeutic impact in the present work.

In order to explore these hypotheses, we assessed whether the reduction in aggregate accumulation in treated animals is directly related with viral transduction (GFP expression) in lobules 9/10 and lobule 6 (Figure 3.11A and Supplementary Figure 6). In the first region, we found that animals with more efficient transduction exhibit less aggregates in the PC layer. However, the same correlation could not be applied to lobule 6, suggesting that in regions less transduced with rAAV9 particles, the therapeutic impact is probably dependent on other parameters, such as the intercellular transfer of miR constructs.

Additionally, we assessed whether different motor performances in treated animals might be also explained by distinct viral concentrations in the cerebellum. Given the technical difficulty of intrafacial administration in neonatal mice, combined with the large injected volume, some animals could have received different vector doses. Moreover, the quantity of viral particles that reach the cerebellum may also vary between different animals, possibly due to differences in vascularization or AAV receptor levels, something that we can possibly evaluate in future studies. Therefore, we also tried to establish a relation between the viral transduction levels in all cerebellar lobules (by quantifying GFP fluorescence) and behavioral performance in treated subjects. Interestingly, we found a dose-dependent response, in which higher transgene

expression levels correspond to better rotarod performances (Figure 3.11B). This hypothesis could be further explored, by quantifying the number of viral genome copies in the cerebellum through quantitative real-time PCR. Based on these results we can conclude that the therapeutic effect could potentially be maximized by increasing injected vector doses, i.e. the number of viral particles per animal.

Apart from the proved efficacy, the safety profile of our therapeutic strategy should be assessed to enable a possible translation to the clinic. Recent studies have reported immune responses triggered in the brain after rAAV9 delivery (Ciesielska et al., 2013; Samaranch et al., 2014) and toxicity due to miR-induced off-target silencing (Boudreau et al., 2011b; Monteys et al., 2014). Although we have not explored these parameters in the present work, wild-type mice rotarod performance was normal 85 days after rAAV9-miR-ATXN3 delivery, indicating no major neurological deficits (Supplementary Figure 3). However, in the future, it would be important to evaluate potential toxicity in the brain due to our treatment, by analyzing neuroinflammation markers. Moreover, AAV9 transduction is not restricted to the CNS following systemic injection, since viral vectors also get access to peripheral organs, particularly the liver (Zincarelli et al., 2008). Therefore, it would be interesting to evaluate rAAV9 transduction levels in liver samples from rAAV9-injected animals. Consequently, we could investigate whether viral vectors induce toxic effects in this organ, by analyzing the presence of inflammatory cytokines in the liver, as well as the levels of serum transaminases.

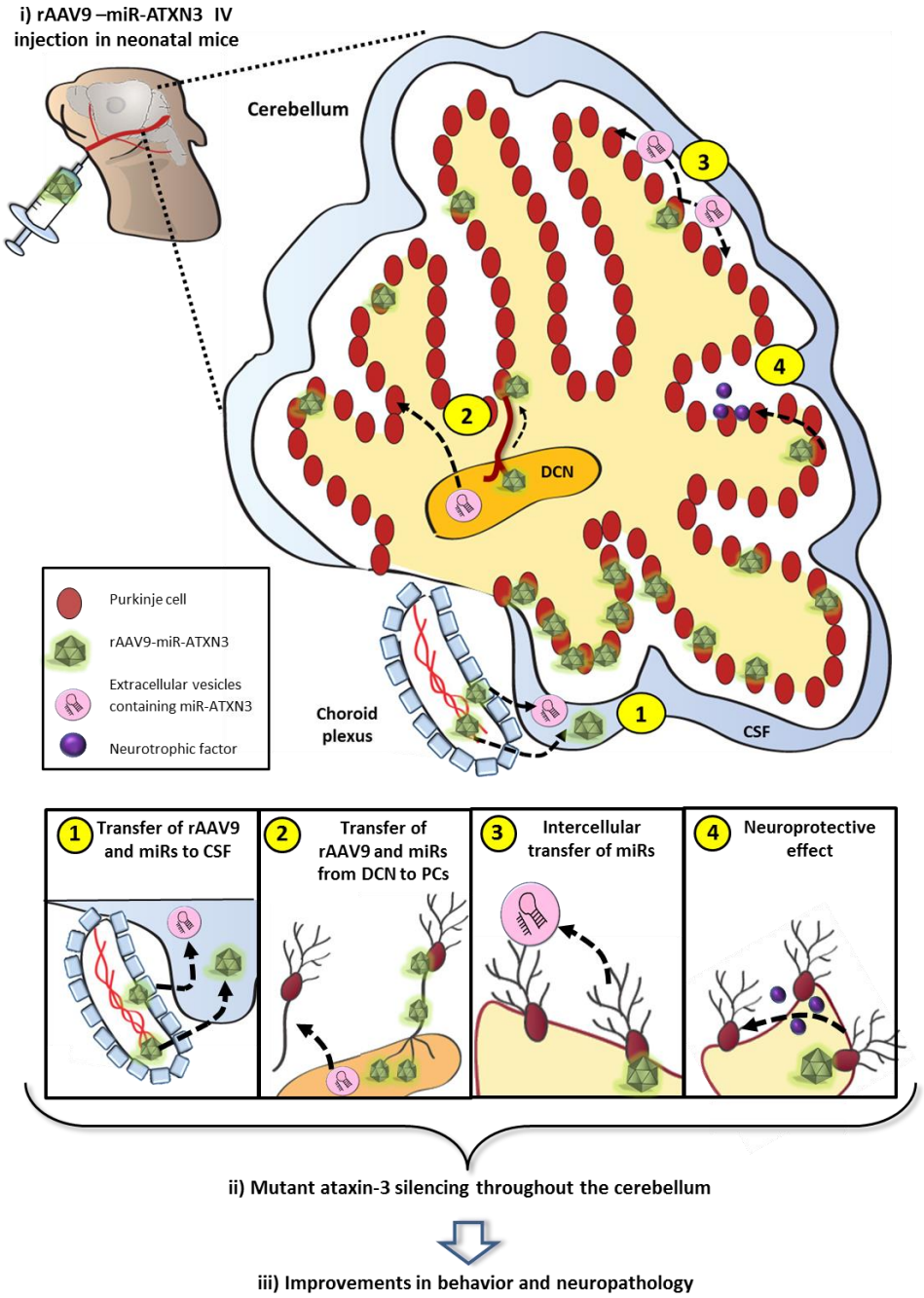

Graphical abstract: Schematic representation of possible mechanisms underlying AAV9-miR-ATXN3 therapeutic impact in the present work. In this project, i) rAAV9 vectors encoding miR-ATXN3 were intravenously injected into neonatal MJD transgenic mice, resulting in ii) mutant ataxin-3 silencing in the cerebellum and consequently iii) alleviation of neuropathological and behavioral impairments. Although rAAV9 vectors have efficiently transduced Purkinje cells (PCs) in lobules 10 and 9, other mechanisms could potentially increase their transduction levels and/or benefic effects, such as: 1) Transfer of viral vectors from the blood to the CSF and/or secretion of miR constructs to the CSF by transduced epithelial cells in the choroid plexus; 2) rAAV9 retrograde transport from DCN to PC layer and/or transfer of miRs from transduced cells in the DCN to PC projections; 3) Transfer or miRs between neighbor PCs; 4) Neuroprotective effects induced by rAAV9-positive PCs.

CSF - cerebrospinal fluid; DCN - Deep Cerebellar Nuclei; PC - Purkinje cell

5. Conclusions

In conclusion, this study provides compelling evidence that a single intravenous injection of rAAV9-miRNA-ATXN3 at postnatal day is able to: i) transpose the blood-brain barrier, ii) silence mutant ataxin-3 and iii) alleviate MJD neuropathological changes and motor impairments.

To our knowledge, this is the first report of significant behavioral improvements in polyglutamine disorders following rAAV9 intravenous administration. Moreover, this strategy also exhibited significant advantages when compared to previous studies exploring silencing strategies in MJD. In summary, our work constitutes the first MJD therapeutic approach capable of inducing widespread and long-term ataxin-3 silencing through a non-invasive system.

References

Aagaard, L., and Rossi, J.J. (2007). RNAi therapeutics: principles, prospects and challenges. Advanced drug delivery reviews *59*, 75-86.

Abbott, N.J. (2013). Blood-brain barrier structure and function and the challenges for CNS drug delivery. Journal of inherited metabolic disease *36*, 437-449.

Abbott, N.J., Ronnback, L., and Hansson, E. (2006). Astrocyte-endothelial interactions at the blood-brain barrier. Nature reviews Neuroscience *7*, 41-53.

Albrecht, M., Golatta, M., Wullner, U., and Lengauer, T. (2004). Structural and functional analysis of ataxin-2 and ataxin-3. European journal of biochemistry / FEBS *271*, 3155-3170.

Alves, S., Nascimento-Ferreira, I., Auregan, G., Hassig, R., Dufour, N., Brouillet, E., Pedroso de Lima, M.C., Hantraye, P., Pereira de Almeida, L., and Deglon, N. (2008a). Allele-specific RNA silencing of mutant ataxin-3 mediates neuroprotection in a rat model of Machado-Joseph disease. PloS one *3*, e3341.

Alves, S., Nascimento-Ferreira, I., Dufour, N., Hassig, R., Auregan, G., Nobrega, C., Brouillet, E., Hantraye, P., Pedroso de Lima, M.C., Deglon, N.*, et al.* (2010). Silencing ataxin-3 mitigates degeneration in a rat model of Machado-Joseph disease: no role for wild-type ataxin-3? Human molecular genetics *19*, 2380-2394.

Alves, S., Regulier, E., Nascimento-Ferreira, I., Hassig, R., Dufour, N., Koeppen, A., Carvalho, A.L., Simoes, S., de Lima, M.C., Brouillet, E.*, et al.* (2008b). Striatal and nigral pathology in a lentiviral rat model of Machado-Joseph disease. Human molecular genetics *17*, 2071-2083.

Antony, P.M., Mantele, S., Mollenkopf, P., Boy, J., Kehlenbach, R.H., Riess, O., and Schmidt, T. (2009). Identification and functional dissection of localization signals within ataxin-3. Neurobiology of disease *36*, 280-292.

Arrasate, M., Mitra, S., Schweitzer, E.S., Segal, M.R., and Finkbeiner, S. (2004). Inclusion body formation reduces levels of mutant huntingtin and the risk of neuronal death. Nature *431*, 805-810.

Aschauer, D.F., Kreuz, S., and Rumpel, S. (2013). Analysis of transduction efficiency, tropism and axonal transport of AAV serotypes 1, 2, 5, 6, 8 and 9 in the mouse brain. PloS one *8*, e76310.

Atchison, R.W., Casto, B.C., and Hammon, W.M. (1965). Adenovirus-Associated Defective Virus Particles. Science *149*, 754-756.

Balakrishnan, B., and Jayandharan, G.R. (2014). Basic biology of adeno-associated virus (AAV) vectors used in gene therapy. Current gene therapy *14*, 86-100.

Banez-Coronel, M., Porta, S., Kagerbauer, B., Mateu-Huertas, E., Pantano, L., Ferrer, I., Guzman, M., Estivill, X., and Marti, E. (2012). A pathogenic mechanism in Huntington's disease involves small CAG-repeated RNAs with neurotoxic activity. PLoS genetics *8*, e1002481.

Benkhelifa-Ziyyat, S., Besse, A., Roda, M., Duque, S., Astord, S., Carcenac, R., Marais, T., and Barkats, M. (2013). Intramuscular scAAV9-SMN injection mediates widespread gene delivery to the spinal cord and decreases disease severity in SMA mice. Molecular therapy : the journal of the American Society of Gene Therapy *21*, 282-290.

Berger, S., Schurer, L., Hartl, R., Messmer, K., and Baethmann, A. (1995). Reduction of post-traumatic intracranial hypertension by hypertonic/hyperoncotic saline/dextran and hypertonic mannitol. Neurosurgery *37*, 98-107; discussion 107-108.

Berke, S.J., Chai, Y., Marrs, G.L., Wen, H., and Paulson, H.L. (2005). Defining the role of ubiquitin-interacting motifs in the polyglutamine disease protein, ataxin-3. The Journal of biological chemistry *280*, 32026-32034.

Berke, S.J., Schmied, F.A., Brunt, E.R., Ellerby, L.M., and Paulson, H.L. (2004). Caspase-mediated proteolysis of the polyglutamine disease protein ataxin-3. Journal of neurochemistry *89*, 908-918.

Berns, K.I., and Linden, R.M. (1995). The cryptic life style of adeno-associated virus. BioEssays : news and reviews in molecular, cellular and developmental biology *17*, 237-245.

Bessis, N., GarciaCozar, F.J., and Boissier, M.C. (2004). Immune responses to gene therapy vectors: influence on vector function and effector mechanisms. Gene therapy *11 Suppl 1*, S10-17.

Bettencourt, C., and Lima, M. (2011). Machado-Joseph Disease: from first descriptions to new perspectives. Orphanet journal of rare diseases *6*, 35.

Bettencourt, C., Santos, C., Coutinho, P., Rizzu, P., Vasconcelos, J., Kay, T., Cymbron, T., Raposo, M., Heutink, P., and Lima, M. (2011). Parkinsonian phenotype in Machado-Joseph disease (MJD/SCA3): a two-case report. BMC neurology *11*, 131.

Bettencourt, C., Santos, C., Montiel, R., Costa Mdo, C., Cruz-Morales, P., Santos, L.R., Simoes, N., Kay, T., Vasconcelos, J., Maciel, P.*, et al.* (2010). Increased transcript diversity: novel splicing variants of Machado-Joseph disease gene (ATXN3). Neurogenetics *11*, 193-202.

Bevan, A.K., Duque, S., Foust, K.D., Morales, P.R., Braun, L., Schmelzer, L., Chan, C.M., McCrate, M., Chicoine, L.G., Coley, B.D.*, et al.* (2011). Systemic gene delivery in large species for targeting spinal cord, brain, and peripheral tissues for pediatric disorders. Molecular therapy : the journal of the American Society of Gene Therapy *19*, 1971-1980.

Bichelmeier, U., Schmidt, T., Hubener, J., Boy, J., Ruttiger, L., Habig, K., Poths, S., Bonin, M., Knipper, M., Schmidt, W.J.*, et al.* (2007). Nuclear localization of ataxin-3 is required for the manifestation of symptoms in SCA3: in vivo evidence. The Journal of neuroscience : the official journal of the Society for Neuroscience *27*, 7418-7428.

Bonanomi, M., Mazzucchelli, S., D'Urzo, A., Nardini, M., Konarev, P.V., Invernizzi, G., Svergun, D.I., Vanoni, M., Regonesi, M.E., and Tortora, P. (2014). Interactions of ataxin-3 with its molecular partners in the protein machinery that sorts protein aggregates to the aggresome. The international journal of biochemistry & cell biology *51*, 58-64.

Boudreau, R.L., Martins, I., and Davidson, B.L. (2009a). Artificial microRNAs as siRNA shuttles: improved safety as compared to shRNAs in vitro and in vivo. Molecular therapy : the journal of the American Society of Gene Therapy *17*, 169-175.

Boudreau, R.L., McBride, J.L., Martins, I., Shen, S., Xing, Y., Carter, B.J., and Davidson, B.L. (2009b). Nonallele-specific silencing of mutant and wild-type huntingtin demonstrates therapeutic efficacy in Huntington's disease mice. Molecular therapy : the journal of the American Society of Gene Therapy *17*, 1053-1063.

Boudreau, R.L., Monteys, A.M., and Davidson, B.L. (2008). Minimizing variables among hairpin-based RNAi vectors reveals the potency of shRNAs. RNA *14*, 1834-1844.

Boudreau, R.L., Rodriguez-Lebron, E., and Davidson, B.L. (2011a). RNAi medicine for the brain: progresses and challenges. Human molecular genetics *20*, R21-27.

Boudreau, R.L., Spengler, R.M., and Davidson, B.L. (2011b). Rational design of therapeutic siRNAs: minimizing off-targeting potential to improve the safety of RNAi therapy for Huntington's disease. Molecular therapy : the journal of the American Society of Gene Therapy *19*, 2169-2177.

Boy, J., Schmidt, T., Schumann, U., Grasshoff, U., Unser, S., Holzmann, C., Schmitt, I., Karl, T., Laccone, F., Wolburg, H*., et al.* (2010). A transgenic mouse model of spinocerebellar ataxia type 3 resembling late disease onset and gender-specific instability of CAG repeats. Neurobiology of disease *37*, 284-293.

Boy, J., Schmidt, T., Wolburg, H., Mack, A., Nuber, S., Bottcher, M., Schmitt, I., Holzmann, C., Zimmermann, F., Servadio, A*., et al.* (2009). Reversibility of symptoms in a conditional mouse model of spinocerebellar ataxia type 3. Human molecular genetics *18*, 4282-4295.

Breuer, P., Haacke, A., Evert, B.O., and Wullner, U. (2010). Nuclear aggregation of polyglutamine-expanded ataxin-3: fragments escape the cytoplasmic quality control. The Journal of biological chemistry *285*, 6532-6537.

Burger, C., Gorbatyuk, O.S., Velardo, M.J., Peden, C.S., Williams, P., Zolotukhin, S., Reier, P.J., Mandel, R.J., and Muzyczka, N. (2004). Recombinant AAV viral vectors pseudotyped with viral capsids from serotypes 1, 2, and 5 display differential efficiency and cell tropism after delivery to different regions of the central nervous system. Molecular therapy : the journal of the American Society of Gene Therapy *10*, 302-317.

Burger, C., Nguyen, F.N., Deng, J., and Mandel, R.J. (2005). Systemic mannitol-induced hyperosmolality amplifies rAAV2-mediated striatal transduction to a greater extent than local co-infusion. Molecular therapy : the journal of the American Society of Gene Therapy *11*, 327-331.

Burgos, K.L., Javaherian, A., Bomprezzi, R., Ghaffari, L., Rhodes, S., Courtright, A., Tembe, W., Kim, S., Metpally, R., and Van Keuren-Jensen, K. (2013). Identification of extracellular miRNA in human cerebrospinal fluid by next-generation sequencing. RNA *19*, 712-722.

Burk, K., Abele, M., Fetter, M., Dichgans, J., Skalej, M., Laccone, F., Didierjean, O., Brice, A., and Klockgether, T. (1996). Autosomal dominant cerebellar ataxia type I clinical features and MRI in families with SCA1, SCA2 and SCA3. Brain : a journal of neurology *119 (Pt 5)*, 1497-1505.

Burnett, B., Li, F., and Pittman, R.N. (2003). The polyglutamine neurodegenerative protein ataxin-3 binds polyubiquitylated proteins and has ubiquitin protease activity. Human molecular genetics *12*, 3195-3205.

Camargos, S.T., Marques, W., Jr., and Santos, A.C. (2011). Brain stem and cerebellum volumetric analysis of Machado Joseph disease patients. Arquivos de neuro-psiquiatria *69*, 292-296.

Cancel, G., Gourfinkel-An, I., Stevanin, G., Didierjean, O., Abbas, N., Hirsch, E., Agid, Y., and Brice, A. (1998). Somatic mosaicism of the CAG repeat expansion in spinocerebellar ataxia type 3/Machado-Joseph disease. Human mutation *11*, 23-27.

Carrington, J.C., and Ambros, V. (2003). Role of microRNAs in plant and animal development. Science *301*, 336-338.

Carvalho, D.R., La Rocque-Ferreira, A., Rizzo, I.M., Imamura, E.U., and Speck-Martins, C.E. (2008). Homozygosity enhances severity in spinocerebellar ataxia type 3. Pediatric neurology *38*, 296-299.

Castanotto, D., Sakurai, K., Lingeman, R., Li, H., Shively, L., Aagaard, L., Soifer, H., Gatignol, A., Riggs, A., and Rossi, J.J. (2007). Combinatorial delivery of small interfering RNAs reduces RNAi efficacy by selective incorporation into RISC. Nucleic acids research *35*, 5154-5164.

Castle, M.J., Perlson, E., Holzbaur, E.L., and Wolfe, J.H. (2014). Long-distance axonal transport of AAV9 is driven by dynein and kinesin-2 and is trafficked in a highly motile Rab7-positive compartment. Molecular therapy : the journal of the American Society of Gene Therapy *22*, 554-566.

Castro-Alvarez, J.F., Uribe-Arias, A., and Cardona-Gomez, G.P. (2015). Cyclin-Dependent kinase 5 targeting prevents beta-Amyloid aggregation involving glycogen synthase kinase 3beta and phosphatases. Journal of neuroscience research *93*, 1258-1266.

Cearley, C.N., and Wolfe, J.H. (2006). Transduction characteristics of adeno-associated virus vectors expressing cap serotypes 7, 8, 9, and Rh10 in the mouse brain. Molecular therapy : the journal of the American Society of Gene Therapy *13*, 528-537.

Cemal, C.K., Carroll, C.J., Lawrence, L., Lowrie, M.B., Ruddle, P., Al-Mahdawi, S., King, R.H., Pook, M.A., Huxley, C., and Chamberlain, S. (2002). YAC transgenic mice carrying pathological alleles of the MJD1 locus exhibit a mild and slowly progressive cerebellar deficit. Human molecular genetics *11*, 1075-1094.

Cervelli, T., Palacios, J.A., Zentilin, L., Mano, M., Schwartz, R.A., Weitzman, M.D., and Giacca, M. (2008). Processing of recombinant AAV genomes occurs in specific nuclear structures that overlap with foci of DNA-damage-response proteins. Journal of cell science *121*, 349-357.

Cetin, A., Komai, S., Eliava, M., Seeburg, P.H., and Osten, P. (2006). Stereotaxic gene delivery in the rodent brain. Nature protocols *1*, 3166-3173.

Chai, Y., Shao, J., Miller, V.M., Williams, A., and Paulson, H.L. (2002). Live-cell imaging reveals divergent intracellular dynamics of polyglutamine disease proteins and supports a sequestration model of pathogenesis. Proceedings of the National Academy of Sciences of the United States of America *99*, 9310-9315.

Chen, X., Tang, T.S., Tu, H., Nelson, O., Pook, M., Hammer, R., Nukina, N., and Bezprozvanny, I. (2008). Deranged calcium signaling and neurodegeneration in spinocerebellar ataxia type 3. The Journal of neuroscience : the official journal of the Society for Neuroscience *28*, 12713-12724.

Choi, V.W., McCarty, D.M., and Samulski, R.J. (2006). Host cell DNA repair pathways in adeno-associated viral genome processing. Journal of virology *80*, 10346-10356.

Chou, A.H., Chen, S.Y., Yeh, T.H., Weng, Y.H., and Wang, H.L. (2011). HDAC inhibitor sodium butyrate reverses transcriptional downregulation and ameliorates ataxic symptoms in a transgenic mouse model of SCA3. Neurobiology of disease *41*, 481-488.

Chou, A.H., Chen, Y.L., Chiu, C.C., Yuan, S.J., Weng, Y.H., Yeh, T.H., Lin, Y.L., Fang, J.M., and Wang, H.L. (2015). T1-11 and JMF1907 ameliorate polyglutamine-expanded ataxin-3-induced neurodegeneration, transcriptional dysregulation and ataxic symptom in the SCA3 transgenic mouse. Neuropharmacology *99*, 308-317.

Chou, A.H., Chen, Y.L., Hu, S.H., Chang, Y.M., and Wang, H.L. (2014). Polyglutamine-expanded ataxin-3 impairs long-term depression in Purkinje neurons of SCA3 transgenic mouse by inhibiting HAT and impairing histone acetylation. Brain research *1583*, 220-229.

Chou, A.H., Yeh, T.H., Ouyang, P., Chen, Y.L., Chen, S.Y., and Wang, H.L. (2008). Polyglutamine-expanded ataxin-3 causes cerebellar dysfunction of SCA3 transgenic mice by inducing transcriptional dysregulation. Neurobiology of disease *31*, 89-101.

Choudhury, S.R., Harris, A.F., Cabral, D.J., Keeler, A.M., Sapp, E., Ferreira, J.S., Gray-Edwards, H.L., Johnson, J.A., Johnson, A.K., Su, Q.*, et al.* (2016a). Widespread Central Nervous System Gene Transfer and Silencing After Systemic Delivery of Novel AAV-AS Vector. Molecular therapy : the journal of the American Society of Gene Therapy *24*, 726-735.

Choudhury, S.R., Hudry, E., Maguire, C.A., Sena-Esteves, M., Breakefield, X.O., and Grandi, P. (2016b). Viral vectors for therapy of neurologic diseases. Neuropharmacology.

Ciesielska, A., Hadaczek, P., Mittermeyer, G., Zhou, S., Wright, J.F., Bankiewicz, K.S., and Forsayeth, J. (2013). Cerebral infusion of AAV9 vector-encoding non-self proteins can elicit cell-mediated immune responses. Molecular therapy : the journal of the American Society of Gene Therapy *21*, 158-166.

Collaco, R.F., Cao, X., and Trempe, J.P. (1999). A helper virus-free packaging system for recombinant adeno-associated virus vectors. Gene *238*, 397-405.

Colomer Gould, V.F., Goti, D., Pearce, D., Gonzalez, G.A., Gao, H., Bermudez de Leon, M., Jenkins, N.A., Copeland, N.G., Ross, C.A., and Brown, D.R. (2007). A mutant ataxin-3 fragment results from processing at a site N-terminal to amino acid 190 in brain of Machado-Joseph disease-like transgenic mice. Neurobiology of disease *27*, 362-369.

Conceicao, M., Mendonca, L., Nobrega, C., Gomes, C., Costa, P., Hirai, H., Moreira, J.N., Lima, M.C., Manjunath, N., and de Almeida, L.P. (2016a). Safety profile of the intravenous administration of brain-targeted stable nucleic acid lipid particles. Data in brief *6*, 700-705.

Conceicao, M., Mendonca, L., Nobrega, C., Gomes, C., Costa, P., Hirai, H., Moreira, J.N., Lima, M.C., Manjunath, N., and Pereira de Almeida, L. (2016b). Intravenous administration of brain-targeted stable nucleic acid lipid particles alleviates Machado-Joseph disease neurological phenotype. Biomaterials *82*, 124-137.

Costa Mdo, C., Luna-Cancalon, K., Fischer, S., Ashraf, N.S., Ouyang, M., Dharia, R.M., Martin-Fishman, L., Yang, Y., Shakkottai, V.G., Davidson, B.L.*, et al.* (2013). Toward RNAi therapy for the polyglutamine disease Machado-Joseph disease. Molecular therapy : the journal of the American Society of Gene Therapy *21*, 1898-1908.

Coutinho, P., and Andrade, C. (1978). Autosomal dominant system degeneration in Portuguese families of the Azores Islands. A new genetic disorder involving cerebellar, pyramidal, extrapyramidal and spinal cord motor functions. Neurology *28*, 703-709.

Cunha-Santos, J., Duarte-Neves, J., Carmona, V., Guarente, L., Pereira de Almeida, L., and Cavadas, C. (2016). Caloric restriction blocks neuropathology and motor deficits in Machado-Joseph disease mouse models through SIRT1 pathway. Nature communications *7*, 11445.

D'Abreu, A., Franca, M., Jr., Appenzeller, S., Lopes-Cendes, I., and Cendes, F. (2009). Axonal dysfunction in the deep white matter in Machado-Joseph disease. Journal of neuroimaging : official journal of the American Society of Neuroimaging *19*, 9-12.

D'Abreu, A., Franca, M.C., Jr., Paulson, H.L., and Lopes-Cendes, I. (2010). Caring for Machado-Joseph disease: current understanding and how to help patients. Parkinsonism & related disorders *16*, 2-7.

D'Abreu, A., Franca, M.C., Jr., Yasuda, C.L., Campos, B.A., Lopes-Cendes, I., and Cendes, F. (2012). Neocortical atrophy in Machado-Joseph disease: a longitudinal neuroimaging study. Journal of neuroimaging : official journal of the American Society of Neuroimaging *22*, 285-291.

Davidson, B.L., Stein, C.S., Heth, J.A., Martins, I., Kotin, R.M., Derksen, T.A., Zabner, J., Ghodsi, A., and Chiorini, J.A. (2000). Recombinant adeno-associated virus type 2, 4, and 5 vectors: transduction of variant cell types and regions in the mammalian central nervous system. Proceedings of the National Academy of Sciences of the United States of America *97*, 3428-3432.

de Almeida, L.P., Zala, D., Aebischer, P., and Deglon, N. (2001). Neuroprotective effect of a CNTF-expressing lentiviral vector in the quinolinic acid rat model of Huntington's disease. Neurobiology of disease *8*, 433-446.

de Mezer, M., Wojciechowska, M., Napierala, M., Sobczak, K., and Krzyzosiak, W.J. (2011). Mutant CAG repeats of Huntingtin transcript fold into hairpins, form nuclear foci and are targets for RNA interference. Nucleic acids research *39*, 3852-3863.

Dehay, B., Dalkara, D., Dovero, S., Li, Q., and Bezard, E. (2012). Systemic scAAV9 variant mediates brain transduction in newborn rhesus macaques. Scientific reports *2*, 253.

Deverman, B.E., Pravdo, P.L., Simpson, B.P., Kumar, S.R., Chan, K.Y., Banerjee, A., Wu, W.L., Yang, B., Huber, N., Pasca, S.P*., et al.* (2016). Cre-dependent selection yields AAV variants for widespread gene transfer to the adult brain. Nature biotechnology *34*, 204-209.

DiFiglia, M., Sena-Esteves, M., Chase, K., Sapp, E., Pfister, E., Sass, M., Yoder, J., Reeves, P., Pandey, R.K., Rajeev, K.G*., et al.* (2007). Therapeutic silencing of mutant huntingtin with siRNA attenuates striatal and cortical neuropathology and behavioral deficits. Proceedings of the National Academy of Sciences of the United States of America *104*, 17204-17209.

Dominguez, E., Marais, T., Chatauret, N., Benkhelifa-Ziyyat, S., Duque, S., Ravassard, P., Carcenac, R., Astord, S., Pereira de Moura, A., Voit, T*., et al.* (2011). Intravenous scAAV9 delivery of a codon-optimized SMN1 sequence rescues SMA mice. Human molecular genetics *20*, 681-693.

Donaldson, K.M., Li, W., Ching, K.A., Batalov, S., Tsai, C.C., and Joazeiro, C.A. (2003). Ubiquitin-mediated sequestration of normal cellular proteins into polyglutamine aggregates. Proceedings of the National Academy of Sciences of the United States of America *100*, 8892-8897.

Dong, B., Nakai, H., and Xiao, W. (2010). Characterization of genome integrity for oversized recombinant AAV vector. Molecular therapy : the journal of the American Society of Gene Therapy *18*, 87-92.

Doss-Pepe, E.W., Stenroos, E.S., Johnson, W.G., and Madura, K. (2003). Ataxin-3 interactions with rad23 and valosin-containing protein and its associations with ubiquitin chains and the proteasome are consistent with a role in ubiquitin-mediated proteolysis. Molecular and cellular biology *23*, 6469-6483.

Dragatsis, I., Levine, M.S., and Zeitlin, S. (2000). Inactivation of Hdh in the brain and testis results in progressive neurodegeneration and sterility in mice. Nature genetics *26*, 300-306.

Drouet, V., Perrin, V., Hassig, R., Dufour, N., Auregan, G., Alves, S., Bonvento, G., Brouillet, E., Luthi-Carter, R., Hantraye, P*., et al.* (2009). Sustained effects of nonallele-specific Huntingtin silencing. Annals of neurology *65*, 276-285.

Drouet, V., Ruiz, M., Zala, D., Feyeux, M., Auregan, G., Cambon, K., Troquier, L., Carpentier, J., Aubert, S., Merienne, N*., et al.* (2014). Allele-specific silencing of mutant huntingtin in rodent brain and human stem cells. PloS one *9*, e99341.

Duarte-Neves, J., Goncalves, N., Cunha-Santos, J., Simoes, A.T., den Dunnen, W.F., Hirai, H., Kugler, S., Cavadas, C., and Pereira de Almeida, L. (2015). Neuropeptide Y mitigates neuropathology and motor deficits in mouse models of Machado-Joseph disease. Human molecular genetics *24*, 5451-5463.

Dufour, B.D., Smith, C.A., Clark, R.L., Walker, T.R., and McBride, J.L. (2014). Intrajugular vein delivery of AAV9-RNAi prevents neuropathological changes and weight loss in Huntington's disease mice. Molecular therapy : the journal of the American Society of Gene Therapy *22*, 797-810.

Duque, S., Joussemet, B., Riviere, C., Marais, T., Dubreil, L., Douar, A.M., Fyfe, J., Moullier, P., Colle, M.A., and Barkats, M. (2009). Intravenous administration of self-complementary AAV9 enables transgene delivery to adult motor neurons. Molecular therapy : the journal of the American Society of Gene Therapy *17*, 1187-1196.

Durr, A., Stevanin, G., Cancel, G., Duyckaerts, C., Abbas, N., Didierjean, O., Chneiweiss, H., Benomar, A., Lyon-Caen, O., Julien, J.*, et al.* (1996). Spinocerebellar ataxia 3 and Machado-Joseph disease: clinical, molecular, and neuropathological features. Annals of neurology *39*, 490-499.

Ehlert, E.M., Eggers, R., Niclou, S.P., and Verhaagen, J. (2010). Cellular toxicity following application of adeno-associated viral vector-mediated RNA interference in the nervous system. BMC neuroscience *11*, 20.

Elbashir, S.M., Lendeckel, W., and Tuschl, T. (2001). RNA interference is mediated by 21- and 22-nucleotide RNAs. Genes & development *15*, 188-200.

Esteves, S., Duarte-Silva, S., Naia, L., Neves-Carvalho, A., Teixeira-Castro, A., Rego, A.C., Silva-Fernandes, A., and Maciel, P. (2015). Limited Effect of Chronic Valproic Acid Treatment in a Mouse Model of Machado-Joseph Disease. PloS one *10*, e0141610.

Evers, M.M., Toonen, L.J., and van Roon-Mom, W.M. (2014). Ataxin-3 protein and RNA toxicity in spinocerebellar ataxia type 3: current insights and emerging therapeutic strategies. Molecular neurobiology *49*, 1513-1531.

Evert, B.O., Araujo, J., Vieira-Saecker, A.M., de Vos, R.A., Harendza, S., Klockgether, T., and Wullner, U. (2006). Ataxin-3 represses transcription via chromatin binding, interaction with histone deacetylase 3, and histone deacetylation. The Journal of neuroscience : the official journal of the Society for Neuroscience *26*, 11474-11486.

Ferrari, F.K., Samulski, T., Shenk, T., and Samulski, R.J. (1996). Second-strand synthesis is a rate-limiting step for efficient transduction by recombinant adeno-associated virus vectors. Journal of virology *70*, 3227-3234.

Foust, K.D., Nurre, E., Montgomery, C.L., Hernandez, A., Chan, C.M., and Kaspar, B.K. (2009). Intravascular AAV9 preferentially targets neonatal neurons and adult astrocytes. Nature biotechnology *27*, 59-65.

Foust, K.D., Salazar, D.L., Likhite, S., Ferraiuolo, L., Ditsworth, D., Ilieva, H., Meyer, K., Schmelzer, L., Braun, L., Cleveland, D.W.*, et al.* (2013). Therapeutic AAV9-mediated suppression of mutant SOD1 slows disease progression and extends survival in models of inherited ALS. Molecular therapy : the journal of the American Society of Gene Therapy *21*, 2148-2159.

Foust, K.D., Wang, X., McGovern, V.L., Braun, L., Bevan, A.K., Haidet, A.M., Le, T.T., Morales, P.R., Rich, M.M., Burghes, A.H.*, et al.* (2010). Rescue of the spinal muscular atrophy phenotype in a mouse model by early postnatal delivery of SMN. Nature biotechnology *28*, 271-274.

Franich, N.R., Fitzsimons, H.L., Fong, D.M., Klugmann, M., During, M.J., and Young, D. (2008). AAV vector-mediated RNAi of mutant huntingtin expression is neuroprotective in a novel genetic rat model of Huntington's disease. Molecular therapy : the journal of the American Society of Gene Therapy *16*, 947-956.

Franklin, K.B.J., and Paxinos, G. Paxinos and Franklin's The mouse brain in stereotaxic coordinates, Fourth edition. edn.

Fu, H., Dirosario, J., Killedar, S., Zaraspe, K., and McCarty, D.M. (2011). Correction of neurological disease of mucopolysaccharidosis IIIB in adult mice by rAAV9 trans-blood-brain barrier gene delivery. Molecular therapy : the journal of the American Society of Gene Therapy *19*, 1025-1033.

Gao, G., Vandenberghe, L.H., Alvira, M.R., Lu, Y., Calcedo, R., Zhou, X., and Wilson, J.M. (2004). Clades of Adeno-associated viruses are widely disseminated in human tissues. Journal of virology *78*, 6381-6388.

Garg, S.K., Lioy, D.T., Cheval, H., McGann, J.C., Bissonnette, J.M., Murtha, M.J., Foust, K.D., Kaspar, B.K., Bird, A., and Mandel, G. (2013). Systemic delivery of MeCP2 rescues behavioral and cellular deficits in female mouse models of Rett syndrome. The Journal of neuroscience : the official journal of the Society for Neuroscience *33*, 13612-13620.

Gaspar, C., Lopes-Cendes, I., DeStefano, A.L., Maciel, P., Silveira, I., Coutinho, P., MacLeod, P., Sequeiros, J., Farrer, L.A., and Rouleau, G.A. (1996). Linkage disequilibrium analysis in Machado-Joseph disease patients of different ethnic origins. Human genetics *98*, 620-624.

Gaspar, C., Lopes-Cendes, I., Hayes, S., Goto, J., Arvidsson, K., Dias, A., Silveira, I., Maciel, P., Coutinho, P., Lima, M.*, et al.* (2001). Ancestral origins of the Machado-Joseph disease mutation: a worldwide haplotype study. American journal of human genetics *68*, 523-528.

Giering, J.C., Grimm, D., Storm, T.A., and Kay, M.A. (2008). Expression of shRNA from a tissue-specific pol II promoter is an effective and safe RNAi therapeutic. Molecular therapy : the journal of the American Society of Gene Therapy *16*, 1630-1636.

Glascock, J.J., Osman, E.Y., Wetz, M.J., Krogman, M.M., Shababi, M., and Lorson, C.L. (2012). Decreasing disease severity in symptomatic, Smn(-/-);SMN2(+/+), spinal muscular atrophy mice following scAAV9-SMN delivery. Human gene therapy *23*, 330-335.

Goncalves, N., Simoes, A.T., Cunha, R.A., and de Almeida, L.P. (2013). Caffeine and adenosine A(2A) receptor inactivation decrease striatal neuropathology in a lentiviral-based model of Machado-Joseph disease. Annals of neurology *73*, 655-666.

Gong, Y., Mu, D., Prabhakar, S., Moser, A., Musolino, P., Ren, J., Breakefield, X.O., Maguire, C.A., and Eichler, F.S. (2015). Adenoassociated virus serotype 9-mediated gene therapy for x-linked

adrenoleukodystrophy. Molecular therapy : the journal of the American Society of Gene Therapy *23*, 824-834.

Gordon, C.R., Joffe, V., Vainstein, G., and Gadoth, N. (2003). Vestibulo-ocular arreflexia in families with spinocerebellar ataxia type 3 (Machado-Joseph disease). Journal of neurology, neurosurgery, and psychiatry *74*, 1403-1406.

Goti, D., Katzen, S.M., Mez, J., Kurtis, N., Kiluk, J., Ben-Haiem, L., Jenkins, N.A., Copeland, N.G., Kakizuka, A., Sharp, A.H.*, et al.* (2004). A mutant ataxin-3 putative-cleavage fragment in brains of Machado-Joseph disease patients and transgenic mice is cytotoxic above a critical concentration. The Journal of neuroscience : the official journal of the Society for Neuroscience *24*, 10266-10279.

Goto, J., Watanabe, M., Ichikawa, Y., Yee, S.B., Ihara, N., Endo, K., Igarashi, S., Takiyama, Y., Gaspar, C., Maciel, P.*, et al.* (1997). Machado-Joseph disease gene products carrying different carboxyl termini. Neuroscience research *28*, 373-377.

Gray, S.J., Matagne, V., Bachaboina, L., Yadav, S., Ojeda, S.R., and Samulski, R.J. (2011). Preclinical differences of intravascular AAV9 delivery to neurons and glia: a comparative study of adult mice and nonhuman primates. Molecular therapy : the journal of the American Society of Gene Therapy *19*, 1058-1069.

Green, F., Samaranch, L., Zhang, H.S., Manning-Bog, A., Meyer, K., Forsayeth, J., and Bankiewicz, K.S. (2016). Axonal transport of AAV9 in nonhuman primate brain. Gene therapy *23*, 520-526.

Grimm, D., Streetz, K.L., Jopling, C.L., Storm, T.A., Pandey, K., Davis, C.R., Marion, P., Salazar, F., and Kay, M.A. (2006). Fatality in mice due to oversaturation of cellular microRNA/short hairpin RNA pathways. Nature *441*, 537-541.

Grimm, D., Wang, L., Lee, J.S., Schurmann, N., Gu, S., Borner, K., Storm, T.A., and Kay, M.A. (2010). Argonaute proteins are key determinants of RNAi efficacy, toxicity, and persistence in the adult mouse liver. The Journal of clinical investigation *120*, 3106-3119.

Grondin, R., Kaytor, M.D., Ai, Y., Nelson, P.T., Thakker, D.R., Heisel, J., Weatherspoon, M.R., Blum, J.L., Burright, E.N., Zhang, Z.*, et al.* (2012). Six-month partial suppression of Huntingtin is well tolerated in the adult rhesus striatum. Brain : a journal of neurology *135*, 1197-1209.

Grossman, Z., Mendelson, E., Brok-Simoni, F., Mileguir, F., Leitner, Y., Rechavi, G., and Ramot, B. (1992). Detection of adeno-associated virus type 2 in human peripheral blood cells. The Journal of general virology *73 (Pt 4)*, 961-966.

Gu, W., Ma, H., Wang, K., Jin, M., Zhou, Y., Liu, X., Wang, G., and Shen, Y. (2004). The shortest expanded allele of the MJD1 gene in a Chinese MJD kindred with autonomic dysfunction. European neurology *52*, 107-111.

Gurda, B.L., De Guilhem De Lataillade, A., Bell, P., Zhu, Y., Yu, H., Wang, P., Bagel, J., Vite, C.H., Sikora, T., Hinderer, C.*, et al.* (2015). Evaluation of AAV-mediated Gene Therapy for Central Nervous System Disease in Canine Mucopolysaccharidosis VII. Molecular therapy : the journal of the American Society of Gene Therapy.

Haacke, A., Broadley, S.A., Boteva, R., Tzvetkov, N., Hartl, F.U., and Breuer, P. (2006). Proteolytic cleavage of polyglutamine-expanded ataxin-3 is critical for aggregation and sequestration of non-expanded ataxin-3. Human molecular genetics *15*, 555-568.

Hadaczek, P., Eberling, J.L., Pivirotto, P., Bringas, J., Forsayeth, J., and Bankiewicz, K.S. (2010). Eight years of clinical improvement in MPTP-lesioned primates after gene therapy with AAV2-hAADC. Molecular therapy : the journal of the American Society of Gene Therapy *18*, 1458-1461.

Hands, S.L., and Wyttenbach, A. (2010). Neurotoxic protein oligomerisation associated with polyglutamine diseases. Acta neuropathologica *120*, 419-437.

Harper, S.Q., Staber, P.D., He, X., Eliason, S.L., Martins, I.H., Mao, Q., Yang, L., Kotin, R.M., Paulson, H.L., and Davidson, B.L. (2005). RNA interference improves motor and neuropathological abnormalities in a Huntington's disease mouse model. Proceedings of the National Academy of Sciences of the United States of America *102*, 5820-5825.

Harris, G.M., Dodelzon, K., Gong, L., Gonzalez-Alegre, P., and Paulson, H.L. (2010). Splice isoforms of the polyglutamine disease protein ataxin-3 exhibit similar enzymatic yet different aggregation properties. PloS one *5*, e13695.

Hayashi, M., Kobayashi, K., and Furuta, H. (2003). Immunohistochemical study of neuronal intranuclear and cytoplasmic inclusions in Machado-Joseph disease. Psychiatry and clinical neurosciences *57*, 205-213.

Higa, G.S., de Sousa, E., Walter, L.T., Kinjo, E.R., Resende, R.R., and Kihara, A.H. (2014). MicroRNAs in neuronal communication. Molecular neurobiology *49*, 1309-1326.

High, K.H., Nathwani, A., Spencer, T., and Lillicrap, D. (2014). Current status of haemophilia gene therapy. Haemophilia : the official journal of the World Federation of Hemophilia *20 Suppl 4*, 43-49.

Hironaka, K., Yamazaki, Y., Hirai, Y., Yamamoto, M., Miyake, N., Miyake, K., Okada, T., Morita, A., and Shimada, T. (2015). Enzyme replacement in the CSF to treat metachromatic leukodystrophy in mouse model using single intracerebroventricular injection of self-complementary AAV1 vector. Scientific reports *5*, 13104.

Holmes, S.E., O'Hearn, E.E., McInnis, M.G., Gorelick-Feldman, D.A., Kleiderlein, J.J., Callahan, C., Kwak, N.G., Ingersoll-Ashworth, R.G., Sherr, M., Sumner, A.J.*, et al.* (1999). Expansion of a novel CAG trinucleotide repeat in the 5' region of PPP2R2B is associated with SCA12. Nature genetics *23*, 391-392.

Hsu, P.H., Wei, K.C., Huang, C.Y., Wen, C.J., Yen, T.C., Liu, C.L., Lin, Y.T., Chen, J.C., Shen, C.R., and Liu, H.L. (2013). Noninvasive and targeted gene delivery into the brain using microbubble-facilitated focused ultrasound. PloS one *8*, e57682.

Hsu, R.J., Hsiao, K.M., Lin, M.J., Li, C.Y., Wang, L.C., Chen, L.K., and Pan, H. (2011). Long tract of untranslated CAG repeats is deleterious in transgenic mice. PloS one *6*, e16417.

Hu, J., Liu, J., and Corey, D.R. (2010). Allele-selective inhibition of huntingtin expression by switching to an miRNA-like RNAi mechanism. Chemistry & biology *17*, 1183-1188.

Huang, B., Schiefer, J., Sass, C., Landwehrmeyer, G.B., Kosinski, C.M., and Kochanek, S. (2007). High-capacity adenoviral vector-mediated reduction of huntingtin aggregate load in vitro and in vivo. Human gene therapy *18*, 303-311.

Hubener, J., Weber, J.J., Richter, C., Honold, L., Weiss, A., Murad, F., Breuer, P., Wullner, U., Bellstedt, P., Paquet-Durand, F.*, et al.* (2013). Calpain-mediated ataxin-3 cleavage in the molecular pathogenesis of spinocerebellar ataxia type 3 (SCA3). Human molecular genetics *22*, 508-518.

Huda, F., Konno, A., Matsuzaki, Y., Goenawan, H., Miyake, K., Shimada, T., and Hirai, H. (2014). Distinct transduction profiles in the CNS via three injection routes of AAV9 and the application to generation of a neurodegenerative mouse model. Molecular therapy Methods & clinical development *1*, 14032.

Ichikawa, Y., Goto, J., Hattori, M., Toyoda, A., Ishii, K., Jeong, S.Y., Hashida, H., Masuda, N., Ogata, K., Kasai, F.*, et al.* (2001). The genomic structure and expression of MJD, the Machado-Joseph disease gene. Journal of human genetics *46*, 413-422.

Ikeda, H., Yamaguchi, M., Sugai, S., Aze, Y., Narumiya, S., and Kakizuka, A. (1996). Expanded polyglutamine in the Machado-Joseph disease protein induces cell death in vitro and in vivo. Nature genetics *13*, 196-202.

Inagaki, K., Fuess, S., Storm, T.A., Gibson, G.A., McTiernan, C.F., Kay, M.A., and Nakai, H. (2006). Robust systemic transduction with AAV9 vectors in mice: efficient global cardiac gene transfer superior to that of AAV8. Molecular therapy : the journal of the American Society of Gene Therapy *14*, 45-53.

Ito, M. (2002). Historical review of the significance of the cerebellum and the role of Purkinje cells in motor learning. Annals of the New York Academy of Sciences *978*, 273-288.

Iwata, N., Sekiguchi, M., Hattori, Y., Takahashi, A., Asai, M., Ji, B., Higuchi, M., Staufenbiel, M., Muramatsu, S., and Saido, T.C. (2013). Global brain delivery of neprilysin gene by intravascular administration of AAV vector in mice. Scientific reports *3*, 1472.

Kaur, C., Rathnasamy, G., and Ling, E.A. (2016). The Choroid Plexus in Healthy and Diseased Brain. Journal of neuropathology and experimental neurology *75*, 198-213.

Kawaguchi, Y., Okamoto, T., Taniwaki, M., Aizawa, M., Inoue, M., Katayama, S., Kawakami, H., Nakamura, S., Nishimura, M., Akiguchi, I.*, et al.* (1994). CAG expansions in a novel gene for Machado-Joseph disease at chromosome 14q32.1. Nature genetics *8*, 221-228.

Keiser, M.S., Boudreau, R.L., and Davidson, B.L. (2014). Broad therapeutic benefit after RNAi expression vector delivery to deep cerebellar nuclei: implications for spinocerebellar ataxia type 1 therapy. Molecular therapy : the journal of the American Society of Gene Therapy *22*, 588-595.

Keiser, M.S., Geoghegan, J.C., Boudreau, R.L., Lennox, K.A., and Davidson, B.L. (2013). RNAi or overexpression: alternative therapies for Spinocerebellar Ataxia Type 1. Neurobiology of disease *56*, 6-13.

Keiser, M.S., Kordower, J.H., Gonzalez-Alegre, P., and Davidson, B.L. (2015). Broad distribution of ataxin 1 silencing in rhesus cerebella for spinocerebellar ataxia type 1 therapy. Brain : a journal of neurology *138*, 3555-3566.

Kells, A.P., Hadaczek, P., Yin, D., Bringas, J., Varenika, V., Forsayeth, J., and Bankiewicz, K.S. (2009). Efficient gene therapy-based method for the delivery of therapeutics to primate cortex. Proceedings of the National Academy of Sciences of the United States of America *106*, 2407-2411.

Khodr, C.E., Sapru, M.K., Pedapati, J., Han, Y., West, N.C., Kells, A.P., Bankiewicz, K.S., and Bohn, M.C. (2011). An alpha-synuclein AAV gene silencing vector ameliorates a behavioral deficit in a rat model of Parkinson's disease, but displays toxicity in dopamine neurons. Brain research *1395*, 94-107.

Kieling, C., Prestes, P.R., Saraiva-Pereira, M.L., and Jardim, L.B. (2007). Survival estimates for patients with Machado-Joseph disease (SCA3). Clinical genetics *72*, 543-545.

Koch, P., Breuer, P., Peitz, M., Jungverdorben, J., Kesavan, J., Poppe, D., Doerr, J., Ladewig, J., Mertens, J., Tuting, T*., et al.* (2011). Excitation-induced ataxin-3 aggregation in neurons from patients with Machado-Joseph disease. Nature *480*, 543-546.

Konno, A., Shuvaev, A.N., Miyake, N., Miyake, K., Iizuka, A., Matsuura, S., Huda, F., Nakamura, K., Yanagi, S., Shimada, T*., et al.* (2014). Mutant ataxin-3 with an abnormally expanded polyglutamine chain disrupts dendritic development and metabotropic glutamate receptor signaling in mouse cerebellar Purkinje cells. Cerebellum *13*, 29-41.

Kotterman, M.A., and Schaffer, D.V. (2014). Engineering adeno-associated viruses for clinical gene therapy. Nature reviews Genetics *15*, 445-451.

Krauss, S., Griesche, N., Jastrzebska, E., Chen, C., Rutschow, D., Achmuller, C., Dorn, S., Boesch, S.M., Lalowski, M., Wanker, E*., et al.* (2013). Translation of HTT mRNA with expanded CAG repeats is regulated by the MID1-PP2A protein complex. Nature communications *4*, 1511.

Laco, M.N., Oliveira, C.R., Paulson, H.L., and Rego, A.C. (2012). Compromised mitochondrial complex II in models of Machado-Joseph disease. Biochimica et biophysica acta *1822*, 139-149.

Lentz, T.B., Gray, S.J., and Samulski, R.J. (2012). Viral vectors for gene delivery to the central nervous system. Neurobiology of disease *48*, 179-188.

Leone, P., Shera, D., McPhee, S.W., Francis, J.S., Kolodny, E.H., Bilaniuk, L.T., Wang, D.J., Assadi, M., Goldfarb, O., Goldman, H.W*., et al.* (2012). Long-term follow-up after gene therapy for canavan disease. Science translational medicine *4*, 165ra163.

Li, F., Macfarlan, T., Pittman, R.N., and Chakravarti, D. (2002). Ataxin-3 is a histone-binding protein with two independent transcriptional corepressor activities. The Journal of biological chemistry *277*, 45004-45012.

Li, L.B., Yu, Z., Teng, X., and Bonini, N.M. (2008). RNA toxicity is a component of ataxin-3 degeneration in Drosophila. Nature *453*, 1107-1111.

Liang, X., Jiang, H., Chen, C., Zhou, G., Wang, J., Zhang, S., Lei, L., Wang, X., and Tang, B. (2009). The correlation between magnetic resonance imaging features of the brainstem and cerebellum and clinical features of spinocerebellar ataxia 3/Machado-Joseph disease. Neurology India *57*, 578-583.

Lisowski, L., Tay, S.S., and Alexander, I.E. (2015). Adeno-associated virus serotypes for gene therapeutics. Current opinion in pharmacology *24*, 59-67.

Little, D., Valori, C.F., Mutsaers, C.A., Bennett, E.J., Wyles, M., Sharrack, B., Shaw, P.J., Gillingwater, T.H., Azzouz, M., and Ning, K. (2015). PTEN depletion decreases disease severity and modestly prolongs survival in a mouse model of spinal muscular atrophy. Molecular therapy : the journal of the American Society of Gene Therapy *23*, 270-277.

Liu, G., Martins, I., Wemmie, J.A., Chiorini, J.A., and Davidson, B.L. (2005). Functional correction of CNS phenotypes in a lysosomal storage disease model using adeno-associated virus type 4 vectors. The Journal of neuroscience : the official journal of the Society for Neuroscience *25*, 9321-9327.

Machida, Y., Okada, T., Kurosawa, M., Oyama, F., Ozawa, K., and Nukina, N. (2006). rAAV-mediated shRNA ameliorated neuropathology in Huntington disease model mouse. Biochemical and biophysical research communications *343*, 190-197.

Maciel, P., Costa, M.C., Ferro, A., Rousseau, M., Santos, C.S., Gaspar, C., Barros, J., Rouleau, G.A., Coutinho, P., and Sequeiros, J. (2001). Improvement in the molecular diagnosis of Machado-Joseph disease. Archives of neurology *58*, 1821-1827.

Maciel, P., Gaspar, C., DeStefano, A.L., Silveira, I., Coutinho, P., Radvany, J., Dawson, D.M., Sudarsky, L., Guimaraes, J., Loureiro, J.E*., et al.* (1995). Correlation between CAG repeat length and clinical features in Machado-Joseph disease. American journal of human genetics *57*, 54-61.

Maczuga, P., Koornneef, A., Borel, F., Petry, H., van Deventer, S., Ritsema, T., and Konstantinova, P. (2012). Optimization and comparison of knockdown efficacy between polymerase II expressed shRNA and artificial miRNA targeting luciferase and Apolipoprotein B100. BMC biotechnology *12*, 42.

Manfredsson, F.P., Rising, A.C., and Mandel, R.J. (2009). AAV9: a potential blood-brain barrier buster. Molecular therapy : the journal of the American Society of Gene Therapy *17*, 403-405.

Mano, M., Ippodrino, R., Zentilin, L., Zacchigna, S., and Giacca, M. (2015). Genome-wide RNAi screening identifies host restriction factors critical for in vivo AAV transduction. Proceedings of the National Academy of Sciences of the United States of America *112*, 11276-11281.

Mao, Y., Senic-Matuglia, F., Di Fiore, P.P., Polo, S., Hodsdon, M.E., and De Camilli, P. (2005). Deubiquitinating function of ataxin-3: insights from the solution structure of the Josephin domain. Proceedings of the National Academy of Sciences of the United States of America *102*, 12700-12705.

Marks, W.J., Jr., Bartus, R.T., Siffert, J., Davis, C.S., Lozano, A., Boulis, N., Vitek, J., Stacy, M., Turner, D., Verhagen, L.*, et al.* (2010). Gene delivery of AAV2-neurturin for Parkinson's disease: a double-blind, randomised, controlled trial. The Lancet Neurology *9*, 1164-1172.

Marquet, F., Teichert, T., Wu, S.Y., Tung, Y.S., Downs, M., Wang, S., Chen, C., Ferrera, V., and Konofagou, E.E. (2014). Real-time, transcranial monitoring of safe blood-brain barrier opening in non-human primates. PloS one *9*, e84310.

Martin, J.N., Wolken, N., Brown, T., Dauer, W.T., Ehrlich, M.E., and Gonzalez-Alegre, P. (2011). Lethal toxicity caused by expression of shRNA in the mouse striatum: implications for therapeutic design. Gene therapy *18*, 666-673.

Masino, L., Musi, V., Menon, R.P., Fusi, P., Kelly, G., Frenkiel, T.A., Trottier, Y., and Pastore, A. (2003). Domain architecture of the polyglutamine protein ataxin-3: a globular domain followed by a flexible tail. FEBS letters *549*, 21-25.

Matos, C.A., de Macedo-Ribeiro, S., and Carvalho, A.L. (2011). Polyglutamine diseases: the special case of ataxin-3 and Machado-Joseph disease. Progress in neurobiology *95*, 26-48.

McBride, J.L., Boudreau, R.L., Harper, S.Q., Staber, P.D., Monteys, A.M., Martins, I., Gilmore, B.L., Burstein, H., Peluso, R.W., Polisky, B.*, et al.* (2008). Artificial miRNAs mitigate shRNA-mediated toxicity in the brain: implications for the therapeutic development of RNAi. Proceedings of the National Academy of Sciences of the United States of America *105*, 5868-5873.

McBride, J.L., Pitzer, M.R., Boudreau, R.L., Dufour, B., Hobbs, T., Ojeda, S.R., and Davidson, B.L. (2011). Preclinical safety of RNAi-mediated HTT suppression in the rhesus macaque as a potential therapy for Huntington's disease. Molecular therapy : the journal of the American Society of Gene Therapy *19*, 2152-2162.

McCarty, D.M., DiRosario, J., Gulaid, K., Muenzer, J., and Fu, H. (2009). Mannitol-facilitated CNS entry of rAAV2 vector significantly delayed the neurological disease progression in MPS IIIB mice. Gene therapy *16*, 1340-1352.

McCarty, D.M., Fu, H., Monahan, P.E., Toulson, C.E., Naik, P., and Samulski, R.J. (2003). Adeno-associated virus terminal repeat (TR) mutant generates self-complementary vectors to overcome the rate-limiting step to transduction in vivo. Gene therapy *10*, 2112-2118.

McCarty, D.M., Monahan, P.E., and Samulski, R.J. (2001). Self-complementary recombinant adeno-associated virus (scAAV) vectors promote efficient transduction independently of DNA synthesis. Gene therapy *8*, 1248-1254.

McCarty, D.M., Young, S.M., Jr., and Samulski, R.J. (2004). Integration of adeno-associated virus (AAV) and recombinant AAV vectors. Annual review of genetics *38*, 819-845.

McPhee, S.W., Janson, C.G., Li, C., Samulski, R.J., Camp, A.S., Francis, J., Shera, D., Lioutermann, L., Feely, M., Freese, A.*, et al.* (2006). Immune responses to AAV in a phase I study for Canavan disease. The journal of gene medicine *8*, 577-588.

Mendonca, L.S., Nobrega, C., Hirai, H., Kaspar, B.K., and Pereira de Almeida, L. (2015). Transplantation of cerebellar neural stem cells improves motor coordination and neuropathology in Machado-Joseph disease mice. Brain : a journal of neurology *138*, 320-335.

Menzies, F.M., Huebener, J., Renna, M., Bonin, M., Riess, O., and Rubinsztein, D.C. (2010). Autophagy induction reduces mutant ataxin-3 levels and toxicity in a mouse model of spinocerebellar ataxia type 3. Brain : a journal of neurology *133*, 93-104.

Miller, T.M., Kaspar, B.K., Kops, G.J., Yamanaka, K., Christian, L.J., Gage, F.H., and Cleveland, D.W. (2005). Virus-delivered small RNA silencing sustains strength in amyotrophic lateral sclerosis. Annals of neurology *57*, 773-776.

Miyake, K., Miyake, N., Yamazaki, Y., Shimada, T., and Hirai, Y. (2012). Serotype-independent method of recombinant adeno-associated virus (AAV) vector production and purification. Journal of Nippon Medical School = Nippon Ika Daigaku zasshi *79*, 394-402.

Miyake, N., Miyake, K., Asakawa, N., Yamamoto, M., and Shimada, T. (2014). Long-term correction of biochemical and neurological abnormalities in MLD mice model by neonatal systemic injection of an AAV serotype 9 vector. Gene therapy *21*, 427-433.

Miyake, N., Miyake, K., Yamamoto, M., Hirai, Y., and Shimada, T. (2011). Global gene transfer into the CNS across the BBB after neonatal systemic delivery of single-stranded AAV vectors. Brain research *1389*, 19-26.

Monteys, A.M., Spengler, R.M., Dufour, B.D., Wilson, M.S., Oakley, C.K., Sowada, M.J., McBride, J.L., and Davidson, B.L. (2014). Single nucleotide seed modification restores in vivo tolerability of a toxic artificial miRNA sequence in the mouse brain. Nucleic acids research *42*, 13315-13327.

Mueller, T., Breuer, P., Schmitt, I., Walter, J., Evert, B.O., and Wullner, U. (2009). CK2-dependent phosphorylation determines cellular localization and stability of ataxin-3. Human molecular genetics *18*, 3334-3343.

Murlidharan, G., Samulski, R.J., and Asokan, A. (2014). Biology of adeno-associated viral vectors in the central nervous system. Frontiers in molecular neuroscience *7*, 76.

Murrey, D.A., Naughton, B.J., Duncan, F.J., Meadows, A.S., Ware, T.A., Campbell, K.J., Bremer, W.G., Walker, C.M., Goodchild, L., Bolon, B.*, et al.* (2014). Feasibility and safety of systemic rAAV9-hNAGLU delivery for treating mucopolysaccharidosis IIIB: toxicology, biodistribution, and immunological assessments in primates. Human gene therapy Clinical development *25*, 72-84.

Mykowska, A., Sobczak, K., Wojciechowska, M., Kozlowski, P., and Krzyzosiak, W.J. (2011). CAG repeats mimic CUG repeats in the misregulation of alternative splicing. Nucleic acids research *39*, 8938-8951.

Nagai, Y., Inui, T., Popiel, H.A., Fujikake, N., Hasegawa, K., Urade, Y., Goto, Y., Naiki, H., and Toda, T. (2007). A toxic monomeric conformer of the polyglutamine protein. Nature structural & molecular biology *14*, 332-340.

Nakano, K.K., Dawson, D.M., and Spence, A. (1972). Machado disease. A hereditary ataxia in Portuguese emigrants to Massachusetts. Neurology *22*, 49-55.

Nalavade, R., Griesche, N., Ryan, D.P., Hildebrand, S., and Krauss, S. (2013). Mechanisms of RNA-induced toxicity in CAG repeat disorders. Cell death & disease *4*, e752.

Naldini, L., Blomer, U., Gallay, P., Ory, D., Mulligan, R., Gage, F.H., Verma, I.M., and Trono, D. (1996). In vivo gene delivery and stable transduction of nondividing cells by a lentiviral vector. Science *272*, 263-267.

Nascimento-Ferreira, I., Nobrega, C., Vasconcelos-Ferreira, A., Onofre, I., Albuquerque, D., Aveleira, C., Hirai, H., Deglon, N., and Pereira de Almeida, L. (2013). Beclin 1 mitigates motor and neuropathological deficits in genetic mouse models of Machado-Joseph disease. Brain : a journal of neurology *136*, 2173-2188.

Nascimento-Ferreira, I., Santos-Ferreira, T., Sousa-Ferreira, L., Auregan, G., Onofre, I., Alves, S., Dufour, N., Colomer Gould, V.F., Koeppen, A., Deglon, N.*, et al.* (2011). Overexpression of the autophagic beclin-1 protein clears mutant ataxin-3 and alleviates Machado-Joseph disease. Brain : a journal of neurology *134*, 1400-1415.

Nguyen, H.P., Hubener, J., Weber, J.J., Grueninger, S., Riess, O., and Weiss, A. (2013). Cerebellar soluble mutant ataxin-3 level decreases during disease progression in Spinocerebellar Ataxia Type 3 mice. PloS one *8*, e62043.

Nicastro, G., Menon, R.P., Masino, L., Knowles, P.P., McDonald, N.Q., and Pastore, A. (2005). The solution structure of the Josephin domain of ataxin-3: structural determinants for molecular recognition. Proceedings of the National Academy of Sciences of the United States of America *102*, 10493-10498.

Nicastro, G., Todi, S.V., Karaca, E., Bonvin, A.M., Paulson, H.L., and Pastore, A. (2010). Understanding the role of the Josephin domain in the PolyUb binding and cleavage properties of ataxin-3. PloS one *5*, e12430.

Nizzardo, M., Simone, C., Rizzo, F., Salani, S., Dametti, S., Rinchetti, P., Del Bo, R., Foust, K., Kaspar, B.K., Bresolin, N.*, et al.* (2015). Gene therapy rescues disease phenotype in a spinal muscular atrophy with respiratory distress type 1 (SMARD1) mouse model. Science advances *1*, e1500078.

Nobre, R.J., and Almeida, L.P. (2011). Gene therapy for Parkinson's and Alzheimer's diseases: from the bench to clinical trials. Current pharmaceutical design *17*, 3434-3445.

Nobrega, C., Nascimento-Ferreira, I., Onofre, I., Albuquerque, D., Conceicao, M., Deglon, N., and de Almeida, L.P. (2013a). Overexpression of mutant ataxin-3 in mouse cerebellum induces ataxia and cerebellar neuropathology. Cerebellum *12*, 441-455.

Nobrega, C., Nascimento-Ferreira, I., Onofre, I., Albuquerque, D., Deglon, N., and de Almeida, L.P. (2014). RNA interference mitigates motor and neuropathological deficits in a cerebellar mouse model of Machado-Joseph disease. PloS one *9*, e100086.

Nobrega, C., Nascimento-Ferreira, I., Onofre, I., Albuquerque, D., Hirai, H., Deglon, N., and de Almeida, L.P. (2013b). Silencing mutant ataxin-3 rescues motor deficits and neuropathology in Machado-Joseph disease transgenic mice. PloS one *8*, e52396.

Nonnenmacher, M., and Weber, T. (2012). Intracellular transport of recombinant adeno-associated virus vectors. Gene therapy *19*, 649-658.

Ojala, D.S., Amara, D.P., and Schaffer, D.V. (2015). Adeno-associated virus vectors and neurological gene therapy. The Neuroscientist : a review journal bringing neurobiology, neurology and psychiatry *21*, 84-98.

Onofre, I., Mendonca, N., Lopes, S., Nobre, R., de Melo, J.B., Carreira, I.M., Januario, C., Goncalves, A.F., and de Almeida, L.P. (2016). Fibroblasts of Machado Joseph Disease patients reveal autophagy impairment. Scientific reports *6*, 28220.

Paddison, P.J., Caudy, A.A., Bernstein, E., Hannon, G.J., and Conklin, D.S. (2002). Short hairpin RNAs (shRNAs) induce sequence-specific silencing in mammalian cells. Genes & development *16*, 948-958.

Paul, C.P., Good, P.D., Winer, I., and Engelke, D.R. (2002). Effective expression of small interfering RNA in human cells. Nature biotechnology *20*, 505-508.

Paulson, H. (2012). Machado-Joseph disease/spinocerebellar ataxia type 3. Handbook of clinical neurology *103*, 437-449.

Paulson, H.L., Perez, M.K., Trottier, Y., Trojanowski, J.Q., Subramony, S.H., Das, S.S., Vig, P., Mandel, J.L., Fischbeck, K.H., and Pittman, R.N. (1997). Intranuclear inclusions of expanded polyglutamine protein in spinocerebellar ataxia type 3. Neuron *19*, 333-344.

Pedroso, J.L., Franca, M.C., Jr., Braga-Neto, P., D'Abreu, A., Saraiva-Pereira, M.L., Saute, J.A., Teive, H.A., Caramelli, P., Jardim, L.B., Lopes-Cendes, I.*, et al.* (2013). Nonmotor and extracerebellar features in Machado-Joseph disease: a review. Movement disorders : official journal of the Movement Disorder Society *28*, 1200-1208.

Peer, D., and Lieberman, J. (2011). Special delivery: targeted therapy with small RNAs. Gene therapy *18*, 1127-1133.

Pegtel, D.M., Cosmopoulos, K., Thorley-Lawson, D.A., van Eijndhoven, M.A., Hopmans, E.S., Lindenberg, J.L., de Gruijl, T.D., Wurdinger, T., and Middeldorp, J.M. (2010). Functional delivery of viral miRNAs via exosomes. Proceedings of the National Academy of Sciences of the United States of America *107*, 6328-6333.

Pennuto, M., Palazzolo, I., and Poletti, A. (2009). Post-translational modifications of expanded polyglutamine proteins: impact on neurotoxicity. Human molecular genetics *18*, R40-47.

Piedrahita, D., Hernandez, I., Lopez-Tobon, A., Fedorov, D., Obara, B., Manjunath, B.S., Boudreau, R.L., Davidson, B., Laferla, F., Gallego-Gomez, J.C.*, et al.* (2010). Silencing of CDK5 reduces neurofibrillary tangles in transgenic alzheimer's mice. The Journal of neuroscience : the official journal of the Society for Neuroscience *30*, 13966-13976.

Pillay, S., Meyer, N.L., Puschnik, A.S., Davulcu, O., Diep, J., Ishikawa, Y., Jae, L.T., Wosen, J.E., Nagamine, C.M., Chapman, M.S.*, et al.* (2016). An essential receptor for adeno-associated virus infection. Nature *530*, 108-112.

Posadas, I., Guerra, F.J., and Cena, V. (2010). Nonviral vectors for the delivery of small interfering RNAs to the CNS. Nanomedicine (Lond) *5*, 1219-1236.

Pozzi, C., Valtorta, M., Tedeschi, G., Galbusera, E., Pastori, V., Bigi, A., Nonnis, S., Grassi, E., and Fusi, P. (2008). Study of subcellular localization and proteolysis of ataxin-3. Neurobiology of disease *30*, 190-200.

Rabinowitz, J.E., Rolling, F., Li, C., Conrath, H., Xiao, W., Xiao, X., and Samulski, R.J. (2002). Cross-packaging of a single adeno-associated virus (AAV) type 2 vector genome into multiple AAV serotypes enables transduction with broad specificity. Journal of virology *76*, 791-801.

Rahim, A.A., Wong, A.M., Hoefer, K., Buckley, S.M., Mattar, C.N., Cheng, S.H., Chan, J.K., Cooper, J.D., and Waddington, S.N. (2011). Intravenous administration of AAV2/9 to the fetal and neonatal mouse leads to differential targeting of CNS cell types and extensive transduction of the nervous system. FASEB journal : official publication of the Federation of American Societies for Experimental Biology *25*, 3505-3518.

Ralph, G.S., Radcliffe, P.A., Day, D.M., Carthy, J.M., Leroux, M.A., Lee, D.C., Wong, L.F., Bilsland, L.G., Greensmith, L., Kingsman, S.M.*, et al.* (2005). Silencing mutant SOD1 using RNAi protects against neurodegeneration and extends survival in an ALS model. Nature medicine *11*, 429-433.

Ramachandran, P.S., Boudreau, R.L., Schaefer, K.A., La Spada, A.R., and Davidson, B.L. (2014). Nonallele specific silencing of ataxin-7 improves disease phenotypes in a mouse model of SCA7. Molecular therapy : the journal of the American Society of Gene Therapy *22*, 1635-1642.

Ramachandran, P.S., Keiser, M.S., and Davidson, B.L. (2013). Recent advances in RNA interference therapeutics for CNS diseases. Neurotherapeutics : the journal of the American Society for Experimental NeuroTherapeutics *10*, 473-485.

Ramani, B., Harris, G.M., Huang, R., Seki, T., Murphy, G.G., Costa Mdo, C., Fischer, S., Saunders, T.L., Xia, G., McEachin, R.C.*, et al.* (2015). A knockin mouse model of spinocerebellar ataxia type 3 exhibits prominent aggregate pathology and aberrant splicing of the disease gene transcript. Human molecular genetics *24*, 1211-1224.

Ramos, A., Kazachkova, N., Silva, F., Maciel, P., Silva-Fernandes, A., Duarte-Silva, S., Santos, C., and Lima, M. (2015). Differential mtDNA damage patterns in a transgenic mouse model of Machado-Joseph disease (MJD/SCA3). Journal of molecular neuroscience : MN *55*, 449-453.

Raoul, C., Abbas-Terki, T., Bensadoun, J.C., Guillot, S., Haase, G., Szulc, J., Henderson, C.E., and Aebischer, P. (2005). Lentiviral-mediated silencing of SOD1 through RNA interference retards disease onset and progression in a mouse model of ALS. Nature medicine *11*, 423-428.

Rettig, G.R., and Behlke, M.A. (2012). Progress toward in vivo use of siRNAs-II. Molecular therapy : the journal of the American Society of Gene Therapy *20*, 483-512.

Rodrigues, A.J., Coppola, G., Santos, C., Costa Mdo, C., Ailion, M., Sequeiros, J., Geschwind, D.H., and Maciel, P. (2007). Functional genomics and biochemical characterization of the C. elegans orthologue of the Machado-Joseph disease protein ataxin-3. FASEB journal : official publication of the Federation of American Societies for Experimental Biology *21*, 1126-1136.

Rodrigues, A.J., do Carmo Costa, M., Silva, T.L., Ferreira, D., Bajanca, F., Logarinho, E., and Maciel, P. (2010). Absence of ataxin-3 leads to cytoskeletal disorganization and increased cell death. Biochimica et biophysica acta *1803*, 1154-1163.

Rodriguez-Lebron, E., Costa Mdo, C., Luna-Cancalon, K., Peron, T.M., Fischer, S., Boudreau, R.L., Davidson, B.L., and Paulson, H.L. (2013). Silencing mutant ATXN3 expression resolves molecular phenotypes in SCA3 transgenic mice. Molecular therapy : the journal of the American Society of Gene Therapy *21*, 1909-1918.

Rodriguez-Lebron, E., Gouvion, C.M., Moore, S.A., Davidson, B.L., and Paulson, H.L. (2009). Allele-specific RNAi mitigates phenotypic progression in a transgenic model of Alzheimer's disease. Molecular therapy : the journal of the American Society of Gene Therapy *17*, 1563-1573.

Rosenberg, R.N. (1992). Machado-Joseph disease: an autosomal dominant motor system degeneration. Movement disorders : official journal of the Movement Disorder Society *7*, 193-203.

Rub, U., Brunt, E.R., and Deller, T. (2008). New insights into the pathoanatomy of spinocerebellar ataxia type 3 (Machado-Joseph disease). Current opinion in neurology *21*, 111-116.

Rub, U., de Vos, R.A., Brunt, E.R., Sebesteny, T., Schols, L., Auburger, G., Bohl, J., Ghebremedhin, E., Gierga, K., Seidel, K*., et al.* (2006). Spinocerebellar ataxia type 3 (SCA3): thalamic neurodegeneration occurs independently from thalamic ataxin-3 immunopositive neuronal intranuclear inclusions. Brain Pathol *16*, 218-227.

Rub, U., Schols, L., Paulson, H., Auburger, G., Kermer, P., Jen, J.C., Seidel, K., Korf, H.W., and Deller, T. (2013). Clinical features, neurogenetics and neuropathology of the polyglutamine spinocerebellar ataxias type 1, 2, 3, 6 and 7. Progress in neurobiology *104*, 38-66.

Ruzo, A., Marco, S., Garcia, M., Villacampa, P., Ribera, A., Ayuso, E., Maggioni, L., Mingozzi, F., Haurigot, V., and Bosch, F. (2012). Correction of pathological accumulation of glycosaminoglycans

in central nervous system and peripheral tissues of MPSIIIA mice through systemic AAV9 gene transfer. Human gene therapy *23*, 1237-1246.

Saida, H., Matsuzaki, Y., Takayama, K., Iizuka, A., Konno, A., Yanagi, S., and Hirai, H. (2014). One-year follow-up of transgene expression by integrase-defective lentiviral vectors and their therapeutic potential in spinocerebellar ataxia model mice. Gene therapy *21*, 820-827.

Samaranch, L., San Sebastian, W., Kells, A.P., Salegio, E.A., Heller, G., Bringas, J.R., Pivirotto, P., DeArmond, S., Forsayeth, J., and Bankiewicz, K.S. (2014). AAV9-mediated expression of a non-self protein in nonhuman primate central nervous system triggers widespread neuroinflammation driven by antigen-presenting cell transduction. Molecular therapy : the journal of the American Society of Gene Therapy *22*, 329-337.

Samulski, R.J., Berns, K.I., Tan, M., and Muzyczka, N. (1982). Cloning of adeno-associated virus into pBR322: rescue of intact virus from the recombinant plasmid in human cells. Proceedings of the National Academy of Sciences of the United States of America *79*, 2077-2081.

Sapru, M.K., Yates, J.W., Hogan, S., Jiang, L., Halter, J., and Bohn, M.C. (2006). Silencing of human alpha-synuclein in vitro and in rat brain using lentiviral-mediated RNAi. Experimental neurology *198*, 382-390.

Sarkis, C., Philippe, S., Mallet, J., and Serguera, C. (2008). Non-integrating lentiviral vectors. Current gene therapy *8*, 430-437.

Sarna, J.R., and Hawkes, R. (2003). Patterned Purkinje cell death in the cerebellum. Progress in neurobiology *70*, 473-507.

Sathasivam, K., Neueder, A., Gipson, T.A., Landles, C., Benjamin, A.C., Bondulich, M.K., Smith, D.L., Faull, R.L., Roos, R.A., Howland, D*., et al.* (2013). Aberrant splicing of HTT generates the pathogenic exon 1 protein in Huntington disease. Proceedings of the National Academy of Sciences of the United States of America *110*, 2366-2370.

Schaefer, M.H., Wanker, E.E., and Andrade-Navarro, M.A. (2012). Evolution and function of CAG/polyglutamine repeats in protein-protein interaction networks. Nucleic acids research *40*, 4273-4287.

Scherzed, W., Brunt, E.R., Heinsen, H., de Vos, R.A., Seidel, K., Burk, K., Schols, L., Auburger, G., Del Turco, D., Deller, T*., et al.* (2012). Pathoanatomy of cerebellar degeneration in spinocerebellar ataxia type 2 (SCA2) and type 3 (SCA3). Cerebellum *11*, 749-760.

Schmidt, T., Landwehrmeyer, G.B., Schmitt, I., Trottier, Y., Auburger, G., Laccone, F., Klockgether, T., Volpel, M., Epplen, J.T., Schols, L*., et al.* (1998). An isoform of ataxin-3 accumulates in the nucleus of neuronal cells in affected brain regions of SCA3 patients. Brain Pathol *8*, 669-679.

Schmidt, T., Lindenberg, K.S., Krebs, A., Schols, L., Laccone, F., Herms, J., Rechsteiner, M., Riess, O., and Landwehrmeyer, G.B. (2002). Protein surveillance machinery in brains with spinocerebellar ataxia type 3: redistribution and differential recruitment of 26S proteasome subunits and chaperones to neuronal intranuclear inclusions. Annals of neurology *51*, 302-310.

Schmitt, I., Linden, M., Khazneh, H., Evert, B.O., Breuer, P., Klockgether, T., and Wuellner, U. (2007). Inactivation of the mouse Atxn3 (ataxin-3) gene increases protein ubiquitination. Biochemical and biophysical research communications *362*, 734-739.

Scholefield, J., Greenberg, L.J., Weinberg, M.S., Arbuthnot, P.B., Abdelgany, A., and Wood, M.J. (2009). Design of RNAi hairpins for mutation-specific silencing of ataxin-7 and correction of a SCA7 phenotype. PloS one *4*, e7232.

Scholefield, J., Watson, L., Smith, D., Greenberg, J., and Wood, M.J. (2014). Allele-specific silencing of mutant Ataxin-7 in SCA7 patient-derived fibroblasts. European journal of human genetics : EJHG *22*, 1369-1375.

Scholefield, J., and Wood, M.J. (2010). Therapeutic gene silencing strategies for polyglutamine disorders. Trends in genetics : TIG *26*, 29-38.

Schols, L., Bauer, P., Schmidt, T., Schulte, T., and Riess, O. (2004). Autosomal dominant cerebellar ataxias: clinical features, genetics, and pathogenesis. The Lancet Neurology *3*, 291-304.

Seidel, K., den Dunnen, W.F., Schultz, C., Paulson, H., Frank, S., de Vos, R.A., Brunt, E.R., Deller, T., Kampinga, H.H., and Rub, U. (2010). Axonal inclusions in spinocerebellar ataxia type 3. Acta neuropathologica *120*, 449-460.

Seidel, K., Siswanto, S., Brunt, E.R., den Dunnen, W., Korf, H.W., and Rub, U. (2012). Brain pathology of spinocerebellar ataxias. Acta neuropathologica *124*, 1-21.

Shakkottai, V.G., do Carmo Costa, M., Dell'Orco, J.M., Sankaranarayanan, A., Wulff, H., and Paulson, H.L. (2011). Early changes in cerebellar physiology accompany motor dysfunction in the polyglutamine disease spinocerebellar ataxia type 3. The Journal of neuroscience : the official journal of the Society for Neuroscience *31*, 13002-13014.

Shao, J., and Diamond, M.I. (2007). Polyglutamine diseases: emerging concepts in pathogenesis and therapy. Human molecular genetics *16 Spec No. 2*, R115-123.

Shen, S., Bryant, K.D., Brown, S.M., Randell, S.H., and Asokan, A. (2011). Terminal N-linked galactose is the primary receptor for adeno-associated virus 9. The Journal of biological chemistry *286*, 13532-13540.

Shimizu, N., Takiyama, Y., Mizuno, Y., Mizuno, M., Saito, K., and Yoshida, M. (1990). Characteristics of oculomotor disorders of a family with Joseph's disease. Journal of neurology *237*, 393-398.

Shin, K.J., Wall, E.A., Zavzavadjian, J.R., Santat, L.A., Liu, J., Hwang, J.I., Rebres, R., Roach, T., Seaman, W., Simon, M.I.*, et al.* (2006). A single lentiviral vector platform for microRNA-based conditional RNA interference and coordinated transgene expression. Proceedings of the National Academy of Sciences of the United States of America *103*, 13759-13764.

Silva-Fernandes, A., Costa Mdo, C., Duarte-Silva, S., Oliveira, P., Botelho, C.M., Martins, L., Mariz, J.A., Ferreira, T., Ribeiro, F., Correia-Neves, M.*, et al.* (2010). Motor uncoordination and

neuropathology in a transgenic mouse model of Machado-Joseph disease lacking intranuclear inclusions and ataxin-3 cleavage products. Neurobiology of disease *40*, 163-176.

Silva-Fernandes, A., Duarte-Silva, S., Neves-Carvalho, A., Amorim, M., Soares-Cunha, C., Oliveira, P., Thirstrup, K., Teixeira-Castro, A., and Maciel, P. (2014). Chronic treatment with 17-DMAG improves balance and coordination in a new mouse model of Machado-Joseph disease. Neurotherapeutics : the journal of the American Society for Experimental NeuroTherapeutics *11*, 433-449.

Simoes, A.T., Goncalves, N., Koeppen, A., Deglon, N., Kugler, S., Duarte, C.B., and Pereira de Almeida, L. (2012). Calpastatin-mediated inhibition of calpains in the mouse brain prevents mutant ataxin 3 proteolysis, nuclear localization and aggregation, relieving Machado-Joseph disease. Brain : a journal of neurology *135*, 2428-2439.

Simoes, A.T., Goncalves, N., Nobre, R.J., Duarte, C.B., and Pereira de Almeida, L. (2014). Calpain inhibition reduces ataxin-3 cleavage alleviating neuropathology and motor impairments in mouse models of Machado-Joseph disease. Human molecular genetics *23*, 4932-4944.

Singer, O., Marr, R.A., Rockenstein, E., Crews, L., Coufal, N.G., Gage, F.H., Verma, I.M., and Masliah, E. (2005). Targeting BACE1 with siRNAs ameliorates Alzheimer disease neuropathology in a transgenic model. Nature neuroscience *8*, 1343-1349.

Sobczak, K., and Krzyzosiak, W.J. (2005). CAG repeats containing CAA interruptions form branched hairpin structures in spinocerebellar ataxia type 2 transcripts. The Journal of biological chemistry *280*, 3898-3910.

Sonntag, F., Schmidt, K., and Kleinschmidt, J.A. (2010). A viral assembly factor promotes AAV2 capsid formation in the nucleolus. Proceedings of the National Academy of Sciences of the United States of America *107*, 10220-10225.

Soong, B.W., and Liu, R.S. (1998). Positron emission tomography in asymptomatic gene carriers of Machado-Joseph disease. Journal of neurology, neurosurgery, and psychiatry *64*, 499-504.

Spampanato, C., De Leonibus, E., Dama, P., Gargiulo, A., Fraldi, A., Sorrentino, N.C., Russo, F., Nusco, E., Auricchio, A., Surace, E.M.*, et al.* (2011). Efficacy of a combined intracerebral and systemic gene delivery approach for the treatment of a severe lysosomal storage disorder. Molecular therapy : the journal of the American Society of Gene Therapy *19*, 860-869.

Stanek, L.M., Sardi, S.P., Mastis, B., Richards, A.R., Treleaven, C.M., Taksir, T., Misra, K., Cheng, S.H., and Shihabuddin, L.S. (2014). Silencing mutant huntingtin by adeno-associated virus-mediated RNA interference ameliorates disease manifestations in the YAC128 mouse model of Huntington's disease. Human gene therapy *25*, 461-474.

Stoica, L., Todeasa, S.H., Cabrera, G.T., Salameh, J.S., ElMallah, M.K., Mueller, C., Brown, R.H., Jr., and Sena-Esteves, M. (2016). Adeno-associated virus-delivered artificial microRNA extends survival and delays paralysis in an amyotrophic lateral sclerosis mouse model. Annals of neurology *79*, 687-700.

Subramony, S.H., and Currier, R.D. (1996). Intrafamilial variability in Machado-Joseph disease. Movement disorders : official journal of the Movement Disorder Society *11*, 741-743.

Summerford, C., and Samulski, R.J. (1998). Membrane-associated heparan sulfate proteoglycan is a receptor for adeno-associated virus type 2 virions. Journal of virology *72*, 1438-1445.

Switonski, P.M., Szlachcic, W.J., Krzyzosiak, W.J., and Figiel, M. (2015). A new humanized ataxin-3 knock-in mouse model combines the genetic features, pathogenesis of neurons and glia and late disease onset of SCA3/MJD. Neurobiology of disease *73*, 174-188.

Takahashi, T., Kikuchi, S., Katada, S., Nagai, Y., Nishizawa, M., and Onodera, O. (2008). Soluble polyglutamine oligomers formed prior to inclusion body formation are cytotoxic. Human molecular genetics *17*, 345-356.

Takiyama, Y., Igarashi, S., Rogaeva, E.A., Endo, K., Rogaev, E.I., Tanaka, H., Sherrington, R., Sanpei, K., Liang, Y., Saito, M.*, et al.* (1995). Evidence for inter-generational instability in the CAG repeat in the MJD1 gene and for conserved haplotypes at flanking markers amongst Japanese and Caucasian subjects with Machado-Joseph disease. Human molecular genetics *4*, 1137-1146.

Taroni, F., and DiDonato, S. (2004). Pathways to motor incoordination: the inherited ataxias. Nature reviews Neuroscience *5*, 641-655.

Taymans, J.M., Vandenberghe, L.H., Haute, C.V., Thiry, I., Deroose, C.M., Mortelmans, L., Wilson, J.M., Debyser, Z., and Baekelandt, V. (2007). Comparative analysis of adeno-associated viral vector serotypes 1, 2, 5, 7, and 8 in mouse brain. Human gene therapy *18*, 195-206.

Teixeira-Castro, A., Ailion, M., Jalles, A., Brignull, H.R., Vilaca, J.L., Dias, N., Rodrigues, P., Oliveira, J.F., Neves-Carvalho, A., Morimoto, R.I.*, et al.* (2011). Neuron-specific proteotoxicity of mutant ataxin-3 in C. elegans: rescue by the DAF-16 and HSF-1 pathways. Human molecular genetics *20*, 2996-3009.

Teixeira-Castro, A., Jalles, A., Esteves, S., Kang, S., da Silva Santos, L., Silva-Fernandes, A., Neto, M.F., Brielmann, R.M., Bessa, C., Duarte-Silva, S.*, et al.* (2015). Serotonergic signalling suppresses ataxin 3 aggregation and neurotoxicity in animal models of Machado-Joseph disease. Brain : a journal of neurology *138*, 3221-3237.

Thomsen, G.M., Gowing, G., Latter, J., Chen, M., Vit, J.P., Staggenborg, K., Avalos, P., Alkaslasi, M., Ferraiuolo, L., Likhite, S.*, et al.* (2014). Delayed disease onset and extended survival in the SOD1G93A rat model of amyotrophic lateral sclerosis after suppression of mutant SOD1 in the motor cortex. The Journal of neuroscience : the official journal of the Society for Neuroscience *34*, 15587-15600.

Tietje, A., Maron, K.N., Wei, Y., and Feliciano, D.M. (2014). Cerebrospinal fluid extracellular vesicles undergo age dependent declines and contain known and novel non-coding RNAs. PloS one *9*, e113116.

Torashima, T., Koyama, C., Iizuka, A., Mitsumura, K., Takayama, K., Yanagi, S., Oue, M., Yamaguchi, H., and Hirai, H. (2008). Lentivector-mediated rescue from cerebellar ataxia in a mouse model of spinocerebellar ataxia. EMBO reports *9*, 393-399.

Tsoi, H., Lau, T.C., Tsang, S.Y., Lau, K.F., and Chan, H.Y. (2012). CAG expansion induces nucleolar stress in polyglutamine diseases. Proceedings of the National Academy of Sciences of the United States of America *109*, 13428-13433.

Uchihara, T., Fujigasaki, H., Koyano, S., Nakamura, A., Yagishita, S., and Iwabuchi, K. (2001). Non-expanded polyglutamine proteins in intranuclear inclusions of hereditary ataxias--triple-labeling immunofluorescence study. Acta neuropathologica *102*, 149-152.

Uchihara, T., Iwabuchi, K., Funata, N., and Yagishita, S. (2002). Attenuated nuclear shrinkage in neurons with nuclear aggregates--a morphometric study on pontine neurons of Machado-Joseph disease brains. Experimental neurology *178*, 124-128.

Ulusoy, A., Sahin, G., Bjorklund, T., Aebischer, P., and Kirik, D. (2009). Dose optimization for long-term rAAV-mediated RNA interference in the nigrostriatal projection neurons. Molecular therapy : the journal of the American Society of Gene Therapy *17*, 1574-1584.

Valori, C.F., Ning, K., Wyles, M., Mead, R.J., Grierson, A.J., Shaw, P.J., and Azzouz, M. (2010). Systemic delivery of scAAV9 expressing SMN prolongs survival in a model of spinal muscular atrophy. Science translational medicine *2*, 35ra42.

van Gestel, M.A., van Erp, S., Sanders, L.E., Brans, M.A., Luijendijk, M.C., Merkestein, M., Pasterkamp, R.J., and Adan, R.A. (2014). shRNA-induced saturation of the microRNA pathway in the rat brain. Gene therapy *21*, 205-211.

van Hengel, P., Nikken, J.J., de Jong, G.M., Hesp, W.L., and van Bommel, E.F. (1997). Mannitol-induced acute renal failure. The Netherlands journal of medicine *50*, 21-24.

Vandenberghe, L.H., Wilson, J.M., and Gao, G. (2009). Tailoring the AAV vector capsid for gene therapy. Gene therapy *16*, 311-319.

Vite, C.H., Passini, M.A., Haskins, M.E., and Wolfe, J.H. (2003). Adeno-associated virus vector-mediated transduction in the cat brain. Gene therapy *10*, 1874-1881.

Walia, J.S., Altaleb, N., Bello, A., Kruck, C., LaFave, M.C., Varshney, G.K., Burgess, S.M., Chowdhury, B., Hurlbut, D., Hemming, R.*, et al.* (2015). Long-term correction of sandhoff disease following intravenous delivery of rAAV9 to mouse neonates. Molecular therapy : the journal of the American Society of Gene Therapy *23*, 414-422.

Wang, C., Wang, C.M., Clark, K.R., and Sferra, T.J. (2003). Recombinant AAV serotype 1 transduction efficiency and tropism in the murine brain. Gene therapy *10*, 1528-1534.

Wang, D.B., Dayton, R.D., Henning, P.P., Cain, C.D., Zhao, L.R., Schrott, L.M., Orchard, E.A., Knight, D.S., and Klein, R.L. (2010). Expansive gene transfer in the rat CNS rapidly produces amyotrophic

lateral sclerosis relevant sequelae when TDP-43 is overexpressed. Molecular therapy : the journal of the American Society of Gene Therapy *18*, 2064-2074.

Wang, H., Yang, B., Qiu, L., Yang, C., Kramer, J., Su, Q., Guo, Y., Brown, R.H., Jr., Gao, G., and Xu, Z. (2014). Widespread spinal cord transduction by intrathecal injection of rAAV delivers efficacious RNAi therapy for amyotrophic lateral sclerosis. Human molecular genetics *23*, 668-681.

Wang, H.L., Hu, S.H., Chou, A.H., Wang, S.S., Weng, Y.H., and Yeh, T.H. (2013). H1152 promotes the degradation of polyglutamine-expanded ataxin-3 or ataxin-7 independently of its ROCK-inhibiting effect and ameliorates mutant ataxin-3-induced neurodegeneration in the SCA3 transgenic mouse. Neuropharmacology *70*, 1-11.

Wang, L.C., Chen, K.Y., Pan, H., Wu, C.C., Chen, P.H., Liao, Y.T., Li, C., Huang, M.L., and Hsiao, K.M. (2011). Muscleblind participates in RNA toxicity of expanded CAG and CUG repeats in Caenorhabditis elegans. Cellular and molecular life sciences : CMLS *68*, 1255-1267.

Wang, Y.L., Liu, W., Wada, E., Murata, M., Wada, K., and Kanazawa, I. (2005). Clinico-pathological rescue of a model mouse of Huntington's disease by siRNA. Neuroscience research *53*, 241-249.

Warrick, J.M., Morabito, L.M., Bilen, J., Gordesky-Gold, B., Faust, L.Z., Paulson, H.L., and Bonini, N.M. (2005). Ataxin-3 suppresses polyglutamine neurodegeneration in Drosophila by a ubiquitin-associated mechanism. Molecular cell *18*, 37-48.

Watson, L.M., and Wood, M.J. (2012). RNA therapy for polyglutamine neurodegenerative diseases. Expert reviews in molecular medicine *14*, e3.

Weber, M., Rabinowitz, J., Provost, N., Conrath, H., Folliot, S., Briot, D., Cherel, Y., Chenuaud, P., Samulski, J., Moullier, P*., et al.* (2003). Recombinant adeno-associated virus serotype 4 mediates unique and exclusive long-term transduction of retinal pigmented epithelium in rat, dog, and nonhuman primate after subretinal delivery. Molecular therapy : the journal of the American Society of Gene Therapy *7*, 774-781.

Weismann, C.M., Ferreira, J., Keeler, A.M., Su, Q., Qui, L., Shaffer, S.A., Xu, Z., Gao, G., and Sena-Esteves, M. (2015). Systemic AAV9 gene transfer in adult GM1 gangliosidosis mice reduces lysosomal storage in CNS and extends lifespan. Human molecular genetics *24*, 4353-4364.

Winborn, B.J., Travis, S.M., Todi, S.V., Scaglione, K.M., Xu, P., Williams, A.J., Cohen, R.E., Peng, J., and Paulson, H.L. (2008). The deubiquitinating enzyme ataxin-3, a polyglutamine disease protein, edits Lys63 linkages in mixed linkage ubiquitin chains. The Journal of biological chemistry *283*, 26436-26443.

Witter, L., and De Zeeuw, C.I. (2015). Regional functionality of the cerebellum. Current opinion in neurobiology *33*, 150-155.

Wu, Z., Asokan, A., and Samulski, R.J. (2006). Adeno-associated virus serotypes: vector toolkit for human gene therapy. Molecular therapy : the journal of the American Society of Gene Therapy *14*, 316-327.

Wu, Z., Sun, J., Zhang, T., Yin, C., Yin, F., Van Dyke, T., Samulski, R.J., and Monahan, P.E. (2008). Optimization of self-complementary AAV vectors for liver-directed expression results in sustained correction of hemophilia B at low vector dose. Molecular therapy : the journal of the American Society of Gene Therapy *16*, 280-289.

Xia, H., Mao, Q., Eliason, S.L., Harper, S.Q., Martins, I.H., Orr, H.T., Paulson, H.L., Yang, L., Kotin, R.M., and Davidson, B.L. (2004). RNAi suppresses polyglutamine-induced neurodegeneration in a model of spinocerebellar ataxia. Nature medicine *10*, 816-820.

Xia, X., Zhou, H., Huang, Y., and Xu, Z. (2006). Allele-specific RNAi selectively silences mutant SOD1 and achieves significant therapeutic benefit in vivo. Neurobiology of disease *23*, 578-586.

Xiao, X., Xiao, W., Li, J., and Samulski, R.J. (1997). A novel 165-base-pair terminal repeat sequence is the sole cis requirement for the adeno-associated virus life cycle. Journal of virology *71*, 941-948.

Yamada, M., Hayashi, S., Tsuji, S., and Takahashi, H. (2001). Involvement of the cerebral cortex and autonomic ganglia in Machado-Joseph disease. Acta neuropathologica *101*, 140-144.

Yamada, M., Tan, C.F., Inenaga, C., Tsuji, S., and Takahashi, H. (2004). Sharing of polyglutamine localization by the neuronal nucleus and cytoplasm in CAG-repeat diseases. Neuropathology and applied neurobiology *30*, 665-675.

Yamashita, T., Chai, H.L., Teramoto, S., Tsuji, S., Shimazaki, K., Muramatsu, S., and Kwak, S. (2013). Rescue of amyotrophic lateral sclerosis phenotype in a mouse model by intravenous AAV9-ADAR2 delivery to motor neurons. EMBO molecular medicine *5*, 1710-1719.

Yamazaki, Y., Hirai, Y., Miyake, K., and Shimada, T. (2014). Targeted gene transfer into ependymal cells through intraventricular injection of AAV1 vector and long-term enzyme replacement via the CSF. Scientific reports *4*, 5506.

Yang, B., Li, S., Wang, H., Guo, Y., Gessler, D.J., Cao, C., Su, Q., Kramer, J., Zhong, L., Ahmed, S.S., *et al.* (2014a). Global CNS transduction of adult mice by intravenously delivered rAAVrh.8 and rAAVrh.10 and nonhuman primates by rAAVrh.10. Molecular therapy : the journal of the American Society of Gene Therapy *22*, 1299-1309.

Yang, H., Li, J.J., Liu, S., Zhao, J., Jiang, Y.J., Song, A.X., and Hu, H.Y. (2014b). Aggregation of polyglutamine-expanded ataxin-3 sequesters its specific interacting partners into inclusions: implication in a loss-of-function pathology. Scientific reports *4*, 6410.

Yi, R., Doehle, B.P., Qin, Y., Macara, I.G., and Cullen, B.R. (2005). Overexpression of exportin 5 enhances RNA interference mediated by short hairpin RNAs and microRNAs. RNA *11*, 220-226.

Yu, C.J., Liu, W., Chen, H.Y., Wang, L., and Zhang, Z.R. (2014). BACE1 RNA interference improves spatial memory and attenuates Abeta burden in a streptozotocin-induced tau hyperphosphorylated rat model. Cell biochemistry and function *32*, 590-596.

Zeng, S., Zeng, J., He, M., Zeng, X., Zhou, Y., Liu, Z., Jiang, H., Tang, B., and Wang, J. (2015). Chinese homozygous Machado-Joseph disease (MJD)/SCA3: a case report. Journal of human genetics *60*, 157-160.

Zeng, Y., Wagner, E.J., and Cullen, B.R. (2002). Both natural and designed micro RNAs can inhibit the expression of cognate mRNAs when expressed in human cells. Molecular cell *9*, 1327-1333.

Zhang, H., Yang, B., Mu, X., Ahmed, S.S., Su, Q., He, R., Wang, H., Mueller, C., Sena-Esteves, M., Brown, R.*, et al.* (2011). Several rAAV vectors efficiently cross the blood-brain barrier and transduce neurons and astrocytes in the neonatal mouse central nervous system. Molecular therapy : the journal of the American Society of Gene Therapy *19*, 1440-1448.

Zhong, X., and Pittman, R.N. (2006). Ataxin-3 binds VCP/p97 and regulates retrotranslocation of ERAD substrates. Human molecular genetics *15*, 2409-2420.

Zincarelli, C., Soltys, S., Rengo, G., and Rabinowitz, J.E. (2008). Analysis of AAV serotypes 1-9 mediated gene expression and tropism in mice after systemic injection. Molecular therapy : the journal of the American Society of Gene Therapy *16*, 1073-1080.

Zolotukhin, S., Byrne, B.J., Mason, E., Zolotukhin, I., Potter, M., Chesnut, K., Summerford, C., Samulski, R.J., and Muzyczka, N. (1999). Recombinant adeno-associated virus purification using novel methods improves infectious titer and yield. Gene therapy *6*, 973-985.

Appendix

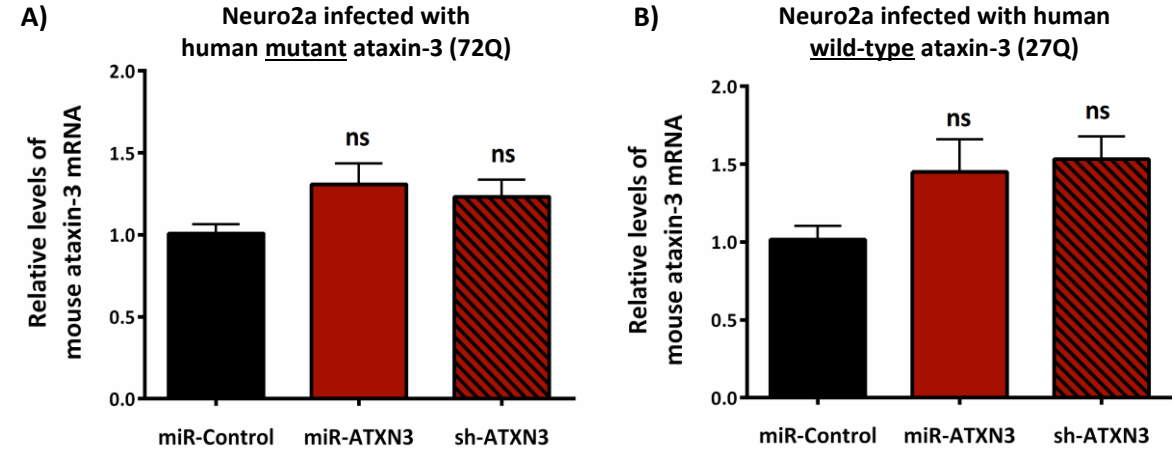

Supplementary Figure 1: miR-ATXN3 treatment does not induce alterations in endogenous mouse ataxin-3 mRNA levels *in vitro*. Neuro2a cells infected with A) human mutant ataxin-3 (72Q) or B) human wild-type ataxin-3 (27Q) were transfected with plasmids encoding miR-Control, miR-ATXN3 and sh-ATXN3. Relative expression levels of mouse ataxin-3 mRNA were determined by quantitative real-time PCR. Results are expressed as the mean relative mRNA level ± SEM (n=5). Internal controls for normalization were mouse Glyceraldehyde 3-phosphate dehydrogenase (GAPDH) and hypoxanthine guanine phosphoribosyl transferase (HPRT). Statistical analysis was performed by Ordinary One-way ANOVA (ns = not significant).

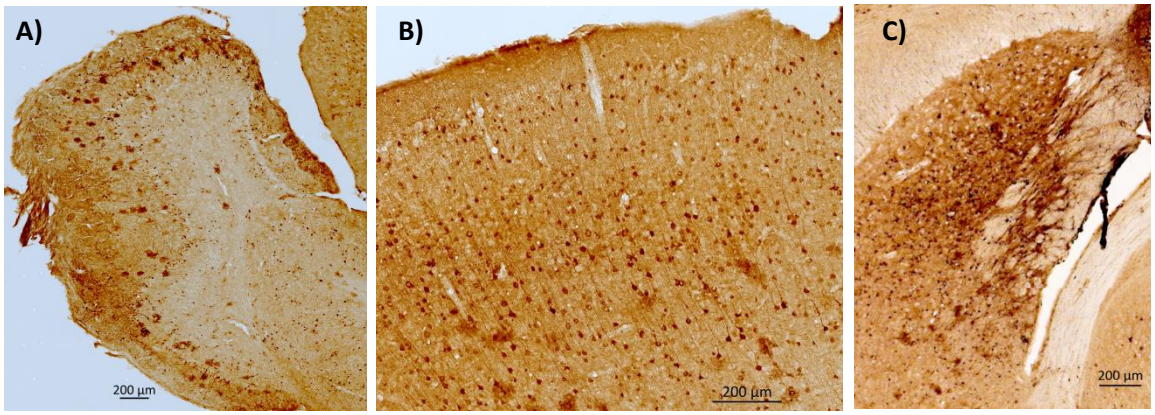

Supplementary Figure 2: Intravenously injected rAAV9 vectors mediate an efficient transduction in several brain regions of transgenic MJD mice. Representative images of GFP immunohistochemistry (in brown) in the brains of 3-month-old MJD mice injected with rAAV9 at P1: A) olfactory bulb; B) cortex; C) striatum. Images were obtained with a 20x objective.

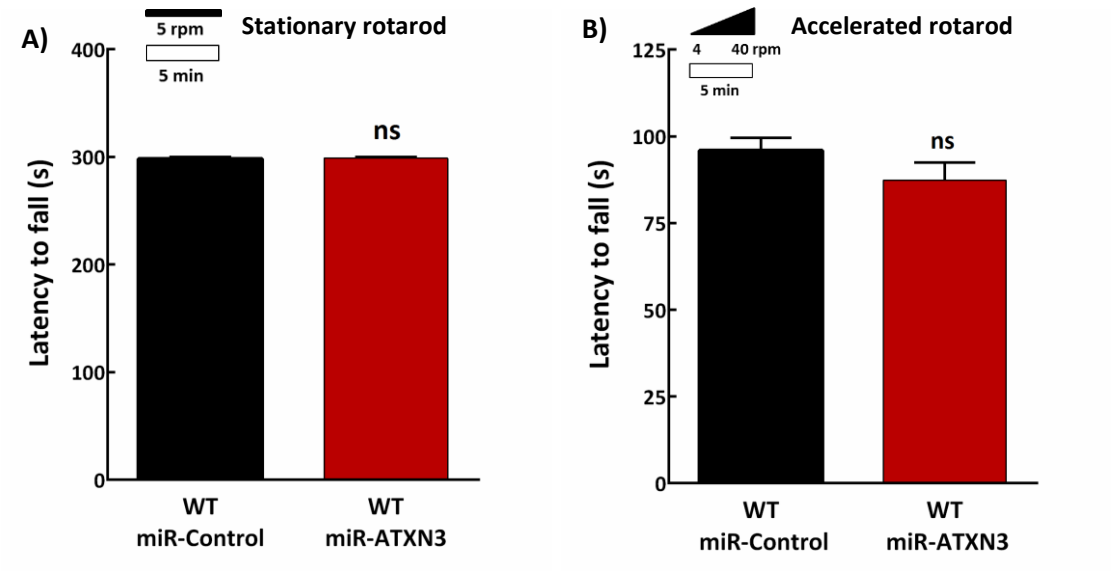

Supplementary Figure 3: rAAV9-miR-ATXN3 IV injection does not affect rotarod performance in wild-type mice. A) Rotarod performance at constant velocity (5 r.p.m). B) Rotarod performance at accelerated velocity. Data are presented as mean latency time to fall ± SEM for wild-type mice (miR-Control, n = 5) and mice injected with AAV9-miR-ATXN3 (n = 5) Statistical analysis was performed using the unpaired Student's t-test (ns = not significant).

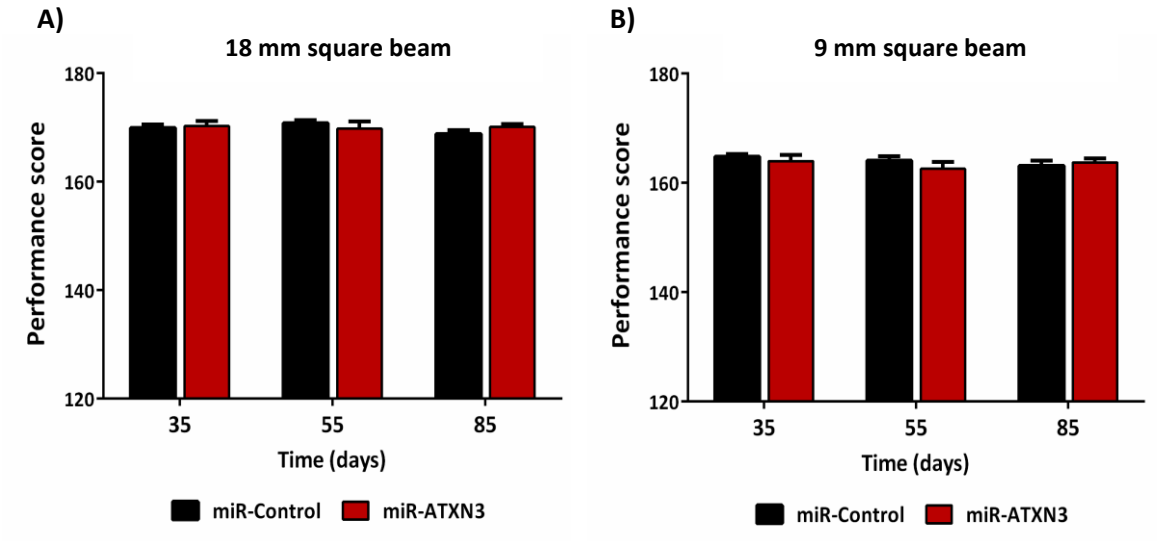

Supplementary Figure 4: rAAV9-miR ATXN3 treatment does not induce alterations in the beam walking test performance, using 18 mm and 9 mm square beams. Animals were evaluated based on their performance when walking on a: A) 18-mm square beam and B) 9-mm square beam. Considering the total time to cross the beam and the motor coordination, each animal received a score (Mendonca et al., 2015). Data are presented as mean performance score ±SEM for control mice (miR-Control, n = 11) and mice injected with AAV9-miR-ATXN3 (n = 8). Statistical analysis was performed using the unpaired Student's t-test.

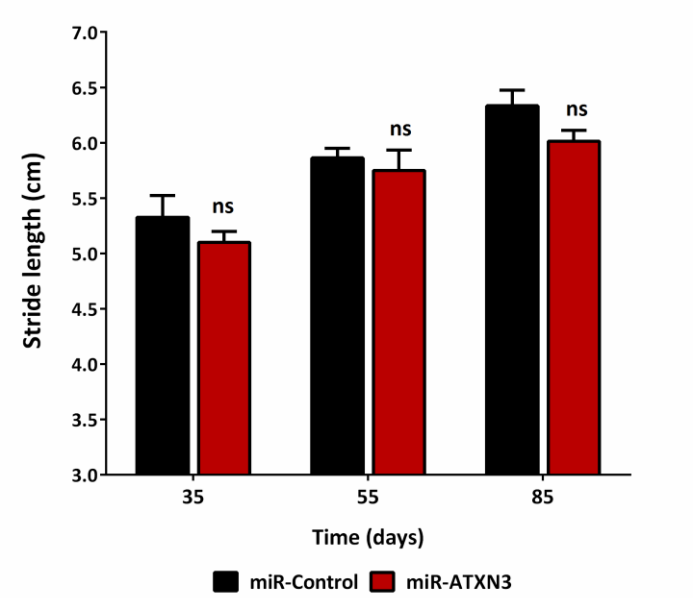

Supplementary Figure 5: rAAV9-miR ATXN3 does not induce alterations in stride length. Data are presented as the mean stride length ±SEM for control mice (miR-Control, n = 11) and mice injected with AAV9-miR-ATXN3 (n = 8). Statistical analysis was performed using the unpaired Student's t-test (ns = not significant).

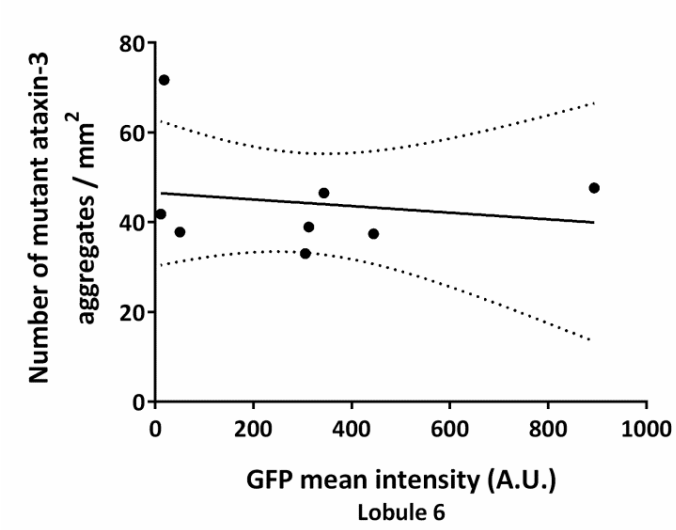

Supplementary Figure 6: rAAV9 transduction levels in lobule 6 do not correlate with neuropathological parameters in treated mice. Linear regression graph between GFP mean intensity in lobule 6 (A.U.= arbitrary units) and number of aggregates/mm^2 in the same region. Statistical analysis was performed using Pearson's correlation (two-tailed p value). Dotted lines represent 95% confidence interval (p=0.6714, R^2=0.03205).

.